



D4.12 - Final Energy Router

Deliverable ID	D4.12
Deliverable Title	Final Energy Router
Work Package	WP4
Dissemination Level	PUBLIC
Version	1.0
Date	29/08/2019
Status	Final
Type	Prototype
Lead Editor	UNINOVA
Main Contributors	UNINOVA (Carlos Roncero-Clemente, Nuno Vilhena, Vasco Delgado-Gomes), UPB (Mihai Sanduleac, Marta Sturzeanu, Mihaela Albu)

Published by the Storage4Grid Consortium



This project has received funding from the European Union's Horizon 2020 research and innovation programme under grant agreement No 731155.

Document History

Version	Date	Author(s)	Description
0.1	2019-03-07	UNINOVA	First draft with the single-phase ER information ready for initial review.
0.2	2019-04-11	UNINOVA	Version addressing the initial reviewer comments.
0.3	2019-08-13	UPB	UPB inputs included.
0.4	2019-08-19	UNINOVA	Final editing and version ready for final internal review.
0.5	2019-08-23	UNINOVA	Addressed reviewer comments and minor corrections.
0.6	2019-08-27	UPB	Addressed reviewer comments and minor corrections.
1.0	2019-08-29	UNINOVA	Final version, ready for submission to the EC.

Internal Review History

Review Date	Reviewer	Summary of Comments
2019-04-01 (v0.1)	Hamidreza Mirtaheri (LINKS)	Reviewed: <ul style="list-style-type: none">Minor comments and edits.
2019-03-28 (v0.1)	Gustavo Aragón (FRAUNHOFER FIT)	Reviewed: <ul style="list-style-type: none">General minor corrections.Comments on pictures.Missing on-site tests.
2019-08-21 (v0.4)	Gustavo Aragón (FRAUNHOFER FIT)	Approved: <ul style="list-style-type: none">General minor corrections.
2019-08-22 (v0.4)	Hamidreza Mirtaheri (LINKS)	Reviewed (2 nd): <ul style="list-style-type: none">General minor corrections.Comments for further information.
2019-08-28 (v0.6)	Hamidreza Mirtaheri (LINKS)	Approved.

Legal Notice

The research work leading to these results has received funding from the European Union's Horizon 2020 research and innovation programme under grant agreement No 731155 - Storage4Grid project. The information in this document is subject to change without notice. The Members of the Storage4Grid Consortium make no warranty of any kind with regard to this document, including, but not limited to, the implied warranties of merchantability and fitness for a particular purpose. The Members of the Storage4Grid Consortium shall not be held liable for errors contained herein or direct, indirect, special, incidental or consequential damages in connection with the furnishing, performance, or use of this material. The European Union and the Innovation and Networks Executive Agency (INEA) are not responsible for any use that may be made of the information contained therein.

Table of Contents

Document History	2
Internal Review History	2
Table of Contents	3
Executive Summary.....	5
1 Introduction.....	6
1.1 Scope	6
1.2 Related documents.....	6
2 Single-phase energy router prototype overview.....	7
3 Single-phase energy router sizing.....	9
3.1 PV interface sizing.....	9
3.2 ESS interface sizing.....	11
3.3 Grid interface sizing	13
3.4 Values of the selected components	15
4 Control algorithms.....	16
5 Operating scenarios	17
6 Simulation results.....	19
6.1 Scenario A1.....	19
6.2 Scenario A2.....	22
6.3 Scenario A3.....	24
6.4 Scenario B1	25
6.5 Scenario B2	26
6.6 Scenario C	27
7 Laboratory tests	30
7.1 Scenario A1.....	30
7.2 Scenario A2.....	31
7.3 Scenario A3.....	32
7.4 Scenario B1	33
7.5 Scenario B2	34
7.6 Scenario C	35
8 On-site tests	37
8.1 Scenario A1.....	37
8.2 Scenario A2.....	39
8.3 Scenario A3.....	41
8.4 Scenario B1	43
8.5 Scenario B2	45
8.6 Scenario C	47
9 Unidirectional neighbourhood DC-DC network	49
10 After deployment tests	51
10.1 LESSAg integration with ER.....	51
10.2 Boost converter evaluation	53

11 Installation/Deployment instructions	55
12 Conclusions.....	58
Acronyms.....	59
Variables nomenclature	61
List of figures.....	64
List of tables.....	66
References	66

Executive Summary

D4.12 – “Final Energy Router” presents the sizing, simulation, laboratory tests and on-site tests of the single-phase Energy Router (ER) prototype. The single-phase ER presented in this document was deployed in Bucharest, Romania at University Politehnica of Bucharest (UPB) MicroDERLab facilities. A photovoltaic (PV) system with 70 V Maximum Power Point (MPP) and 1040 W of nominal power is available in the test site. An Energy Storage System (ESS) composed of 8 lead-acid battery pack with 96 V and 17 Ah of capacity is also available. The sizing and simulations of the ER in this document were performed taking into consideration these values.

Different scenarios were defined in order to validate the correct operation of the single-phase ER. They are divided into three groups: A – Distribution System Operation (DSO) grid available, B – DSO grid unavailable (island mode), and C – black-start operation.

A comprehensive simulation study was performed in the PSCAD/EMTDCⁱ software to validate the calculated values, the main functionalities, control algorithms, and modulation methods. The different previously proposed scenarios were analysed and simulated. The simulations results show a correct operation of the ER in the different scenarios. Furthermore, the different scenarios were also tested in laboratory and at UPB’s MicroDERLab facilities, with similar results.

The boost converter of the unidirectional DC network connection was developed and tested by UPB at the Bucharest test site. The DC network will be used in the third phase of the S4G project to supply the neighbourhood 400 V DC line with power from the 220 V ER DC bus. It will be also used for the evaluation of the neighbourhood energy exchange defined in the Bucharest High-Level Use-Cases (HLUCs) and to be reported in D6.12 – “Phase 3 Evaluation Report” (February 2020).

1 Introduction

D4.12 describes the “Final Energy Router” prototype, developed by the Storage4Grid project. This prototype describes all the steps made to develop and deploy the single-phase ER prototype. More information regarding the ER controller and the S4G architecture can be retrieved from the related documents summarized in Section 1.2.

1.1 Scope

This prototype deliverable has been developed in Task T4.5 – “Energy Router”. Two ER prototypes resulted of this task, a three-phase ER described in D4.11[S4G-D4.11] and a single-phase ER described in this deliverable.

1.2 Related documents

ID	Title	Reference	Version	Date
D2.2	Final Storage Scenarios and Use Cases	[S4G-D2.2]	1.0	2018-07-31
D4.3	Final User-side ESS control system	[S4G-D4.3]	1.0	2019-06-13
D4.9	Updated USM Extensions for Storage Systems	[S4G-D4.9]	1.0	2018-08-31
D4.10	Final USM Extensions for Storage Systems	[S4G-D4.10]	0.2	2019-07-10
D4.11	Initial Energy Router	[S4G-D4.11]	1.0	2018-11-02

2 Single-phase energy router prototype overview

The main diagram of the single-phase ER is show in Figure 1. A DSO switch (S_{DSO}) enables the island operation. The D4.12 prototype, i.e., the single-phase ER is composed of the following power conversion stages:

- DC-DC boost converter as interface between the PV array and the common DC-link.
- Bidirectional DC-DC buck-boost converter for ESS charging/discharging.
- Bidirectional single-phase DC-AC converter.
- Boost converter of the unidirectional neighbourhood DC-DC network (UPB development, orange components).

The single-phase ER is connected to the following power system elements:

- PV generation system.
- ESS.
- DSO single-phase grid.
- Loads.

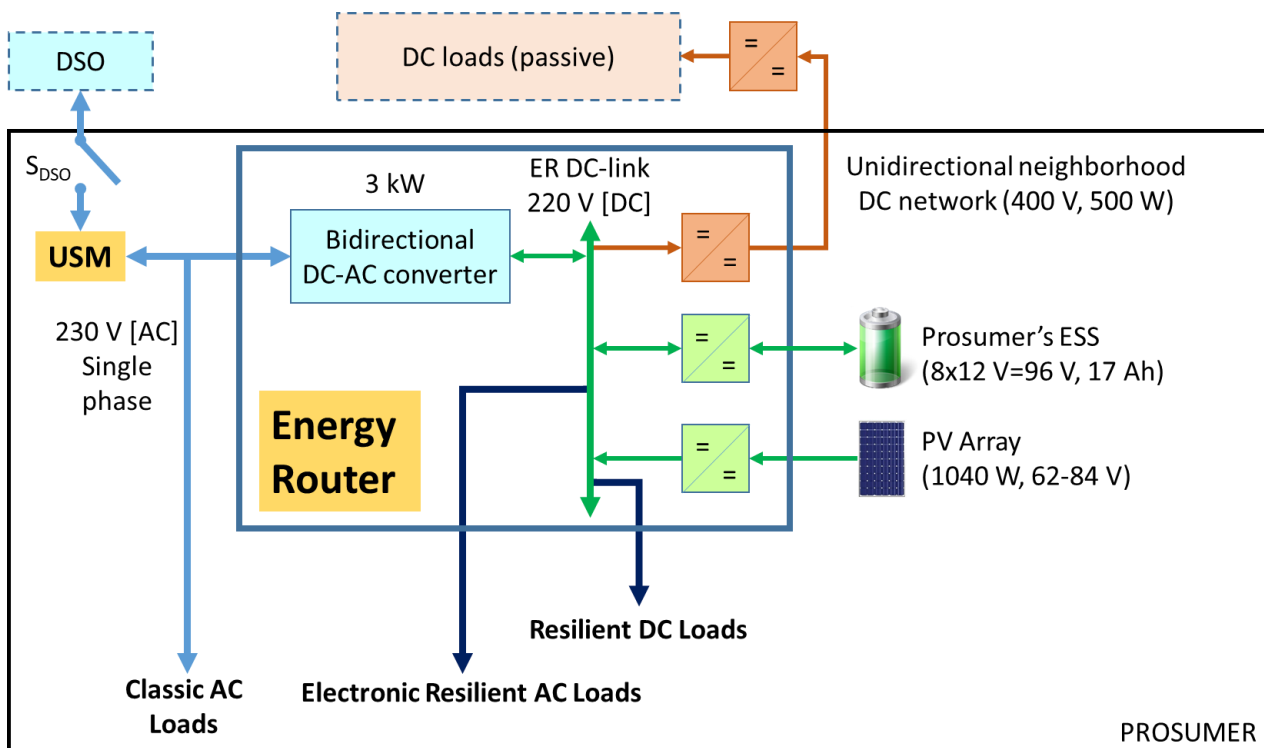


Figure 1. Single-phase ER deployment architecture at Bucharest test site.

The selected topologies of power circuits inside the ER and its connections to other power systems elements are depicted in Figure 2.

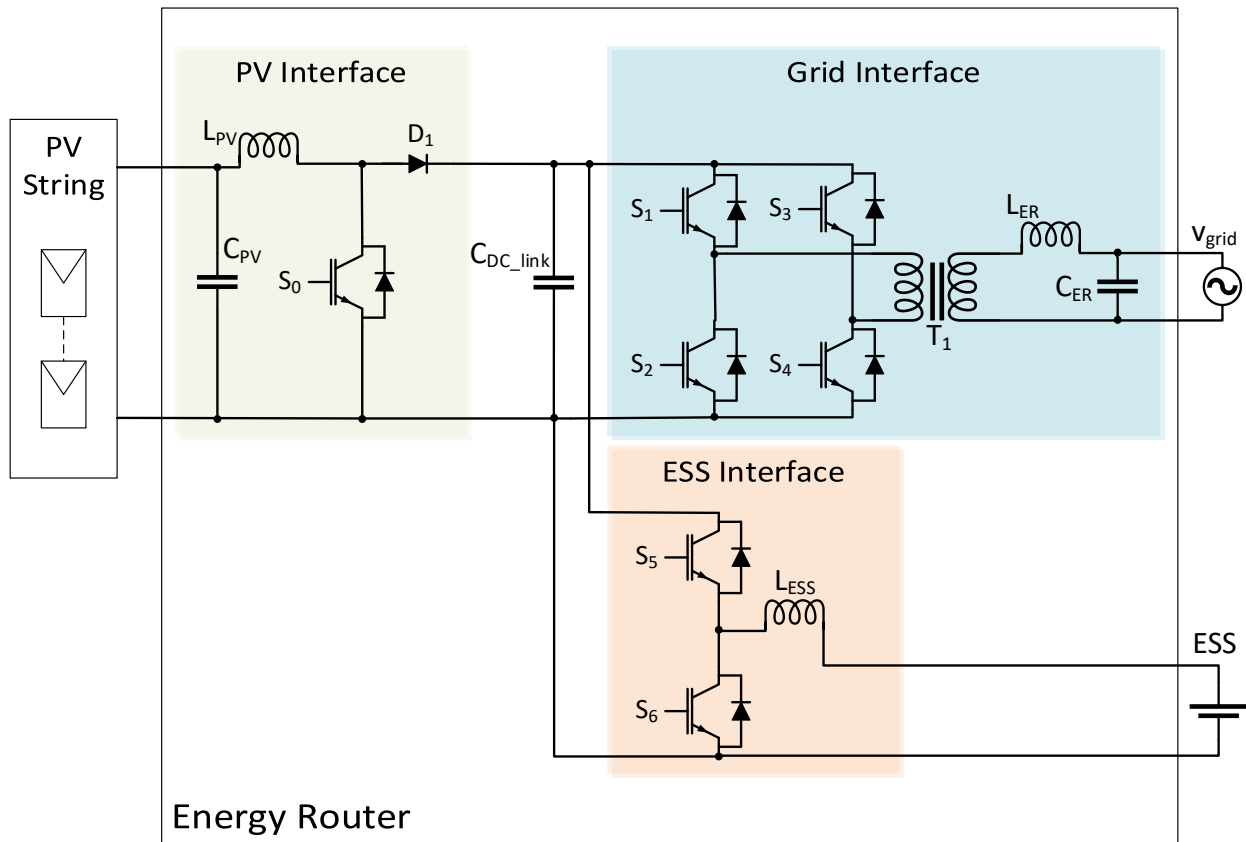


Figure 2. Power topology of the single-phase ER.

For the PV interface it was selected a conventional DC-DC boost converter, composed of a pure inductance filter (L_{PV}), a single switch (S_0) and a diode (D_1). The PV capacitor (C_{PV}) is located at the input stage for stabilizing the PV voltage. The PV panels are directly connected to the DC-DC boost converter, while C_{DC_link} forms the common DC-link for the full system. Its main functionality will be the maximum power extraction from the PV array (MPPT operation) or to provide any feasible reference value of power (RPPT operation). (Figure 2, subsystem highlighted in green).

Due to the difference in the ESS voltage level (96 V) and the considered main DC-link voltage (220 V), a single two-level branch was used to build up the power converter for demanding or injecting power from/to the ESS, working as buck or boost DC-DC converter. It is composed of two switches (S_5 and S_6), and one filter inductance (L_{ESS}). (Figure 2, subsystem highlighted in orange).

A single-phase full bridge DC-AC bidirectional power converter is in charge of interfacing the energy generation system with the utility single-phase grid. Composed of 4 switches (S_1, \dots, S_4), a LC filter (L_{ER} and C_{ER}) and a transformer (T_1) with a turn ratio equal to 1:2, this DC-AC converter will be responsible for the main functionalities and services concerning active and reactive power injection and grid synchronization. (Figure 2, subsystem highlighted in blue).

DC-link voltage will be controlled by the ESS interface converter if the DSO grid is unavailable or by the grid interface if the DSO grid is available.

3 Single-phase energy router sizing

This section presents the sizing of the different ER interfaces, namely: PV, ESS, and grid.

3.1 PV interface sizing

The following four parameters needed to be calculated to size the power circuit that composes the DC-DC boost PV converter:

- 1) PV input voltage range: minimum PV input voltage ($V_{PV,m}$) and maximum PV input voltage ($V_{PV,M}$).
- 2) Nominal DC-link voltage (V_{DC_link}).
- 3) Maximum PV output current ($I_{PV,M}$).
- 4) Integrated circuit, discrete semiconductor or power module to build the boost converter.

For the Romanian test site, it was considered as input voltage 70 V at the Maximum Power Point (MPP), and as nominal power for the PV array 1040 W at standard conditions of irradiance and temperature. V_{DC_link} is 220 V. It is important to note that this value is feasible due to a 1:2 low frequency transformer. This transformer is installed between the DC-AC ER converter and the grid/load, providing galvanic isolation. For safety reasons and possible environmental conditions, it is assumed that $V_{PV,m}$ can get 62 V in case of low irradiance and $V_{PV,M}$ around 84 V (considering this value as open circuit voltage, (V_{oc}) of the PV array).

3.1.1 Calculation of the maximum PV switch current and PV inductor selection

The first step to calculate the maximum PV switch current ($I_{SW_{PV}}$) is to determine the duty cycle ($D_{PV,M}$) for the minimum voltage. This minimum input voltage leads to the maximum PV switch current. In equation (1), η represents the efficiency of the converter, estimated at 80 %. This efficiency is added to the duty cycle calculation since the converter has also to deliver the dissipated energy. This calculation gives a more realistic duty cycle.

$$D_{PV,M} = 1 - \frac{V_{PV,m} \cdot \eta}{V_{DC_link}} \quad (1)$$

The next step to calculate the maximum PV switch current is to determine the PV inductor current ripple ($\Delta I_{L_{PV}}$). The PV inductor was selected according to equation (2), where f_s is the minimum switching frequency of the converter.

$$L_{PV,m} = \frac{V_{PV,m} \cdot (V_{DC_link} - V_{PV,m})}{\Delta I_{L_{PV}} \cdot f_s \cdot V_{DC_link}} \quad (2)$$

The PV inductor current ripple ($\Delta I_{L_{PV}}$) can be estimated using equation (3).

$$\Delta I_{L_{PV}} \approx (0.2 \text{to} 0.4) \cdot I_{PV,M} \cdot \frac{V_{DC_link}}{V_{PV,m}} \quad (3)$$

With equations (1), (2) and (3) it is possible to estimate the required values for this sizing stage. Table 1 presents the specifications and rated values and the calculated values. Using the values in Table 1, the maximum PV switch current ($I_{SW_{PV}}$) is calculated using equation (4).

$$I_{SW_{PV}} \approx I_{PV,M} + \frac{\Delta I_{L_{PV}}}{2} \quad (4)$$

Table 1. Specifications of the PV interface and calculated values (in bold) for L.

Parameter	Value
Maximum power point voltage (V_{MPP})	70 V
Minimum PV input voltage ($V_{PV,m}$)	62 V
Maximum PV input voltage ($V_{PV,M}$)	84 V
Nominal DC-link voltage (V_{DC_link})	220 V
Maximum power point (MPP)	1040 W
Maximum PV output current ($I_{PV,M}$)	16 A
Estimated efficiency of the converter (η)	80 %
Minimum switching frequency (f_s)	15 kHz
PV inductor current ripple ($\Delta I_{L_{PV}}$)	≈2.5 A
Assumed PV inductor current ripple ($\Delta I_{L_{PV}}$)	30 %
Minimum PV inductance ($L_{PV,m}$)	1.3 mH
Maximum PV duty cycle ($D_{PV,M}$)	0.78
Maximum PV switch current ($I_{SW_{PV}}$)	17.25 A

3.1.2 PV input capacitor selection (C_{PV})

This capacitor requires a minimum value necessary to stabilize the input voltage (V_{PV}), due to the switching frequency of S_0 . Equation (5) was used to adjust the minimum input capacitor value ($C_{PV,m}$) for a desired input voltage ripple (ΔV_{PV}).

$$C_{PV,m} = \frac{\Delta I_{L_{PV}}}{8 \cdot f_s \cdot \Delta V_{PV}} \quad (5)$$

At the same time, the minimum input voltage ripple is given by equation (6), where ESR is the equivalent series resistance of the used input capacitor. The estimation of this passive component is summarized in Table 2.

$$\Delta V_{PV} = ESR \cdot \left(I_{PV,M} + \frac{\Delta I_{L_{PV}}}{2} \right) \quad (6)$$

Table 2. Specifications of the PV interface and calculated values (in bold) for C.

Parameter	Value
Equivalent series resistance (ESR)	0.25 Ω
Estimated PV voltage ripple (ΔV_{PV})	4.3 V
Considered PV voltage ripple (ΔV_{PV})	5 V
Minimum PV input capacitor value ($C_{PV,m}$)	4.2 μF

3.1.3 DC-link capacitor selection

Equation (7) was used to adjust the minimum output capacitor value ($C_{DC_link,m}$) for a desired output voltage ripple (ΔV_{DC_link}).

$$C_{DC_link,m} = \frac{I_{PV,M} \cdot D_{PV,M} \cdot (1 - D_{PV,M})}{f_s \cdot \Delta V_{DC_link}} \quad (7)$$

At the same time, the minimum output voltage ripple is given by equation (8), where ESR is the equivalent series resistance of the used capacitor. The estimation of this passive component is summarized in Table 3.

$$\Delta V_{DC_link} = ESR \cdot \left(I_{PV,M} + \frac{\Delta I_{LPV}}{2} \right) \quad (8)$$

Table 3. Specifications of the PV interface and calculated values (in bold) for C.

Parameter	Value
Equivalent series resistance (ESR)	0.25 Ω
Estimated DC-link voltage ripple (ΔV_{DC_link})	4.3 V
Considered DC-link voltage ripple (ΔV_{DC_link})	5 V
Minimum DC-link capacitor value ($C_{DC_link,m}$)	36.6 μF

3.2 ESS interface sizing

Similar considerations and procedure were used for sizing the components of the DC-DC buck-boost converter, which will act as power interface with the ESS. The next four values are needed for calculations.

- 1) ESS input voltage range: minimum ESS input voltage ($V_{ESS,m}$) and maximum ESS input voltage ($V_{ESS,M}$).
- 2) Nominal DC-link voltage (V_{DC_link}).
- 3) Maximum ESS output current ($I_{ESS,M}$).
- 4) Integrated circuit, discrete semiconductor or power module to build the boost converter.

For the Romanian test site, it was considered as input voltage 96 V, obtained as serial association of 8x12 V batteries, and as nominal power around 1000 W for discharging and 500 W for charging. This ESS voltage level is suitable to interact with the DC-link voltage at 220 V.

3.2.1 Calculation of the maximum ESS switch current and ESS inductor selection

The first step for calculating the maximum ESS switching current ($I_{SW_{ESS}}$) is to determine the duty cycle ($D_{ESS,M}$) for the minimum voltage. This minimum input voltage leads to the maximum ESS switch current. In equation (6), η represents the efficiency of the converter, estimated at 80 %.

$$D_{ESS,M} = 1 - \frac{V_{ESS,m} \cdot \eta}{V_{DC_link}} \quad (9)$$

The next step to calculate the maximum ESS switch current is to determine the ESS inductor current ripple ($\Delta I_{L_{ESS}}$). The ESS inductor is calculated using equation (7), where f_s is the minimum switching frequency of the converter.

$$L_{ESS,m} = \frac{V_{ESS,m} \cdot (V_{DC_link} - V_{ESS,m})}{\Delta I_{L_{ESS}} \cdot f_s \cdot V_{DC_link}} \quad (10)$$

The ESS inductor current ripple ($\Delta I_{L_{ESS}}$) can be estimated as shown in equation (8).

$$\Delta I_{L_{ESS}} \approx (0.2 \text{to} 0.4) \cdot I_{ESS,M} \cdot \frac{V_{DC_link}}{V_{ESS,m}} \quad (11)$$

Using equations (9), (10) and (11) it is possible to estimate the required values for the ESS inductor sizing. Table 4 presents the specifications and rated values, and the calculated values. Using the values in Table 4, the maximum ESS switch current is calculated using equation (12).

$$I_{SW_{ESS}} \approx I_{ESS,M} + \frac{\Delta I_{L_{ESS}}}{2} \quad (12)$$

Table 4. Specifications of the ESS interface and calculated values (in bold) for L.

Parameter	Values for Boost operation	Values for Buck operation
Nominal ESS voltage (V_{ESS})	96 V	96 V
Nominal DC-link voltage (V_{DC_link})	220 V	220 V
Nominal ESS power (P_{ESS})	1000 W	500 W
Maximum ESS output current ($I_{ESS,M}$)	10.4 A	5.2 A
Estimated efficiency of the converter (η)	80 %	80 %
Minimum switching frequency (f_s)	15 kHz	15 kHz
ESS inductor current ripple ($\Delta I_{L_{ESS}}$)	≈ 0.2 A	≈ 0.2 A
Assumed ESS inductor current ripple ($\Delta I_{L_{ESS}}$)	8 %	8 %
Minimum ESS inductance filter ($L_{ESS,m}$)	1.9 mH	2.74 mH
Maximum ESS duty cycle ($D_{ESS,M}$)	0.64	0.76
Maximum ESS switch current ($I_{SW_{ESS}}$)	10.5 A	5.3 A

Using the equation (11) to estimate the ESS inductor current ripple gives as result a high current value due to the difference voltage level between the DC-link (220 V) and the ESS side (96 V). The ESS inductor ripple current was limited to a value of 0.5 A, to extend the ESS useful life.

3.2.2 DC-link capacitor selection

Equation (13) was used to adjust the minimum DC-link capacitor value ($C_{DC_link,m}$) for a desired DC-link voltage ripple (ΔV_{DC_link}).

$$C_{DC_link,m} = \frac{I_{ESS,M} \cdot D_{ESS,M} \cdot (1 - D_{ESS,M})}{f_s \cdot \Delta V_{DC_link}} \quad (13)$$

At the same time, the minimum output voltage ripple is given by equation (14), where ESR is the equivalent series resistance of the used capacitor. The estimation of this passive component is summarized in Table 5.

$$\Delta V_{DC_link} = ESR \cdot \left(I_{ESS,M} + \frac{\Delta I_{ESS}}{2} \right) \quad (14)$$

Table 5. Specifications of the ESS interface and calculated values (in bold) for C.

Parameter	Values for Boost operation	Values for Buck operation
Equivalent series resistance (ESR)	0.25 Ω	0.25 Ω
Estimated DC-link voltage ripple (ΔV_{DC_link})	2.6 V	1.3 V
Minimum DC-link capacitor value ($C_{DC_link,m}$)	61 μF	49 μF

3.3 Grid interface sizing

In a single-phase full-bridge DC-AC converter is necessary to calculate and estimate the output filter (C_{ER} and L_{ER} components, shown in Figure 2). This component is essential for Pulse Width Modulation (PWM) converters. Some technical documents cover the output filter design^{ii,iii,iv}. L, LC, LCL and LLCL output filters are commonly used in this kind of power converter. However, it was selected a LC filter to mitigate the high frequency harmonics, to measure the capacitor voltage and to control it during the island operation.

There are several criteria that can be considered for L selection. For instance, the ripple criteria ensures that the error between the reference current and the grid injected current by the converter remains within a margin regulated by the power quality standards (usually between 5% and 15%). The used criteria is based on the current ripple calculation on the switching harmonic. Figure 3 shows a typical harmonic spectrum of the DC-AC converter. It is possible to define the converter voltage harmonic at the switching frequency.

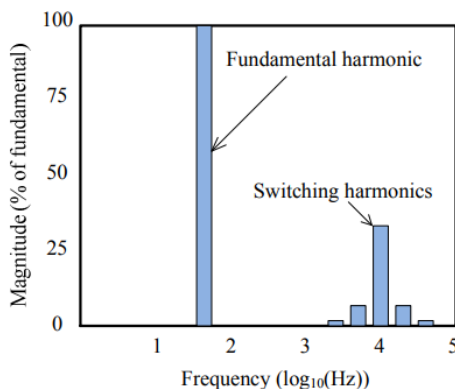


Figure 3. Typical harmonic spectrum of the grid current.

Assuming that the current ripple is directly and exclusively influenced by the switching frequency, equation (15) is considered, where I_{SW} is the grid RMS harmonic current at the switching frequency, I_1 is the RMS value of the current fundamental harmonic of the grid.

$$THD_I \approx \sqrt{\frac{I_{SW}^2}{I_1^2}} = \frac{I_{SW}}{I_1} \quad (15)$$

The current ripple through the converter side to the grid side can be computed upon consideration that at high frequencies, the converter is a harmonic generator, while the grid can be considered as a short circuit, as shown in Figure 4. The transfer function ($G_L(h_{sw})$) of this circuit is expressed as equation (16), where h_{sw} – the number of switching harmonic, ω_1 – fundamental harmonic, and total filter inductance $L_t=L_{ER}+L_{grid}$.

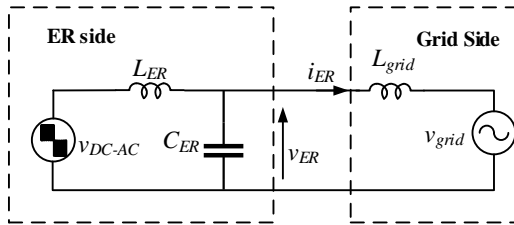


Figure 4. Equivalent grid-connected ER with LC filter.

$$G_L(h_{sw}) = \frac{i_{ER}(h_{sw})}{v_{ER}(h_{sw})} = \left| \frac{-j}{\omega_1 \cdot h_{sw} \cdot (L_{ER} + L_{grid})} \right| \quad (16)$$

From equation (16), the current ripple is defined as shown in equation (17).

$$I_{SW} = I_{ER}(h_{sw}) = V_{ER}(h_{sw}) \frac{1}{\omega_1 \cdot h_{sw} \cdot L_t} \quad (17)$$

To estimate the inductance value, it was necessary to establish the harmonic component of the converter output voltage at the switching frequency $V_{ER}(h_{sw})$. Considering unity power factor and equations (15) and (17), equation (18) can be written, where P_{ER} is the ER rated power.

$$L_t \geq \frac{V_{ER}(h_{sw}) \cdot v_{grid}}{\omega_1 \cdot h_{sw} \cdot P_{ER} \cdot THD_I} \quad (18)$$

As the voltage harmonic component at the switching frequency is unknown, the current ripple can be estimated directly from this calculation using the converter voltage waveform. Typically, such approach gives the same result, since there is a proportional relation between the two magnitudes: ripple and content of harmonics.

The filter capacitor (C_{ER}) is added in parallel to the single-phase grid/load and calculated using equation (19). The cut-off frequency (f_c) is considered 700 Hz, in order to mitigate the high switching components of the output current.

Table 6 presents the specification, rated values and the calculated values.

$$f_c = \frac{1}{2 \cdot \pi \cdot \sqrt{L_t \cdot C_{ER}}} \quad (19)$$

Table 6. Specifications of the grid interface and calculated values (in bold) for L and C.

Parameter	Value
ER Rated Power (P_{ER})	3000 W
RMS Grid phase to neutral voltage (V_{grid})	230 V
ER voltage at switching frequency ($V_{ER}(h_{sw})$)	23 V (10 %)
h_{sw}	300 (15 kHz)

Fundamental frequency (ω_1)	50 Hz
THD _I	5 %
Minimum ER output inductance filter ($L_{ER,m}$)	3.3 mH
Minimum ER output capacitance filter ($C_{ER,m}$)	0.9 μF

3.4 Values of the selected components

Taking into account the calculations in the previous sections, the final values of the selected components are show in Table 7. The Insulated-Gate Bipolar Transistors (IGBTs) selected for the power electronic converters were the 2MBI150U2A-060-50 branch module.

Table 7. Final values of the single-phase ER selected components.

Parameter	Value
PV inductance (L_{PV})	5 mH
PV input capacitor (C_{PV})	1800 μ F
ESS inductance filter (L_{ESS})	5 mH
DC-link capacitor (C_{DC_link})	4400 μ F
ER output inductance filter (L_{ER})	10 mH
ER output capacitance filter (C_{ER})	3 μ F

4 Control algorithms

The general block diagram of the control structure is shown in Figure 5.

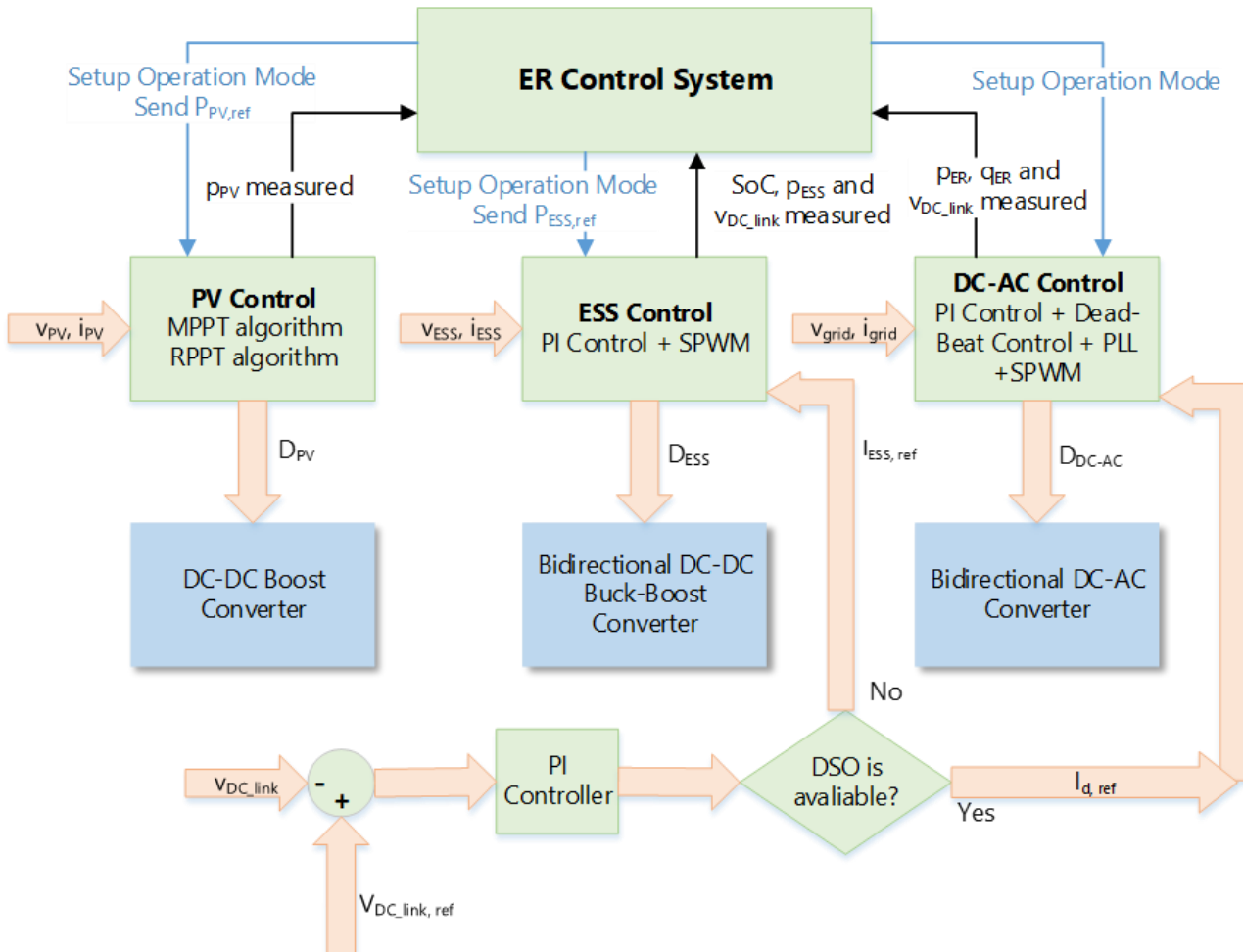


Figure 5. Block diagram of the ER control strategy.

The DC-AC ER converter operates with a direct component reference current (I_d, ref). The converter can work in DSO grid available and DSO grid unavailable (island) modes. When the ER is working connected to the DSO grid, I_d, ref is obtained by a DC-link control loop (the DC-AC converter is set to control the DC-link voltage). This control loop forces the system to maintain a constant voltage at the desired level. If the ER is working without the DSO grid (island mode), I_d, ref is obtained by a capacitor output filter voltage control loop. This control loop forces the ER to maintain a sinusoidal reference voltage at the output of the ER (grid side), at the desired level. The current tracking control is based on the predictive control type with a dead-beat current controller.

The power exchange between ESS and DC-link is controlled using the external control block according to the ESS state of charge (SoC) and user specifications. If the ER is operating in island mode, the DC-DC ESS converter is set to control the DC-link voltage, if the DSO grid is available, then DC-DC ESS converter will only receive setpoint to charge or discharge the ESS. On the PV side, the DC-DC PV boost converter will extract the maximum power (MPP) from the PV array or any feasible active power reference (RPP) to be injected to the DC-link.

5 Operating scenarios

Different scenarios were defined in order to validate the correct operation of the single-phase ER. They are divided into three groups: A – DSO grid available (Figure 6), B – DSO grid unavailable (island mode, Figure 7), and C – black-start operation (Figure 8), as follows:

- A1) PV system is operating at MPPT mode, ESS discharges and charges, and DC-AC ER converter is injecting/absorbing pure active power and/or reactive power into/from the grid.
- A2) PV system is operating at RPPT mode, ESS discharges and charges, and DC-AC ER converter is injecting/absorbing pure active power and/or reactive power into/from the grid.
- A3) PV system is OFF, ESS discharges and charges, and DC-AC ER converter is injecting/absorbing pure active power and/or reactive power into/from the grid.
- B1) PV system is operating at MPPT mode feeding loads. The remaining power charges the ESS.
- B2) PV system is operating at RPPT mode feeding loads. The remaining power charges the ESS.
- C) Black-start operation.

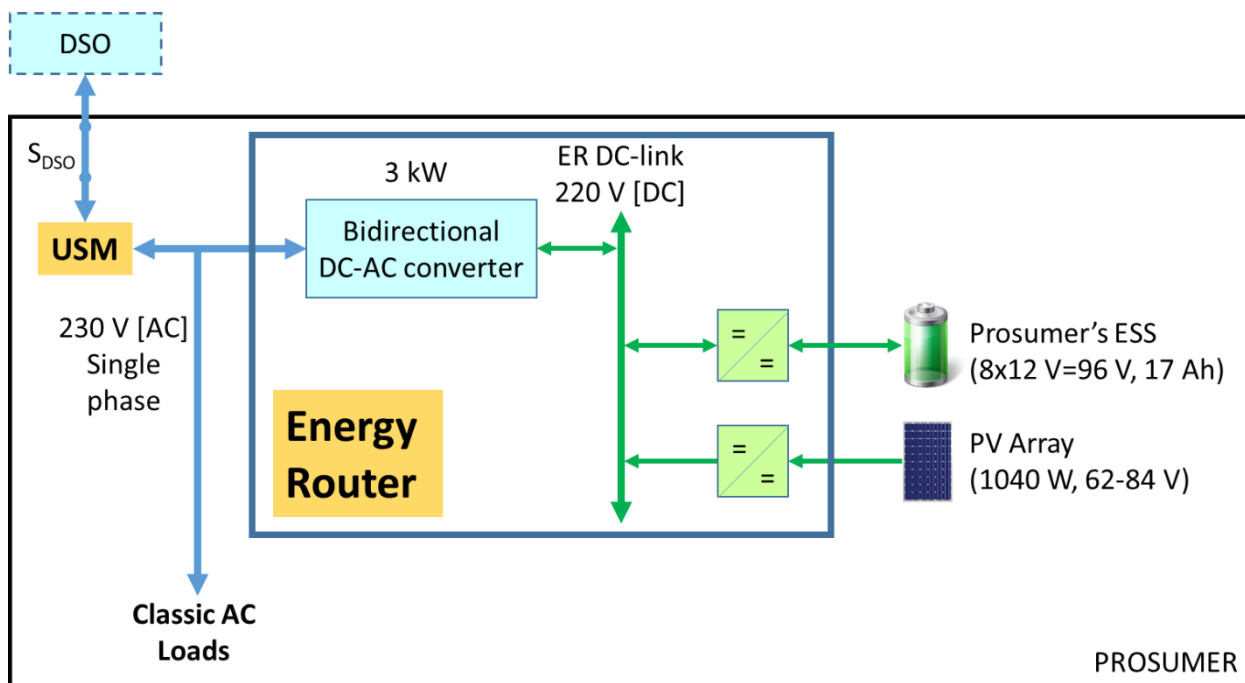


Figure 6. Single-phase ER scenario A architecture.

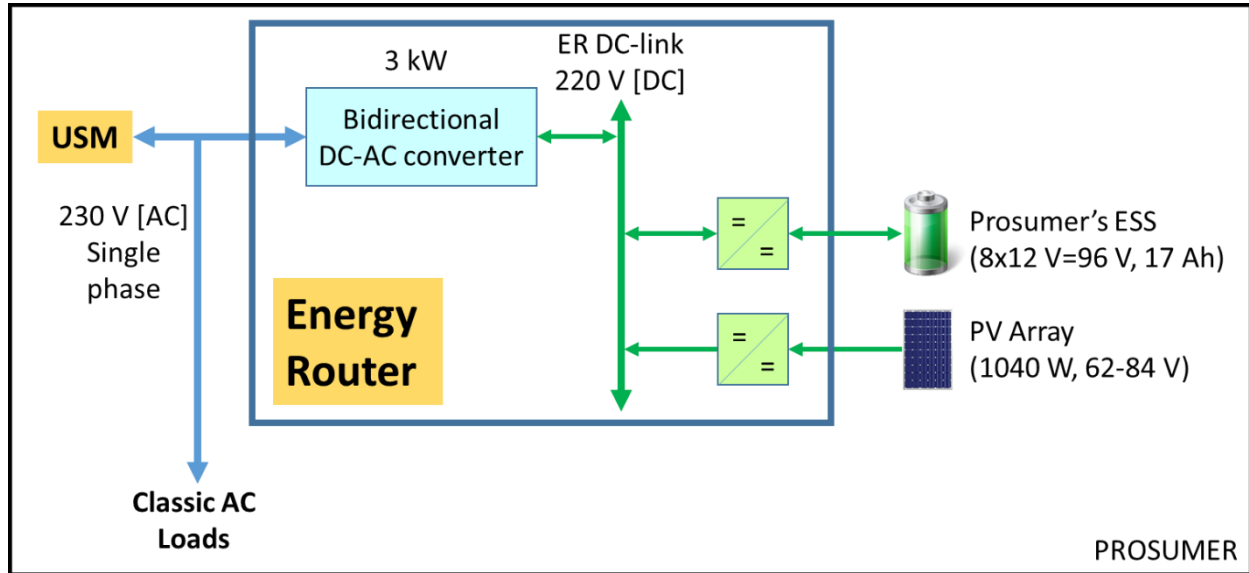


Figure 7. Single-phase ER scenario B architecture.

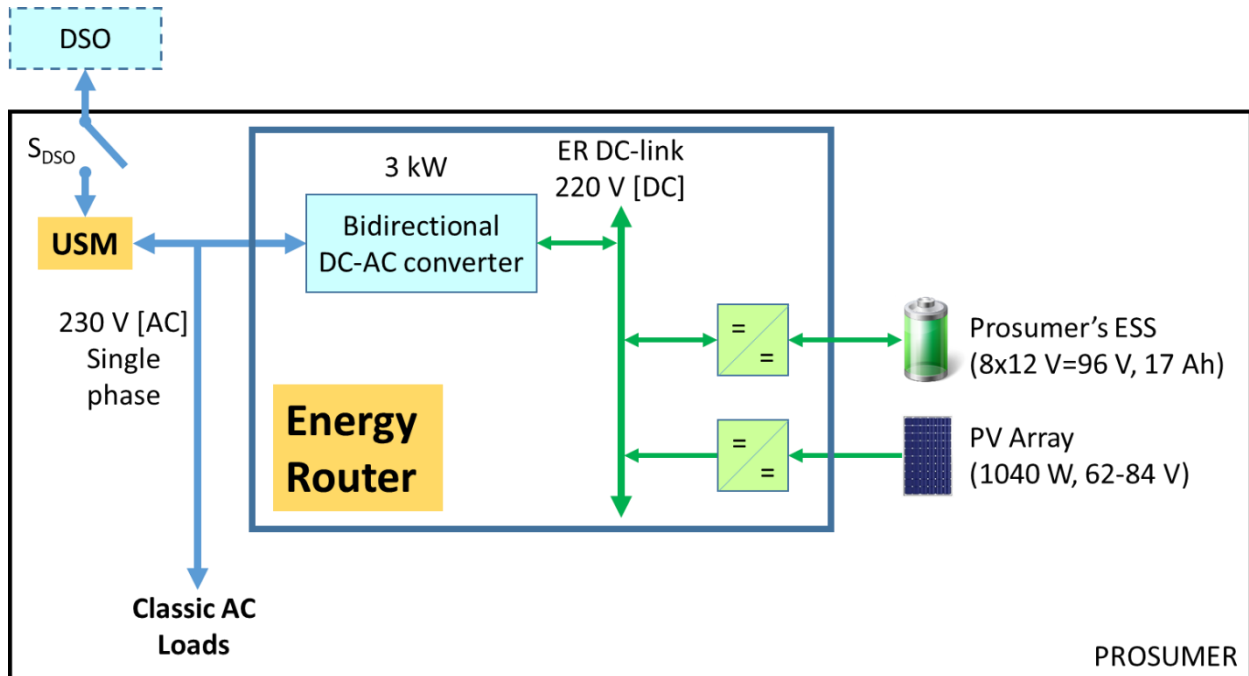


Figure 8. Single-phase ER scenario C architecture.

6 Simulation results

In order to validate the calculated parameters, as well as the main functionalities, control algorithms and modulation methods, a comprehensive simulation study was performed using PSCAD/EMTDCⁱ software. All the details and studied scenarios are given in this section. It is important to note that the required measurements are sampled to match with the control frequency rate implemented in the ER controller, making the simulation more realistic for further real implementation. The scenarios described in section 5 (A – DSO grid available, B – DSO grid unavailable (island mode), and C – black-start operation) were simulated, obtaining the results presented in the following subsections.

6.1 Scenario A1

Scenario A1 aims to validate the steady state conditions. Figure 9 shows the evolution of the reference MPP voltage. This magnitude is obtained by using the MPPT algorithm based on Perturb and Observe (P&O) with adaptive step. The PV voltage and current track the reference and nominal values with accuracy in the steady state respectively.

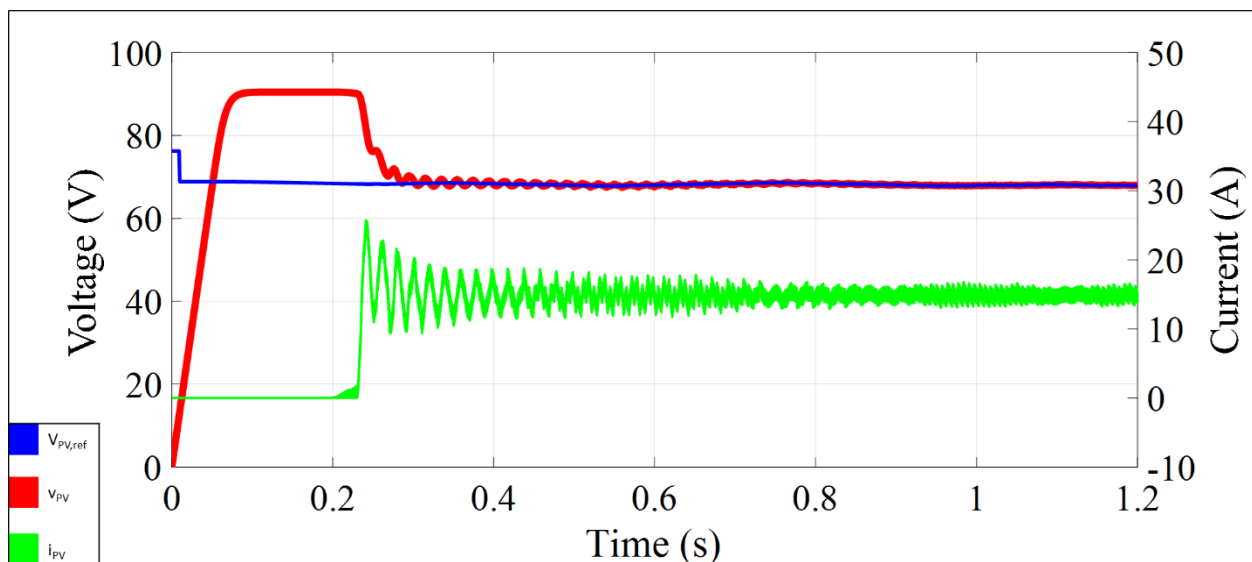


Figure 9. Scenario A1: PV voltage (v_{PV}), MPP reference voltage ($V_{PV,ref}$), and PV current (i_{PV}).

Figure 10 shows the PV current in steady state, once the MPPT is achieved. The PV current ripple demonstrates that this value is under the design limits (Table 1).

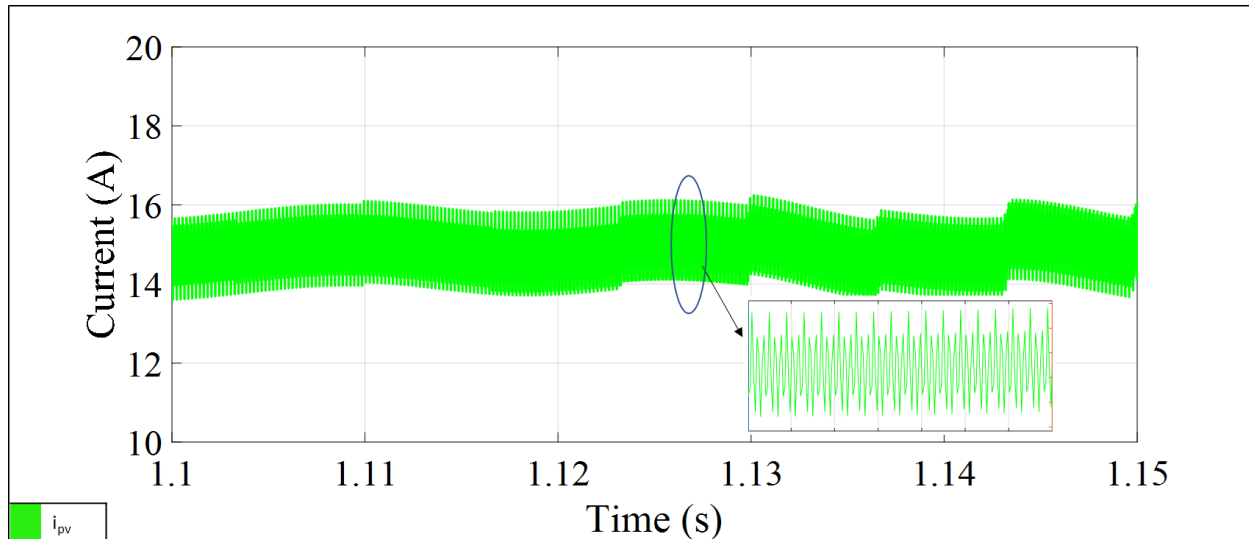


Figure 10. Scenario A1: PV current ripple (i_{pv}).

The magnitudes analysis of the DC-DC buck-boost ESS converter is shown in Figure 11. The ESS is discharged and charged with a reference power of 500 W and -500 W, respectively. The ESS SoC decreases and increases accordingly. The ESS current ripple is under the sizing specifications (8 %). The PV power and ESS powers are injected to the grid using the DC-AC ER converter. Sinusoidal currents are obtained and injected to the grid as shown in Figure 12 and Figure 13, with a setpoint of reactive power (Q) equal to 250 VAr.

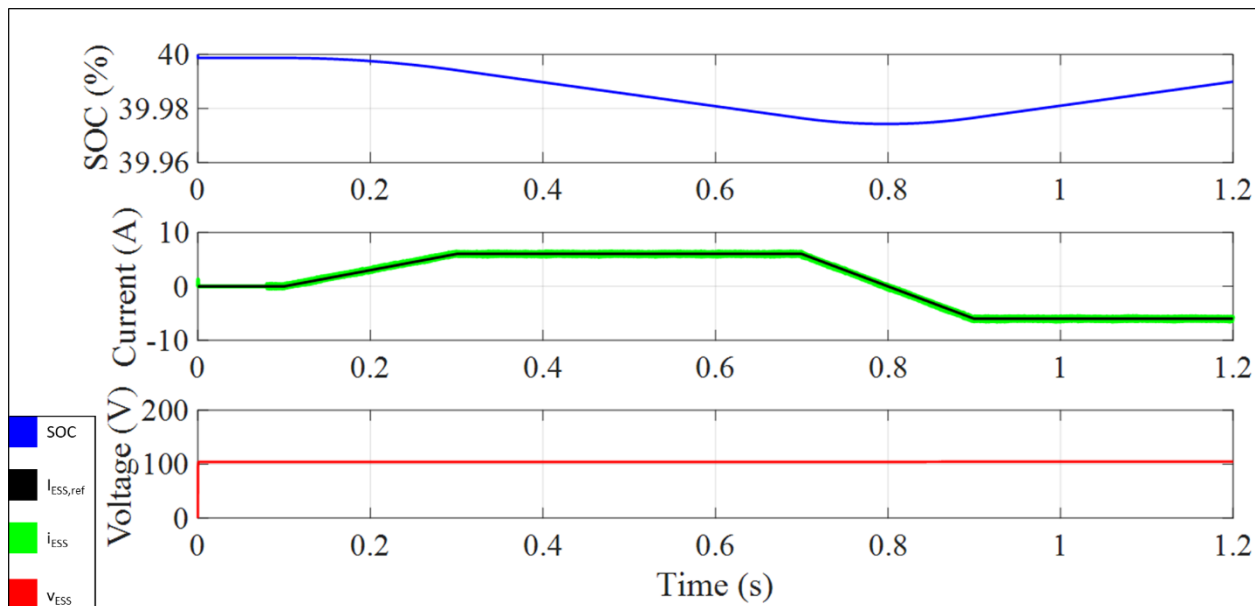


Figure 11. Scenario A1: Main magnitudes of the ESS interface: ESS SoC, ESS reference current ($i_{ESS,ref}$), ESS current (i_{ESS}), and ESS voltage (v_{ESS}).

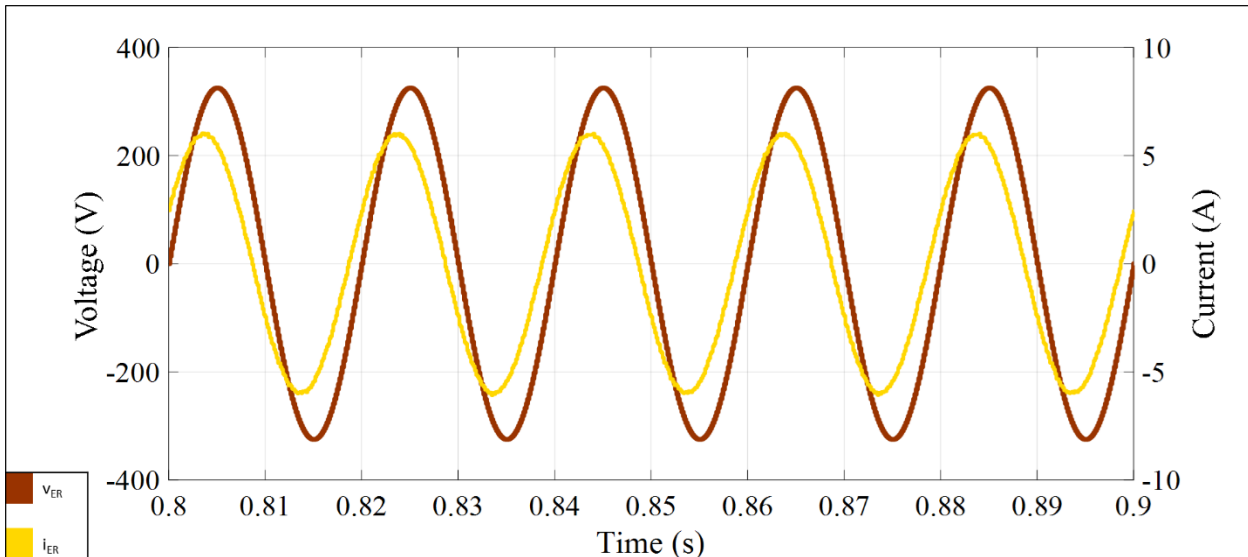


Figure 12. Scenario A1: ER voltage (v_{ER}) and ER current (i_{ER}) during ESS discharge and reactive power injection.

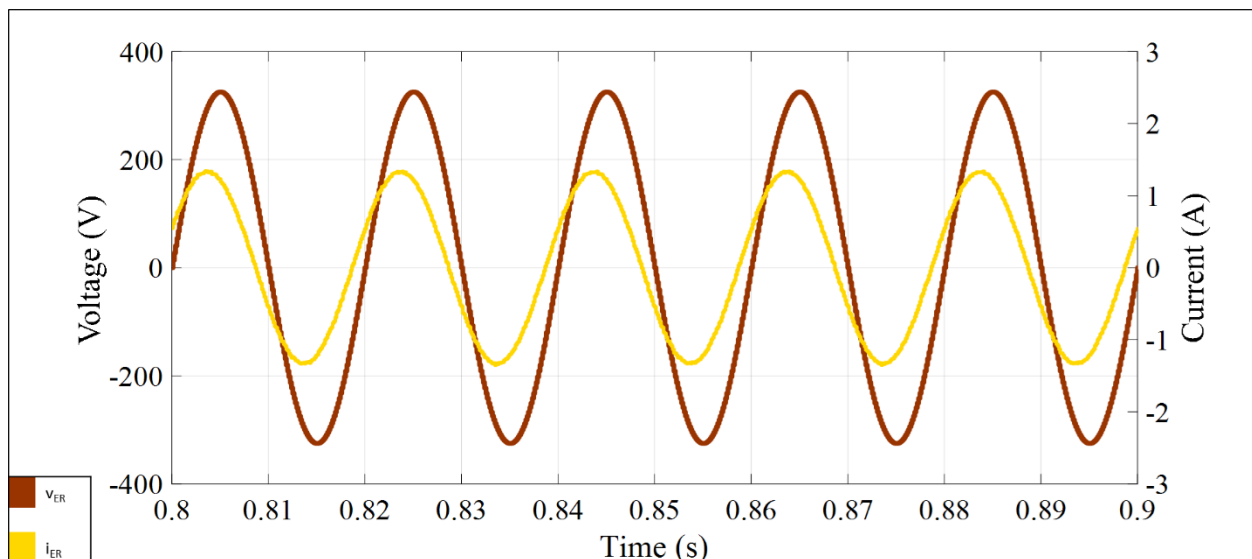


Figure 13. Scenario A1: ER voltage (v_{ER}) and ER current (i_{ER}) during ESS charge and reactive power injection.

The main DC-link voltage is also represented in Figure 14 and its value is maintained in 220 V as defined by the DC-link reference value, which demonstrates the proper operation of the DC-link control loop.

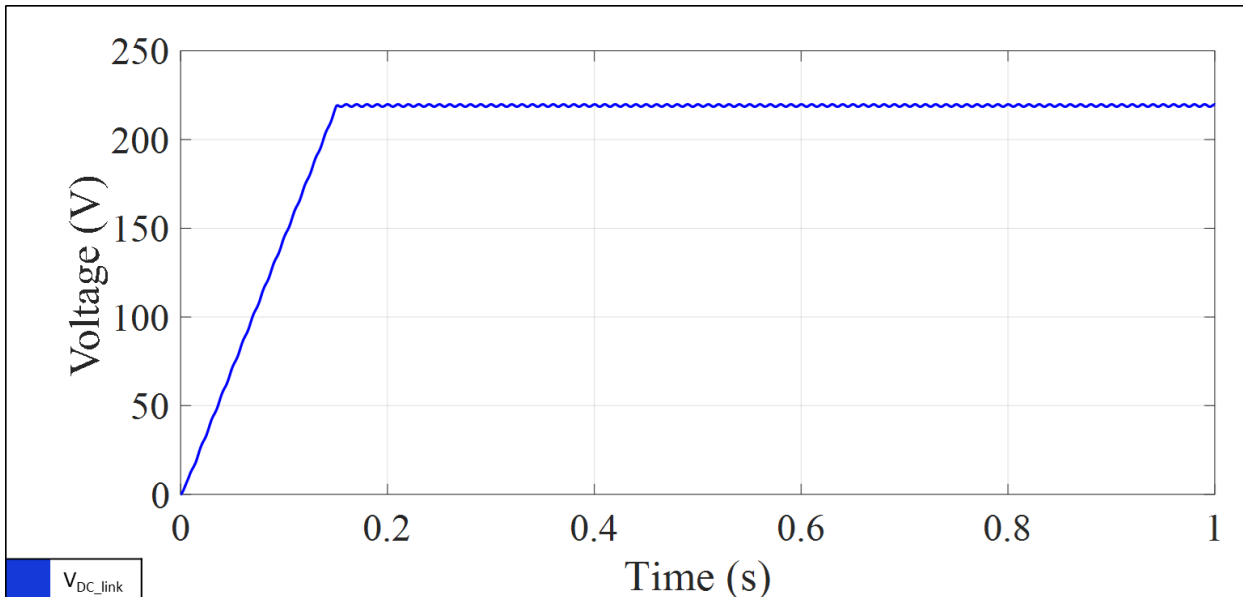


Figure 14. Scenario A1: Evolution of the main DC-link voltage (V_{DC_link}) during ER start-up.

6.2 Scenario A2

Scenario A2 considers that the PV system is operating with a reference equal to 700W (RPPT mode). Same reference power values are given to the ESS converter and reactive power injection as in scenario A1.

A similar response as in scenario A1 is provided by the PV boost converter. Figure 15 depicts the evolution of reference power point. This magnitude is obtained by using the algorithm based on P&O with adaptive step for higher accuracy. The PV voltage and current track the nominal values with accuracy in the steady state.

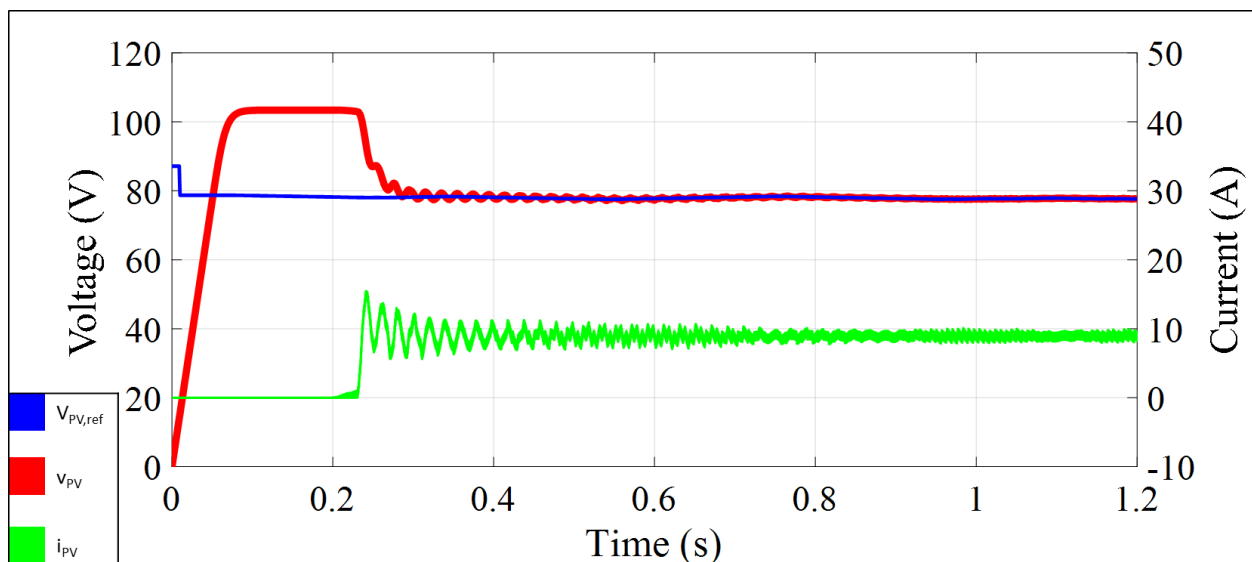


Figure 15. Scenario A2: PV voltage (v_{PV}), RPP reference voltage ($V_{PV,ref}$), and PV current (i_{PV}).

The magnitudes analysis of the DC-DC buck-boost ESS converter is shown in Figure 16. The ESS is discharged and charged with a reference power of 500 W and -500 W as in scenario A1. The ESS SoC decreases and increases accordingly. Sinusoidal currents are obtained and injected to the grid as shown in Figure 17 and Figure 18, with a setpoint of reactive power (Q) equal to 250 VAr.

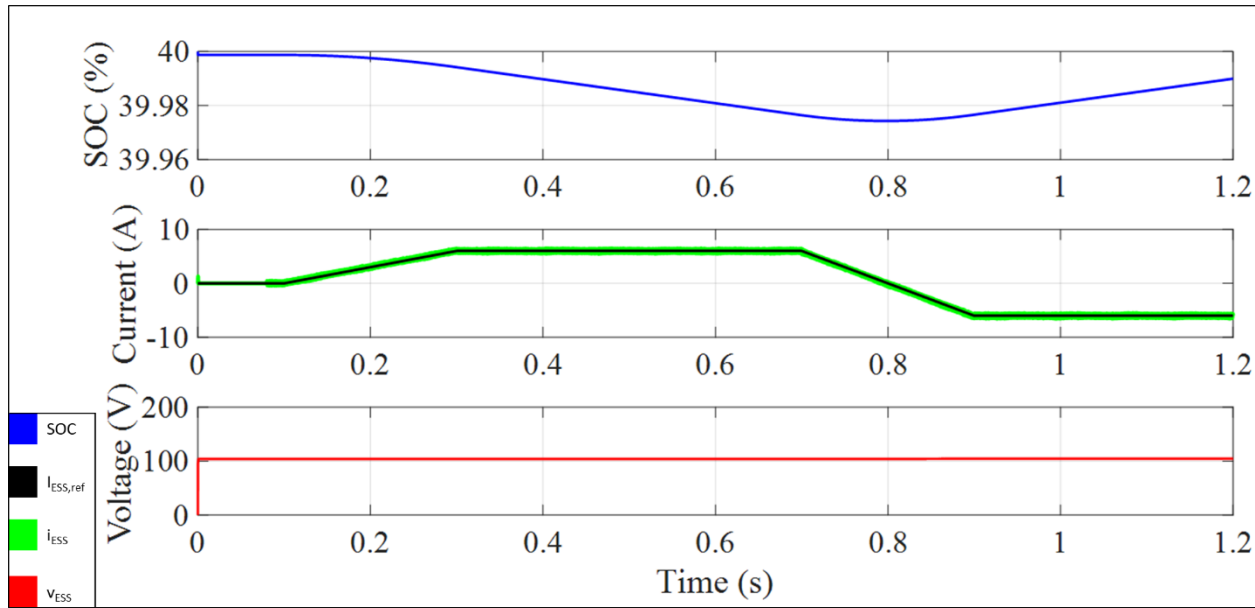


Figure 16. Scenario A2: Main magnitudes of the ESS interface: ESS SoC, ESS reference current ($i_{ESS,ref}$), ESS current (i_{ESS}), and ESS voltage (v_{ESS}).

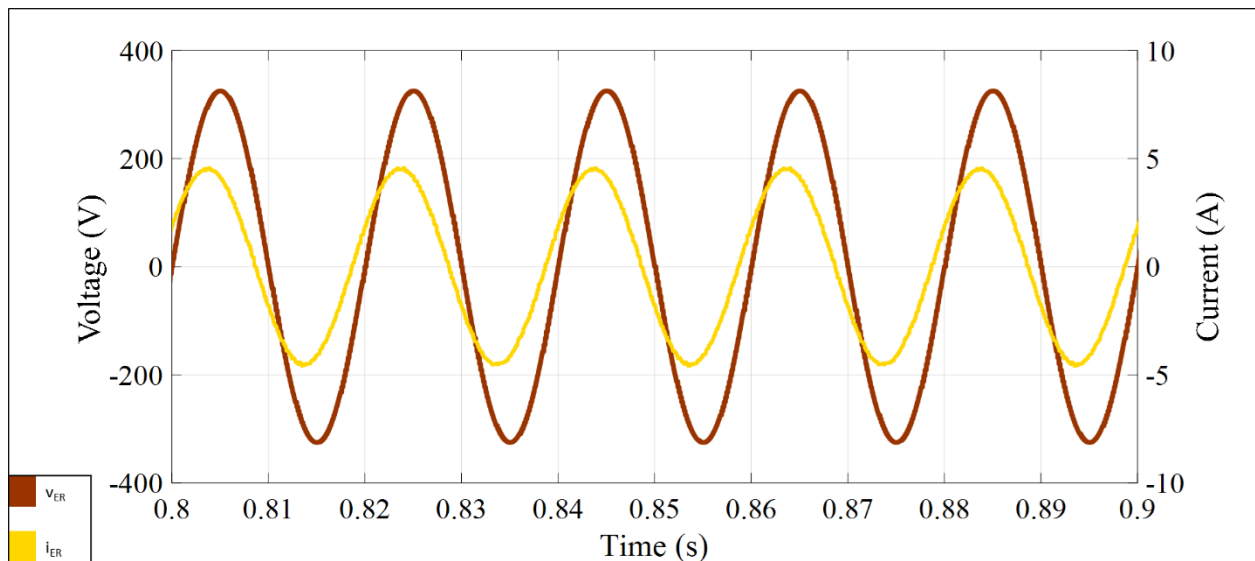


Figure 17. Scenario A2: ER voltage (v_{ER}) and ER current (i_{ER}) during ESS discharge and reactive power injection.

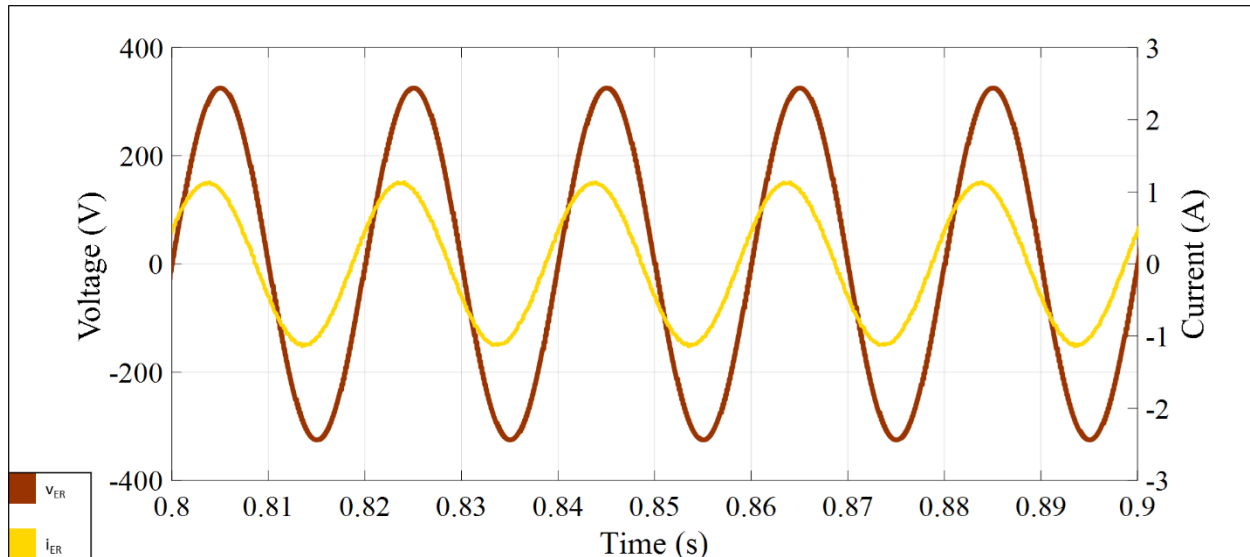


Figure 18. Scenario A2: ER voltage (v_{ER}) and ER current (i_{ER}) during ESS charge and reactive power injection.

6.3 Scenario A3

Scenario A3 demonstrates the ability of the ER when the PV is unavailable (e.g. during night). In scenario A3, the ESS is discharged and charged with a reference power of 600 W and -600 W, respectively. As shown in Figure 19, the ESS SoC decreases and increases accordingly, presenting higher slope rates than in the previous scenarios since the reference is higher in this scenario. Sinusoidal currents are obtained and injected or demanded to/from the grid, as shown in Figure 20 and Figure 21, with a setpoint of reactive power (Q) equal to 250 VAr.

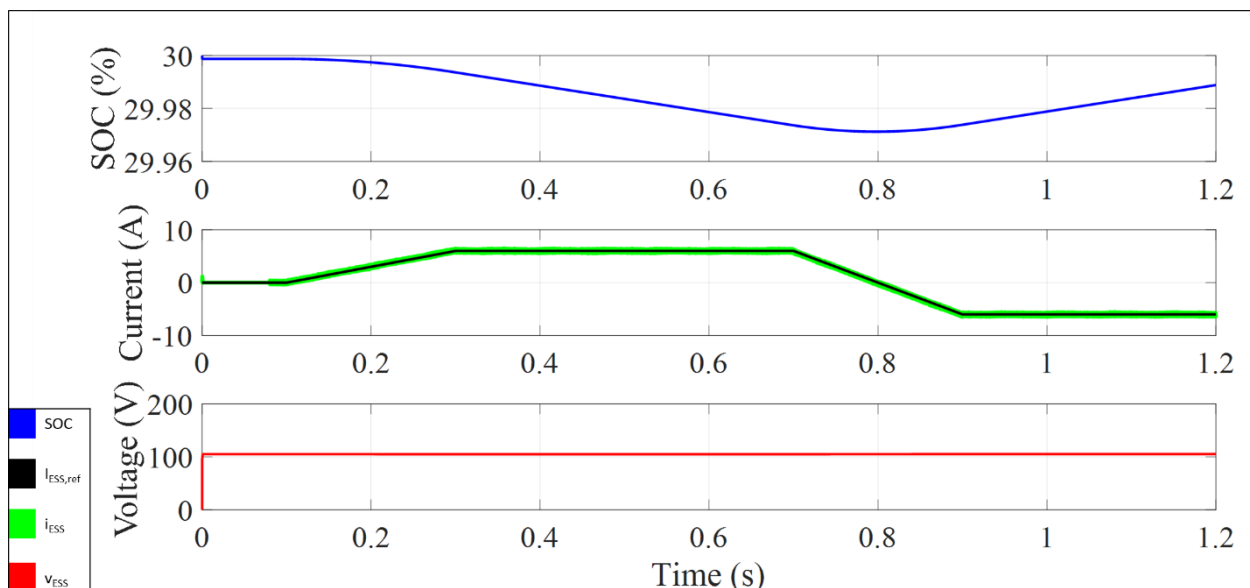


Figure 19. Scenario A3: Main magnitudes of the ESS interface: ESS SoC, ESS reference current ($i_{ESS,ref}$), ESS current (i_{ESS}), and ESS voltage (v_{ESS}).

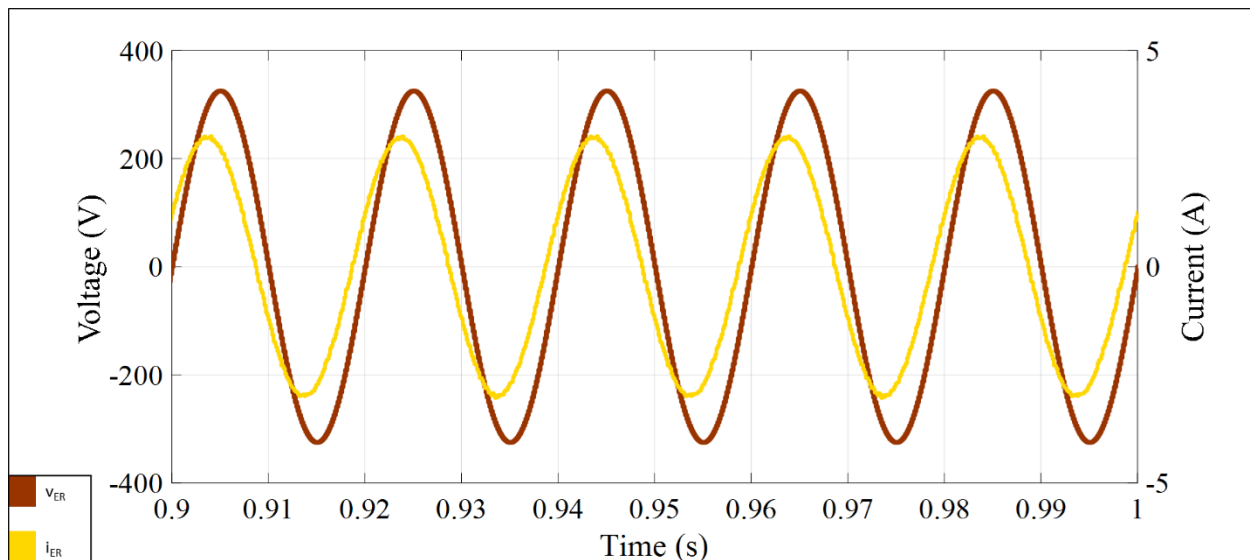


Figure 20. Scenario A3: ER voltage (v_{ER}) and ER current (i_{ER}) during ESS discharge and reactive power injection.

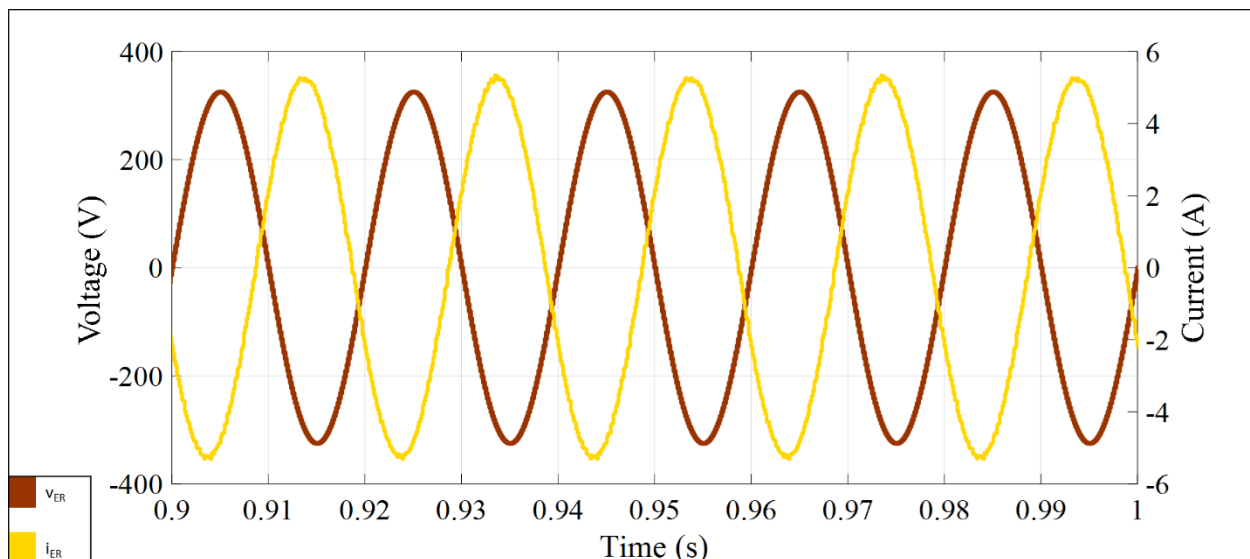


Figure 21. Scenario A3: ER voltage (v_{ER}) and ER current (i_{ER}) during ESS charge and reactive power injection.

6.4 Scenario B1

Scenario B1 illustrates the functionality required for supplying loads when the DSO grid is unavailable, meaning that the ER is operating in island mode. In this scenario, the DC-link is regulated by the ESS interface. The PV is operating in MPP condition and two different loads of 500 W and 1500 W are connected to the AC side. The ESS injects/demands the remaining power to regulate the DC-link voltage at the reference value, as shown in Figure 22 and Figure 23 respectively.

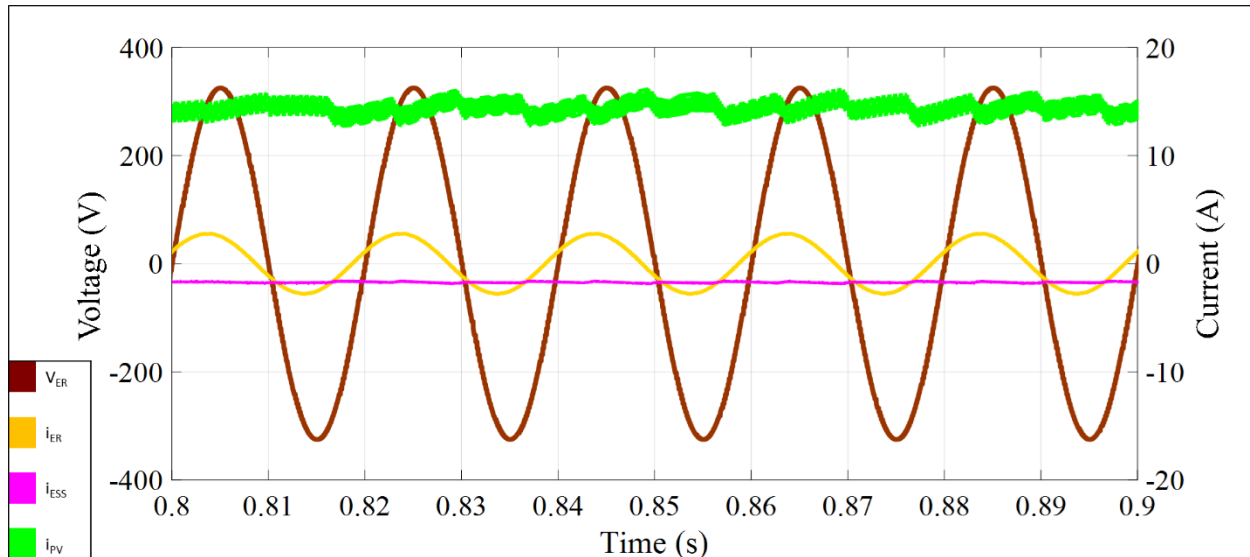


Figure 22. Scenario B1: ER voltage (v_{ER}), ER current (i_{ER}), ESS current (i_{ESS}), and PV current (i_{PV}) with a 500 W AC load.

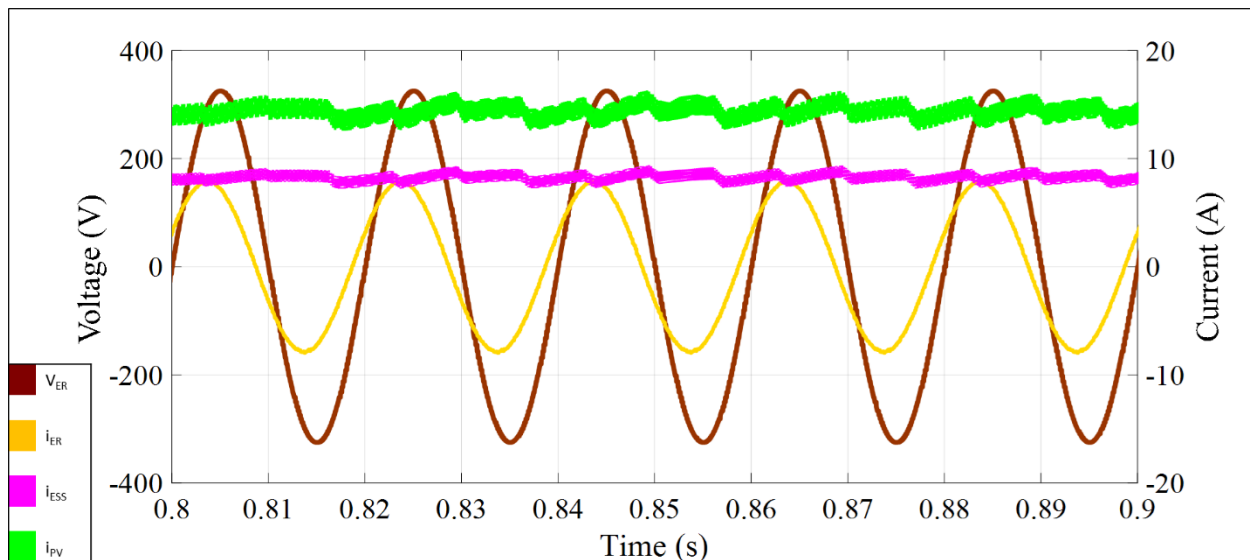


Figure 23. Scenario B1: ER voltage (v_{ER}), ER current (i_{ER}), ESS current (i_{ESS}), and PV current (i_{PV}) with a 1500 W AC load.

6.5 Scenario B2

Scenario B2 illustrates the functionality required for supplying loads when the DSO grid is unavailable, the PV is operating in RPP conditions and two different loads of 500 W and 1500 W are connected to the AC side. The ESS injects/demands the remaining power to regulate the DC-link voltage at the reference value. These conditions are illustrated in Figure 24 and Figure 25 respectively.

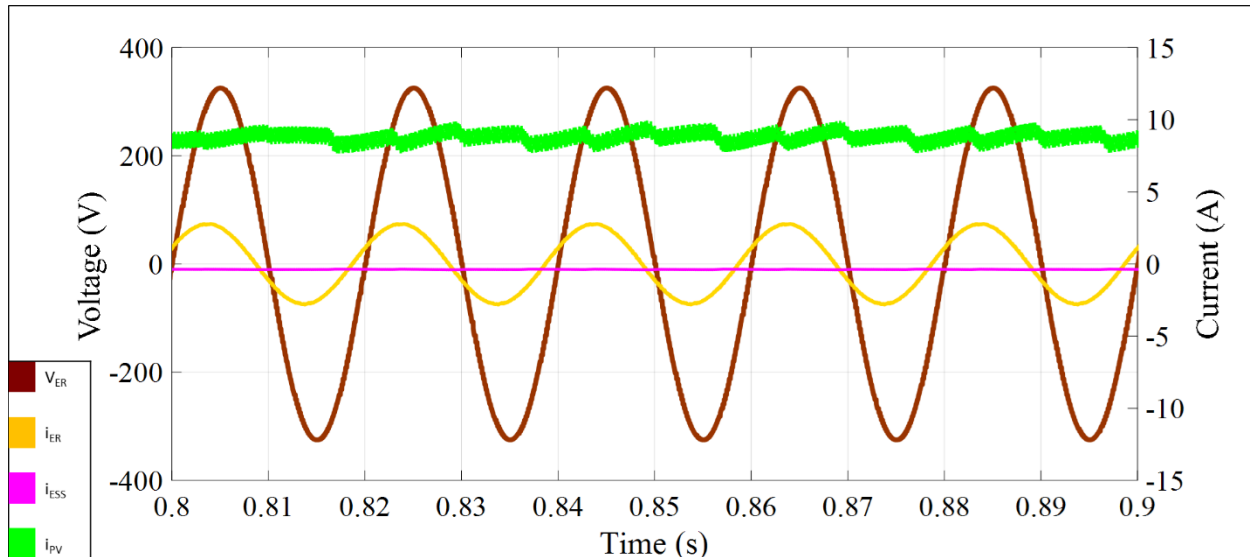


Figure 24. Scenario B2: ER voltage (v_{ER}), ER current (i_{ER}), ESS current (i_{ESS}), and PV current (i_{PV}) with a 500 W AC load.

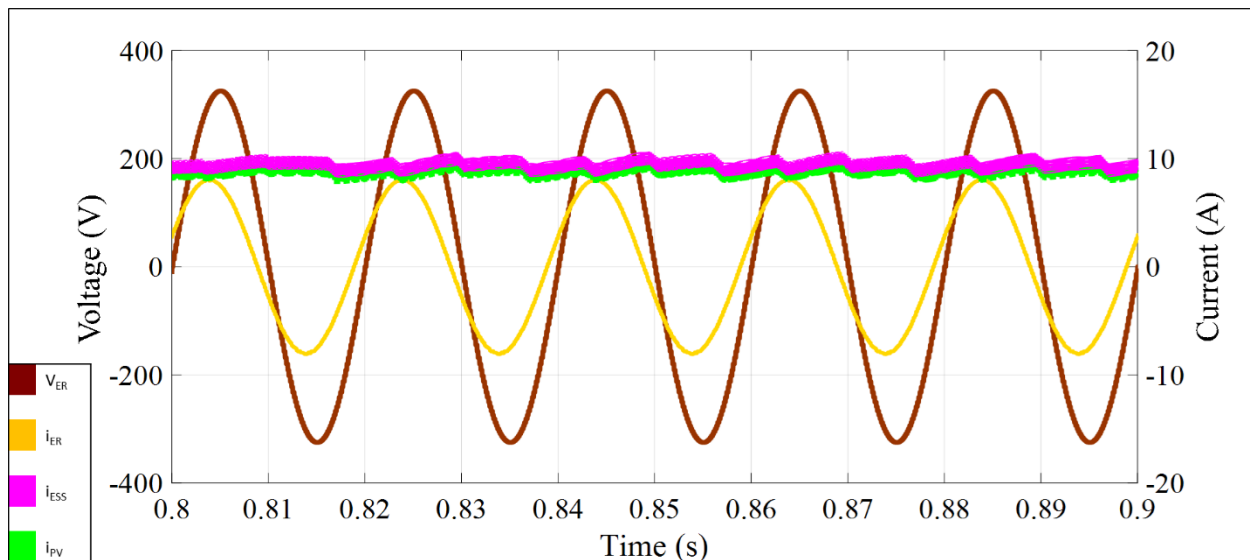


Figure 25. Scenario B2: ER voltage (v_{ER}), ER current (i_{ER}), ESS current (i_{ESS}), and PV current (i_{PV}) with a 1500 W AC load.

6.6 Scenario C

Scenario C demonstrates the ability of the ER to perform a black-start, according to the following sequence. Firstly, the ER is working in island mode regulating the output voltage at the nominal value, i.e. Voltage Control (VC) mode. In second 2, a new load is connected to the island, and the regulation of the nominal voltage is assured. In second 5 the grid is connected to the system, maintaining the reference current as constant (i.e. Current Control (CC) mode), using an internal reference clock signal pulsation. Finally, in second 5.1, the ER operates in synchronism with the grid. It can observe that undesired out of range transients' values are obtained, assuring a safe and proper operation of the ER. The aforementioned sequence can be observed in Figure 26.

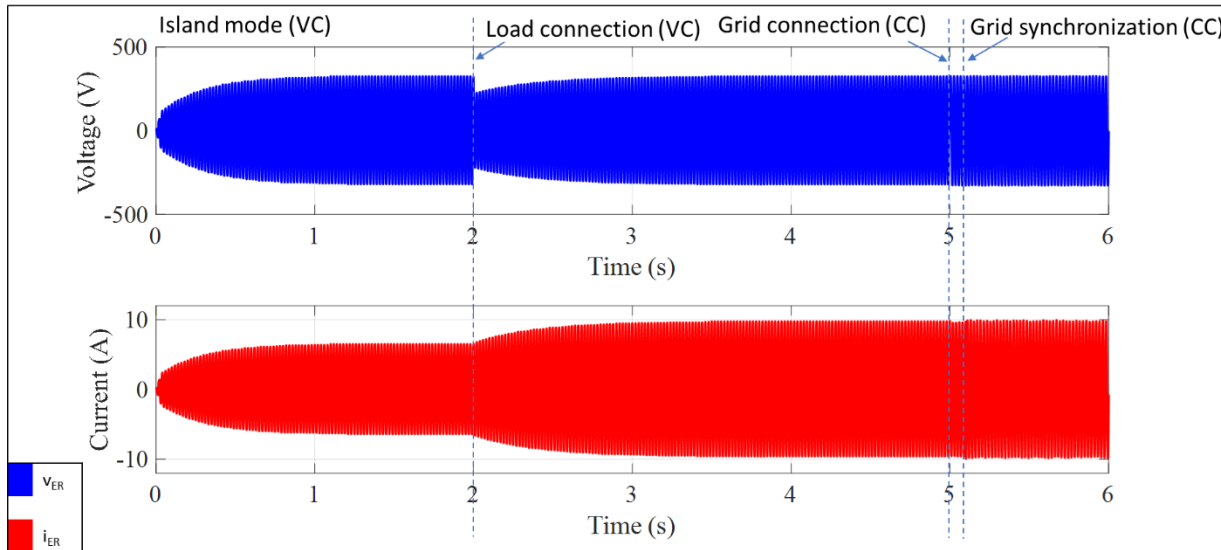


Figure 26. Scenario C: Evolution of the ER voltage (v_{ER}) and ER current (i_{ER}) during black-start operation.

Details of the voltage and current waveforms when the grid is connected, and the ER synchronizes with the grid is represented in Figure 27.

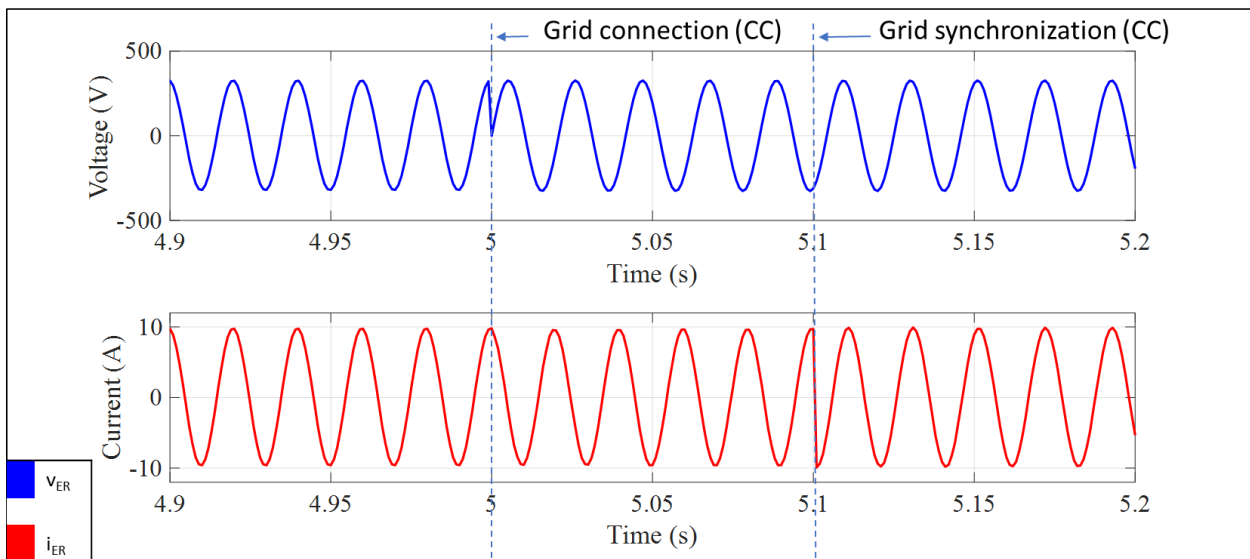


Figure 27. Scenario C: Detailed evolution of the ER voltage (v_{ER}) and ER current (i_{ER}) during black-start operation.

As last part of the simulation study, the transient response under an active power step and reactive power step is analysed. Figure 28 shows the evolution of the injected current when the reference active power (in second 0.23) and the reference reactive power (in second 0.53) are suddenly changed by a step. The system tracks the new reference values with accuracy, demonstrating the good performance of the current controller.

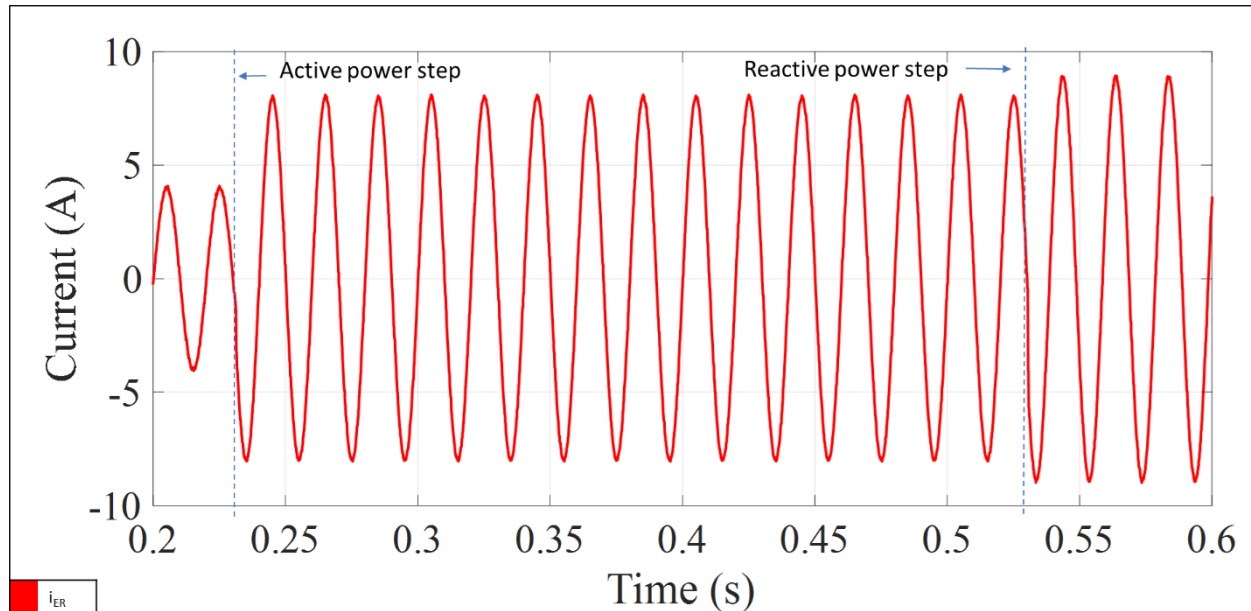


Figure 28. Scenario C: ER current (i_{ER}) during active and reactive power steps.

7 Laboratory tests

The assembled prototype based on the aforementioned specifications and sizing was tested in different scenarios to validate the proper performance.

The photovoltaic array is emulated by means of the Chroma solar array simulator 62000H-S, using the PV panels specifications available on the test site (PV panel KC130GHT-2). The ESS is composed by a serial connection of 8 lead-acid type batteries. The main parameters of the experimental scenarios are described in Table 8.

Table 8. Laboratory specifications of the experimental setup.

PV, ESS and grid	Parameter	Value
PV parameters per panel in standard conditions (array is composed by 7 panels in serial)	Open circuit voltage (V_{oc})	21.90 V
	Short-circuit current (I_{sc})	8.02 A
	Voltage at maximum power (V_{MPP})	17.60 V
	Current at maximum power (I_{MPP})	7.39 A
ESS parameters per single battery (ESS is composed by 8 batteries connected in serial)	Battery voltage	12 V
	Battery capacity	17 Ah
DSO grid	Grid voltage	230 V _{rms}

The scenarios described in section 5 (A – DSO grid available, B – DSO grid unavailable (island mode), and C – black-start operation) were tested in laboratory, obtaining the results shown in the following subsections.

7.1 Scenario A1

The first test aims to validate the proper operation of the full prototype in terms of active power balance between the PV, ESS and the grid. The main waveforms are represented in Figure 29. i_{PV} shows a good tracking of the current at maximum power (I_{MPP}) with its current ripple within the limit. The ESS current (i_{ESS}) is also depicted when the ESS is discharged with a $P_{ESS,ref}$ equal to 500 W. The resulting power is injected into the grid. ER voltage (v_{ER}) and ER current (i_{ER}) present a slight shift angle since the reactive power is set to 250 VAr.

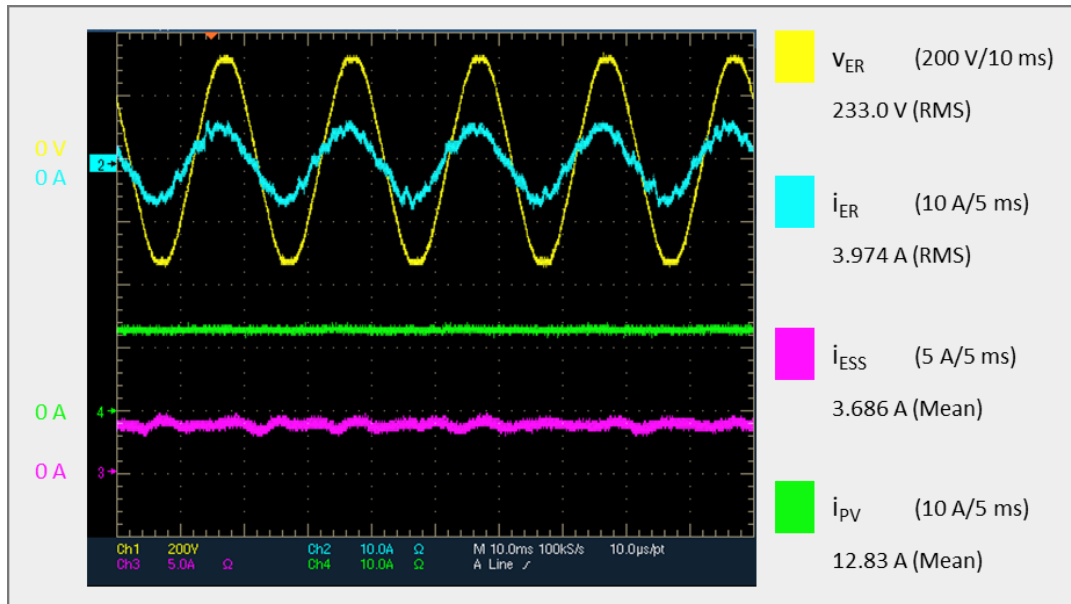


Figure 29. Scenario A1: ER voltage (v_{ER}), ER current, and PV current (i_{PV}).

The same tests but with a charging ESS reference (-500 W) is represented in Figure 30. As the MPPT is higher than the charging reference, the ER is still injecting power to the grid.

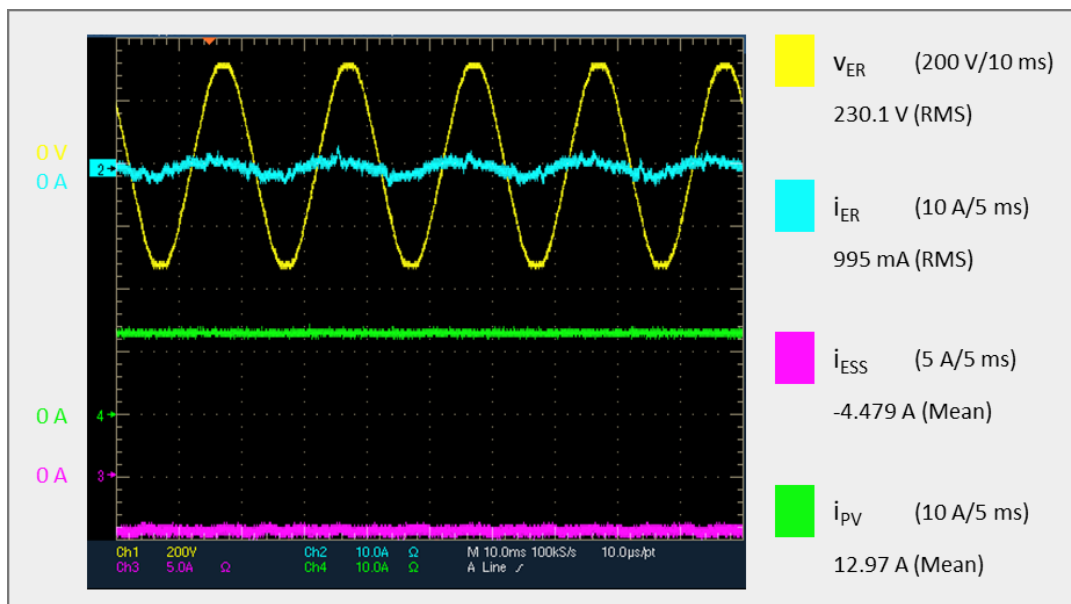


Figure 30. Scenario A1: ER voltage (v_{ER}), ER current (i_{ER}), ESS current (i_{ESS}), and PV current (i_{PV}).

7.2 Scenario A2

In this scenario the PV system is operating in RPPT mode with a setpoint of 700 W and the ESS power reference is set as 500 W. The main waveforms are represented in Figure 31. i_{PV} shows a good tracking of the current at the reference power. The ESS current (i_{ESS}) is also depicted when the ESS is discharged. The resulting power is injected into the grid. ER voltage (v_{ER}) and ER current (i_{ER}) present a slight shift angle since the reactive power is set to 250 VAr as in previous scenario.

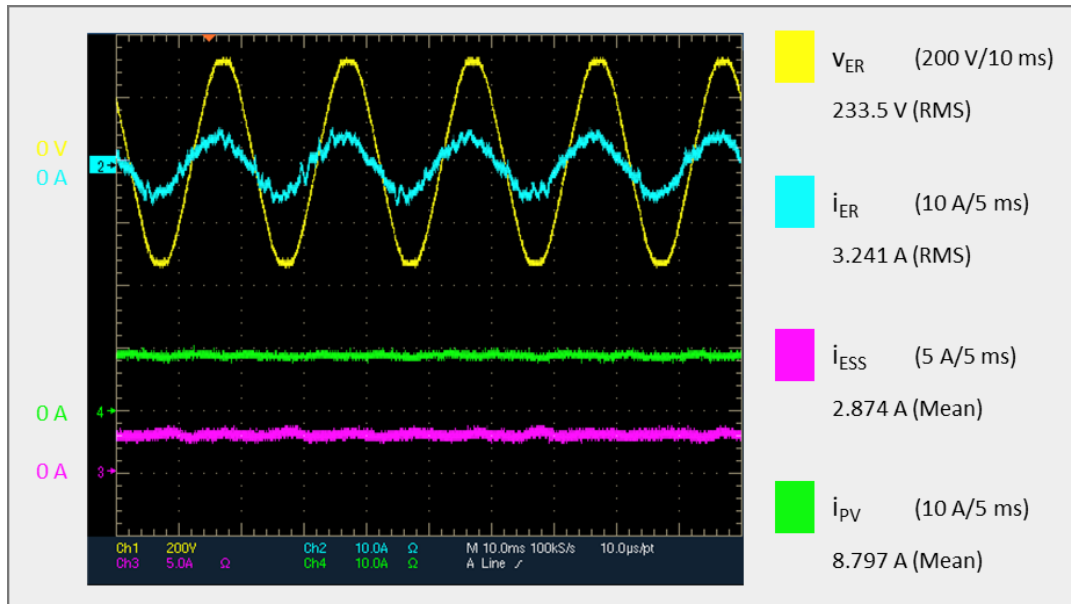


Figure 31. Scenario A2: ER voltage (v_{ER}), ER current (i_{ER}), ESS current (i_{ESS}), and PV current (i_{PV}).

The same test but with a charging ESS reference (-500 W) is represented in Figure 40. As the RPPT is higher than the ESS charging reference, the ER is still injecting power to the grid.

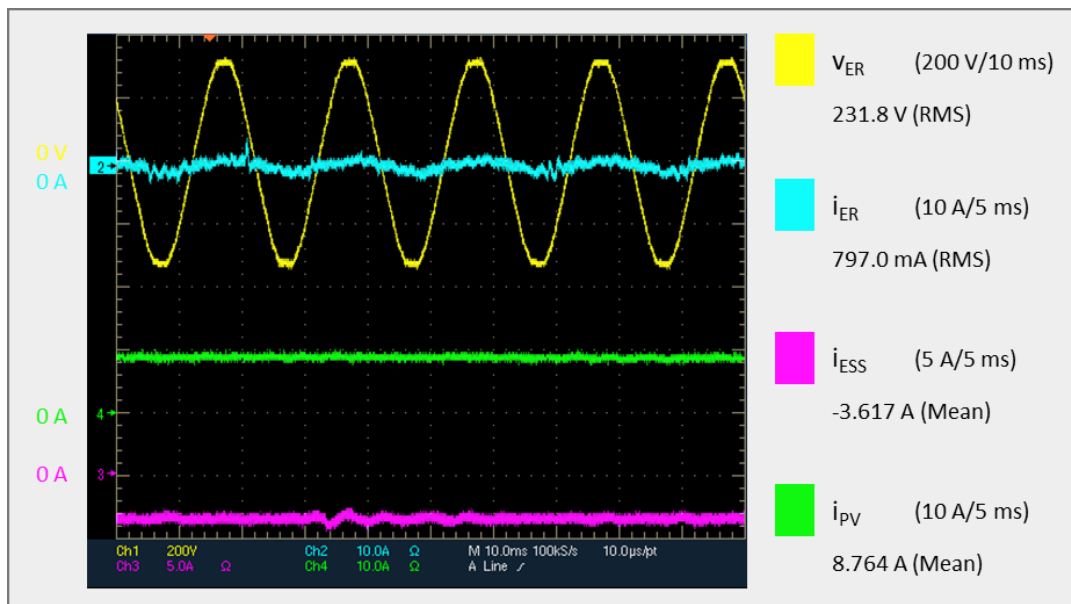


Figure 32. Scenario A2: ER voltage (v_{ER}), ER current (i_{ER}), ESS current (i_{ESS}), and PV current (i_{PV}).

7.3 Scenario A3

This scenario demonstrates experimentally the performance of the ER when the PV is OFF (e.g. during the night). In this scenario, the ESS is discharged and charged with a reference power of 600 W and -600 W (Figure 33 and Figure 34 respectively). Setpoint of reactive power Q was equal to 250 VAr.

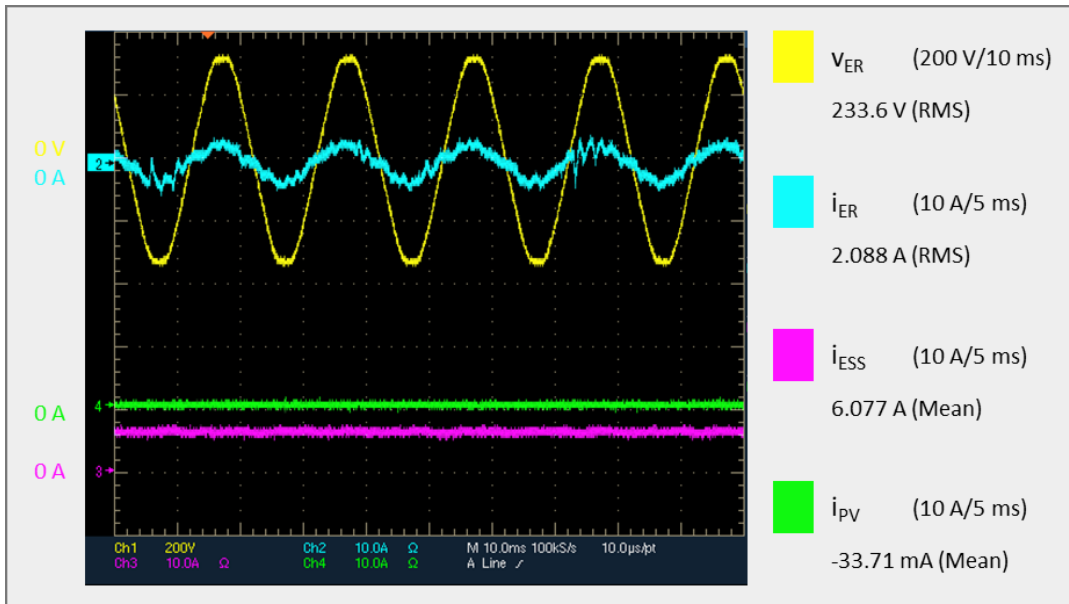


Figure 33. Scenario A3: ER voltage (v_{ER}), ER current (i_{ER}), ESS current (i_{ESS}), and PV current (i_{PV}).

As in scenario A2 in which the ESS must be charged, the demanded current is in opposite phase with the ER voltage.

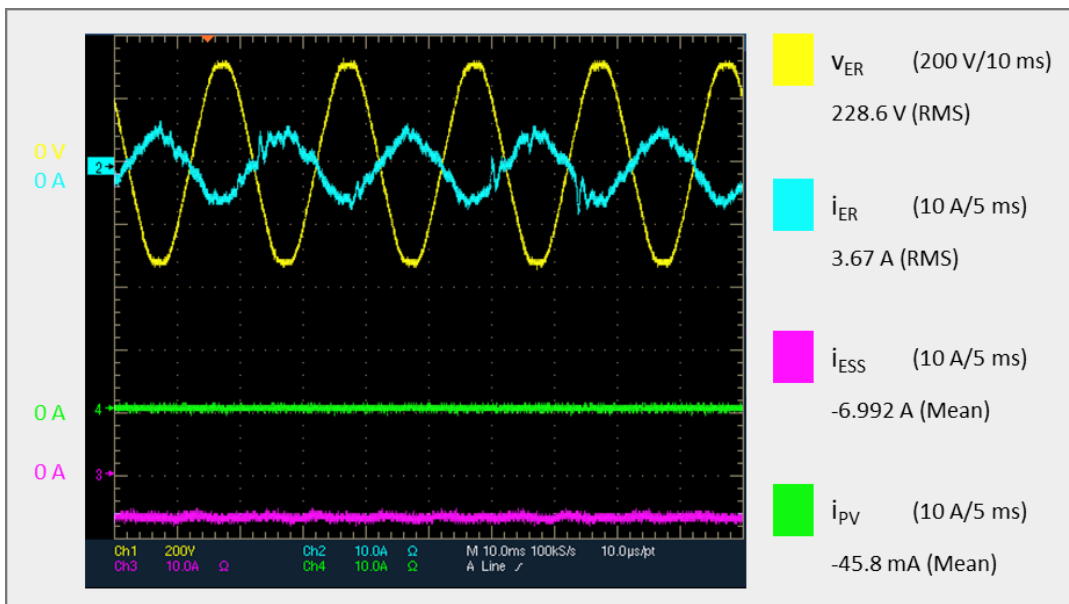


Figure 34. Scenario A3: ER voltage (v_{ER}), ER current (i_{ER}), ESS current (i_{ESS}), and PV current (i_{PV}).

7.4 Scenario B1

This scenario illustrates the ER operating in island mode. In this scenario, the DC-link voltage is regulated by the ESS interface. The PV is operating in MPP condition and two different loads of 500 W and 1000 W are connected to the AC side. The ESS injects/demands the remaining power to regulate the DC-link voltage at the reference value. These tests are illustrated in Figure 35 and Figure 36 respectively. During the operation with the 500 W load, the ESS charges, as P_{MPP} is higher than the load. By connecting the 1500 W load, the ESS discharges.

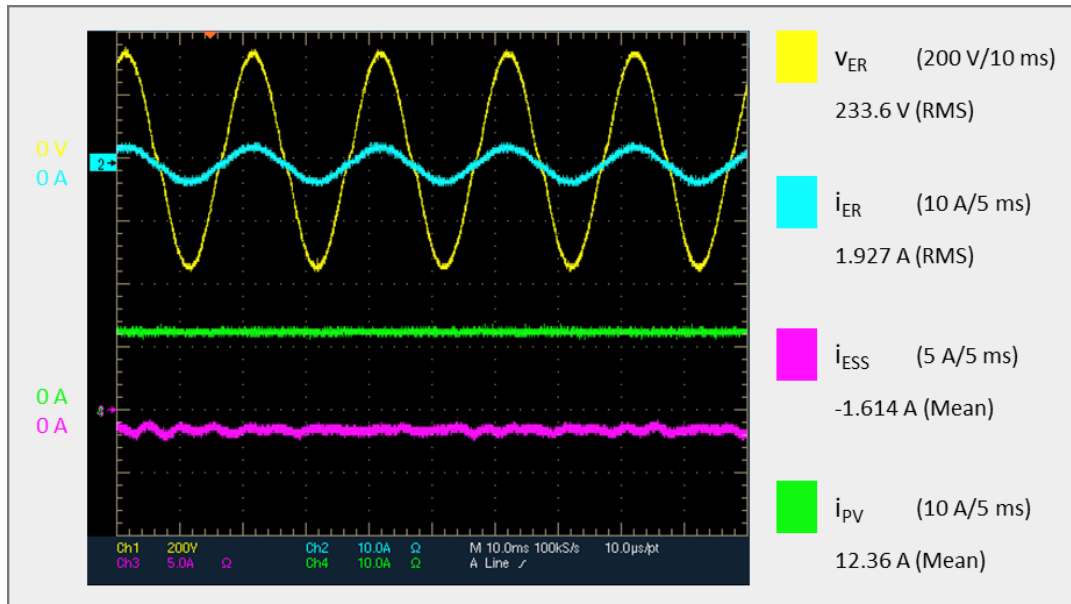


Figure 35. Scenario B1: ER voltage (v_{ER}), ER current (i_{ER}), ESS current (i_{ESS}), and PV current (i_{PV}) with 500 W load.

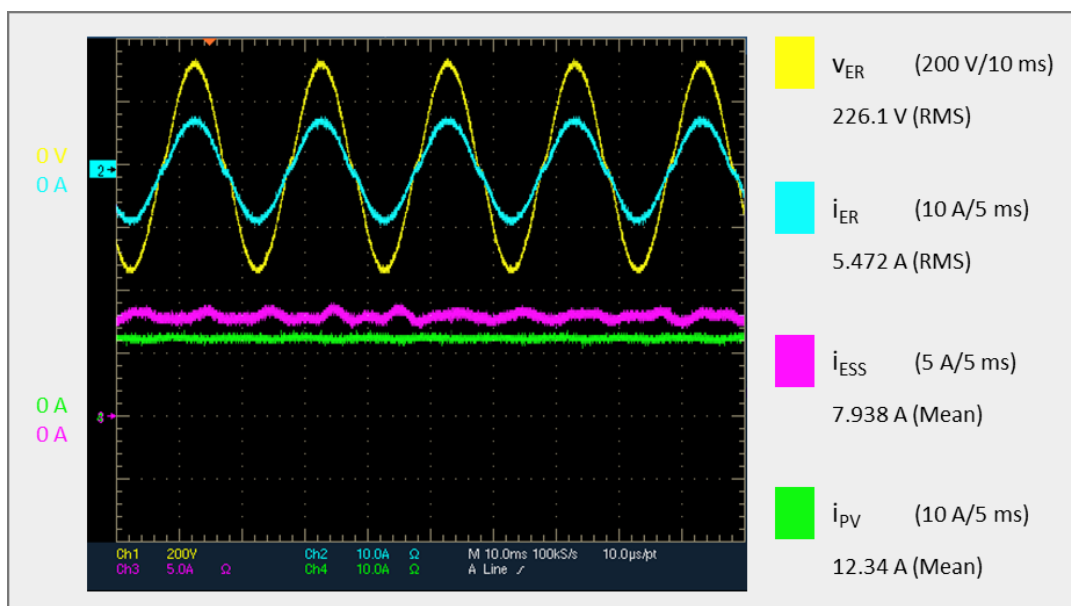


Figure 36. Scenario B1: ER voltage (v_{ER}), ER current (i_{ER}), ESS current (i_{ESS}), and PV current (i_{PV}) with 1500 W load.

7.5 Scenario B2

This scenario illustrates the ER operating in island mode. In this scenario, the DC-link is regulated by the ESS interface. The PV is operating at RPP conditions with 600 W as setpoint, and two different loads of 500 W and 1000 W are connected to the AC side. The ESS injects/demands the remaining power to regulate the DC-link voltage at the reference value. These tests are illustrated in Figure 37 and Figure 38 respectively. During the operation with the 500 W load, the ESS charges, as P_{MPP} is higher than the load. By connecting the 1500 W load, the ESS discharges.

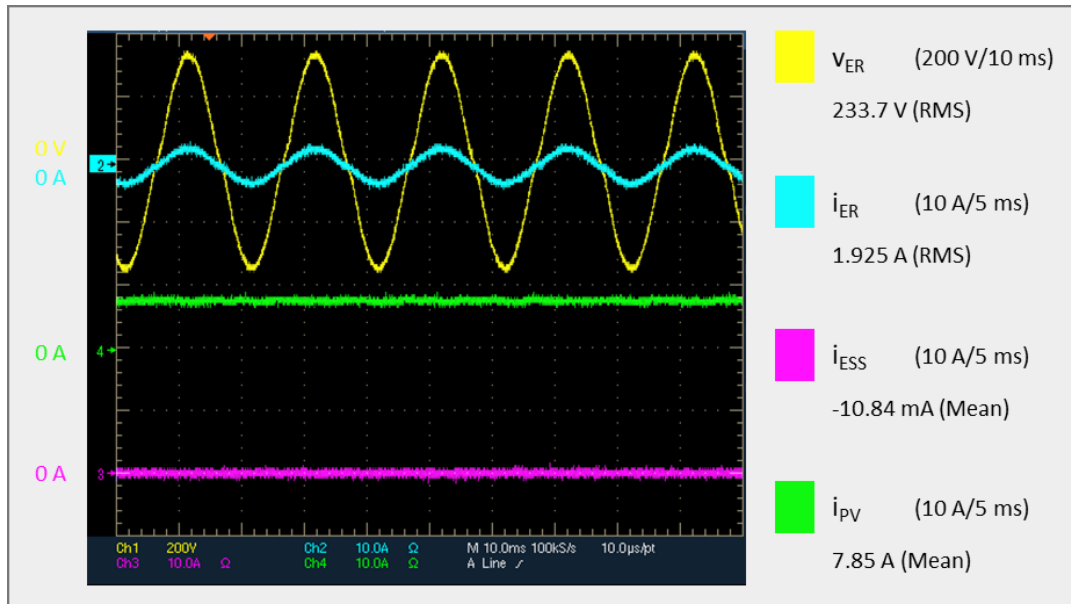


Figure 37. Scenario B2: ER voltage (v_{ER}), ER current (i_{ER}), ESS current (i_{ESS}), and PV current (i_{PV}) with 500 W load.

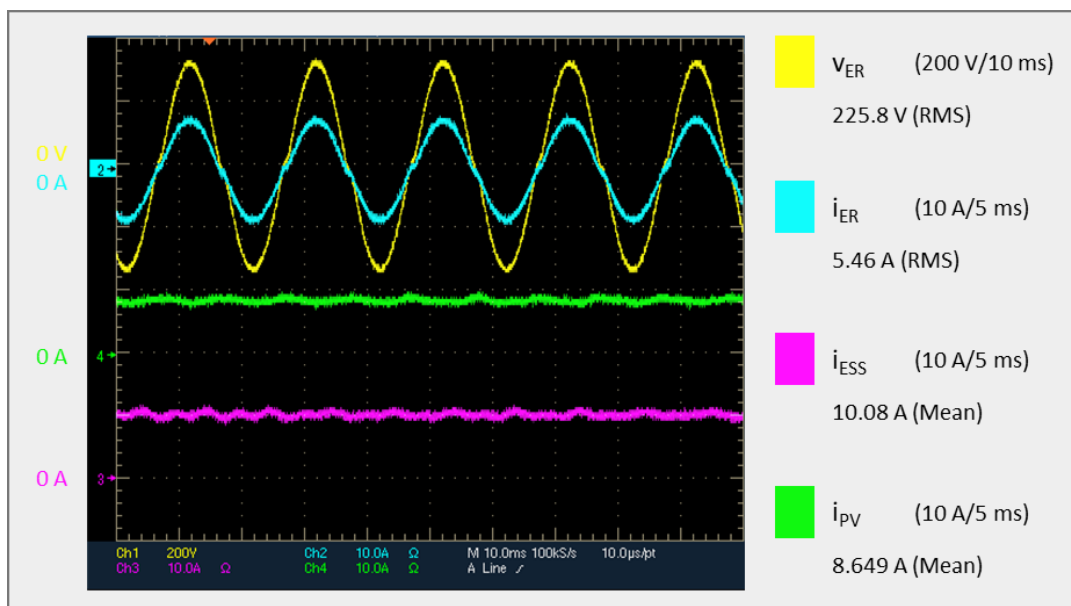


Figure 38. Scenario B2: ER voltage (v_{ER}), ER current (i_{ER}), ESS current (i_{ESS}), and PV current (i_{PV}) with 1500 W load.

7.6 Scenario C

Scenario C demonstrates experimentally the ability of the ER to perform a black-start. The sequence of events is as follows: Firstly, in (22:40:17), the ER starts working in island mode, regulating the output voltage at the nominal value (230 V_{rms}), with the PV working in MPP and the ESS converter controlling the DC-link voltage. During this process the voltage frequency is obtained from an internal clock signal. In (22:40:33) a load is connected to the island and the regulation of the nominal voltage is assured. Once the DSO grid is available, the ER receives this information, and also the grid phase and frequency from the measurement system. Then, the ER regulates the output voltage synchronised with the grid. In (22:41:05) the ER connects to the DSO grid. However, until (22:41:29), the ER is still injecting some active power to the DSO grid and absorbing reactive

power in order to restore the nominal voltage. After this time, the DC-AC ER converter is turned off. This sequence of events is shown in Figure 39.

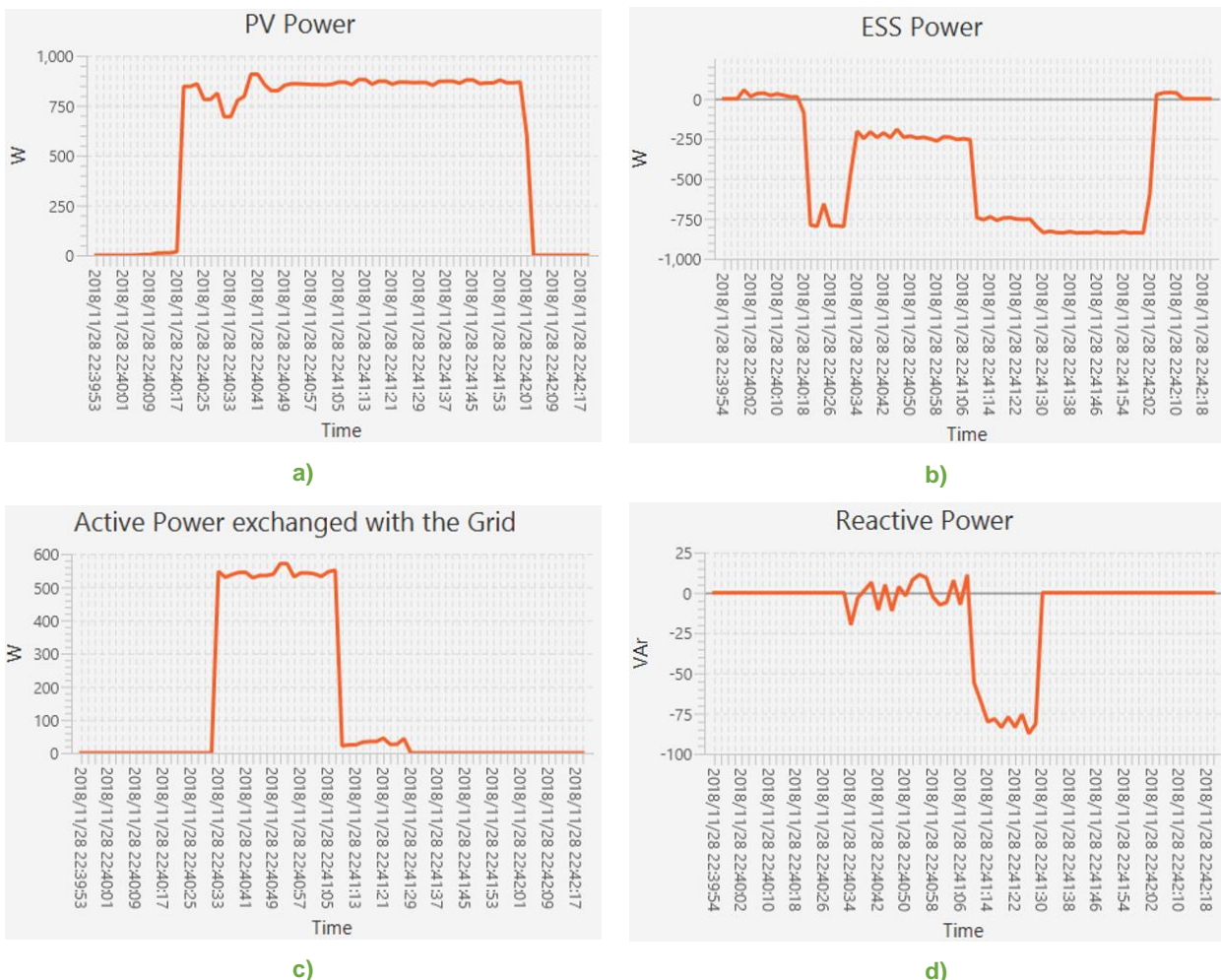


Figure 39. Scenario C: Transient responses of the ER subsystems: a) PV power, b) Power exchanged with the ESS, c) Active power exchanged with the grid, and d) Reactive power.

8 On-site tests

The single-phase ER was deployed during the week of December 11th to 14th 2018, and tested during the last two days. Unfortunately, due to the cloudy weather conditions (Figure 40), it was not possible to extract more than 80 W of the PV system during the on-site tests.

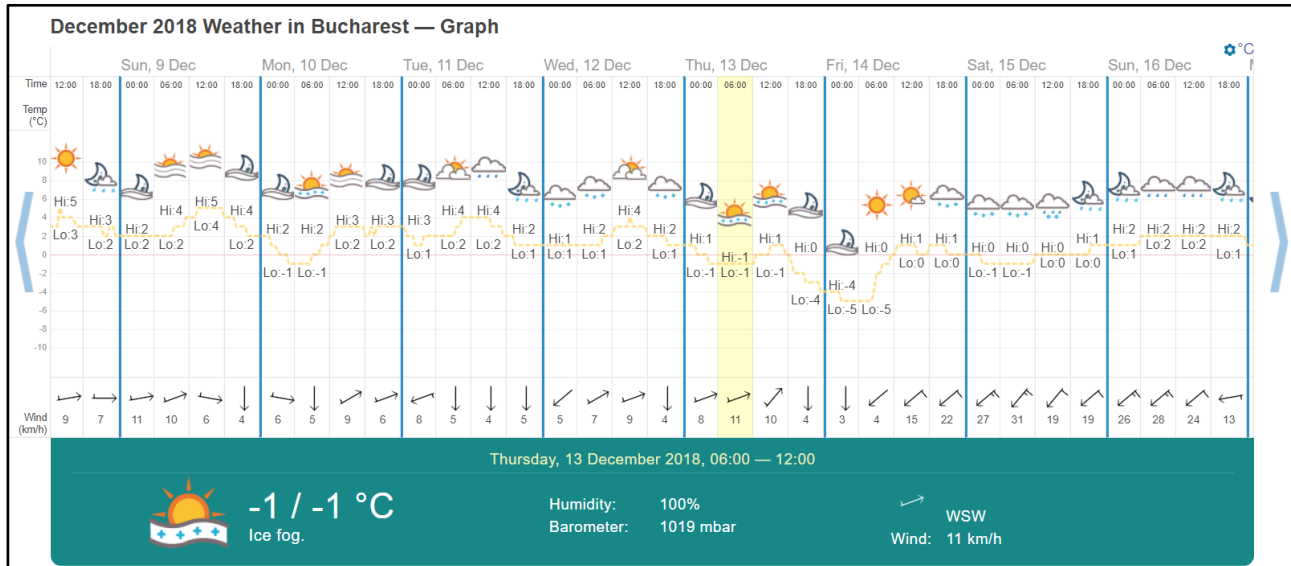


Figure 40. Weather conditions during the last on-site test days (December 11th to 14th, 2018)^v.

Despite that, the scenarios described in section 5 (A – DSO grid available, B – DSO grid unavailable (island mode), and C – black-start operation) were tested at UPB's premises, obtaining the results depicted in the following subsections. In scenario A1 and scenario B1 it was still used the MPPT algorithm, extracting between 50-75 W, and in scenario A2 and scenario B2 it was used the RPPT algorithm with 50 W and 65 W PV references, respectively.

8.1 Scenario A1

The first test aims to validate the proper operation of the ER prototype in terms of active power balance between the PV, ESS and the grid. The main waveforms are represented in Figure 41. i_{PV} shows a good tracking of the current at maximum power (I_{MPP}) with its current ripple within the limit. The ESS current (i_{ESS}) is also depicted when the ESS is discharged with a $P_{ESS,ref}$ equal to 500 W. ER voltage (v_{ER}) and ER current (i_{ER}) present a slight shift angle since the reactive power is set to 300 VAr.

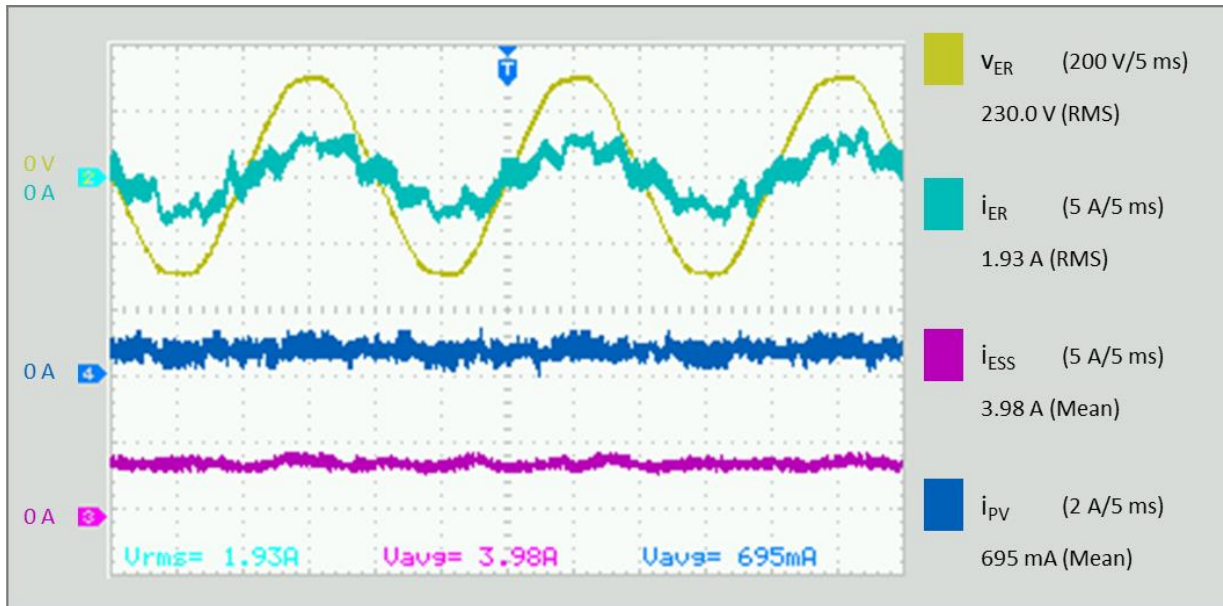


Figure 41. Scenario A1: ER voltage (v_{ER}), ER current (i_{ER}), ESS current (i_{ESS}), and PV current (i_{PV}).

The same test but with a charging ESS reference (-500 W) is represented in Figure 42. As the MPPT is smaller than the ESS charging reference, the ER is demanding power from the grid.

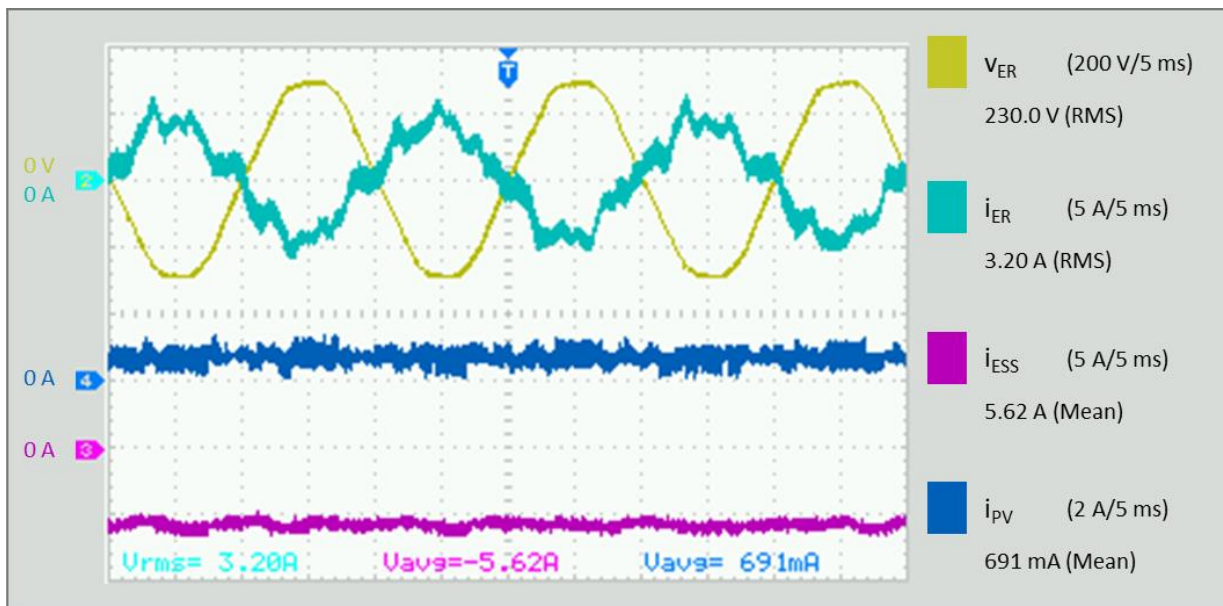


Figure 42. Scenario A1: ER voltage (v_{ER}), ER current (i_{ER}), ESS current (i_{ESS}), and PV current (i_{PV}).

Figure 43 shows the evolution of the powers in each system (PV, ESS and grid) in different setpoints. Figure 43 a) represents the continuous PV MPPT. The presented ripple is justified by the tracking method based on P&O and the low irradiance during the on-site tests. The exchanged power between the ESS and the common DC-link of the ER is also depicted in Figure 43 b), showing a discharging/charging cycle (its reference varies from a positive to negative value). Figure 43 c) and Figure 43 d) show respectively, the corresponding active power and the reactive power injected to the grid. In this scenario of reactive power test, the ability to inject or demand reactive power (inductive or capacitive behaviour) was demonstrated.



Figure 43. Scenario A1: Transient responses of the ER subsystems: a) PV power, b) Power exchanged with the ESS, c) Active power exchanged with the grid, and d) Reactive power.

8.2 Scenario A2

In scenario A2 the PV system is operating in RPP at 50 W. The main waveforms are represented in Figure 44. i_{PV} shows a good tracking of the current at maximum power (I_{MPP}) with its current ripple within the limit. The ESS current (i_{ESS}) is also depicted when the ESS is discharged with a $P_{ESS,ref}$ equal to 400 W. ER voltage (v_{ER}) and ER current (i_{ER}) present a slight shift angle since the reactive power is set to 300 VAr.

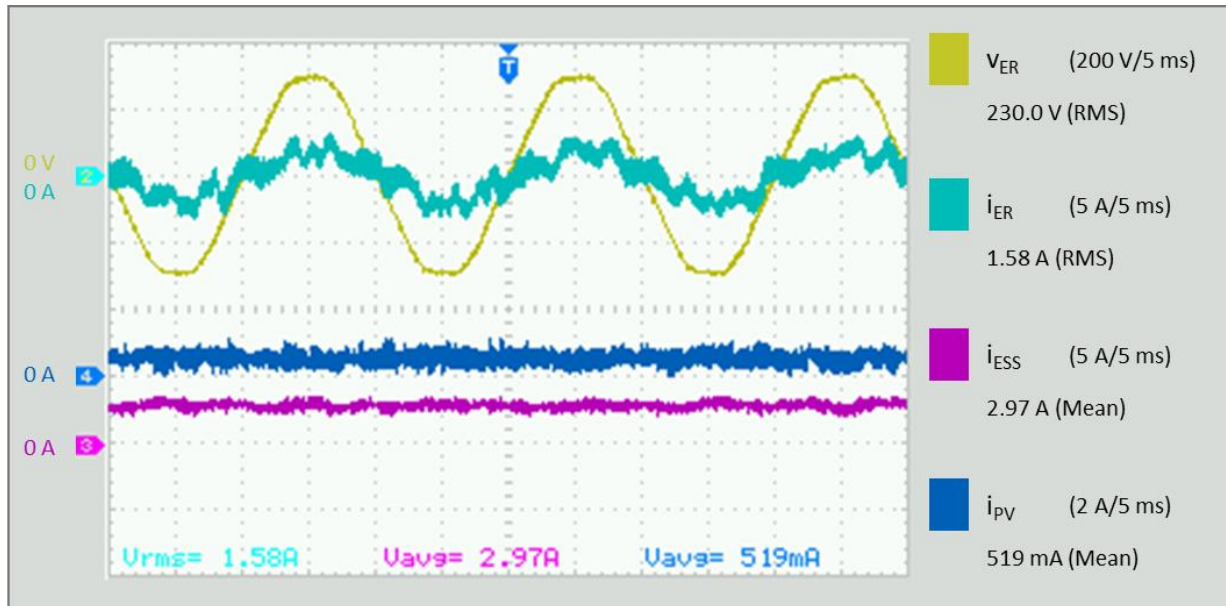


Figure 44. Scenario A2: ER voltage (v_{ER}), ER current (i_{ER}), ESS current (i_{ESS}), and PV current (i_{PV}).

The same tests but with a charging ESS reference (-400 W) is represented in Figure 45. As the RPPT is smaller than the charging reference, the ER is demanding power from the grid.

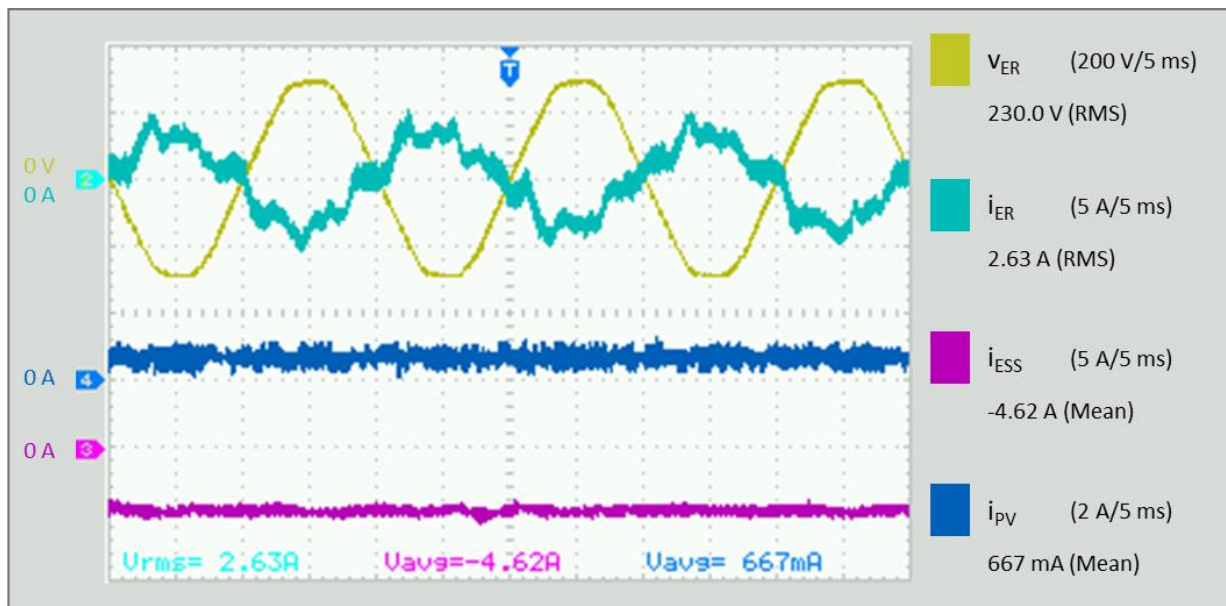


Figure 45. Scenario A2: ER voltage (v_{ER}), ER current (i_{ER}), ESS current (i_{ESS}), and PV current (i_{PV}).

Figure 46 shows the evolution of the powers in each system. Figure 46 a) shows the PV RPPT. A very similar test than in scenario A1 is performed with successful responses.

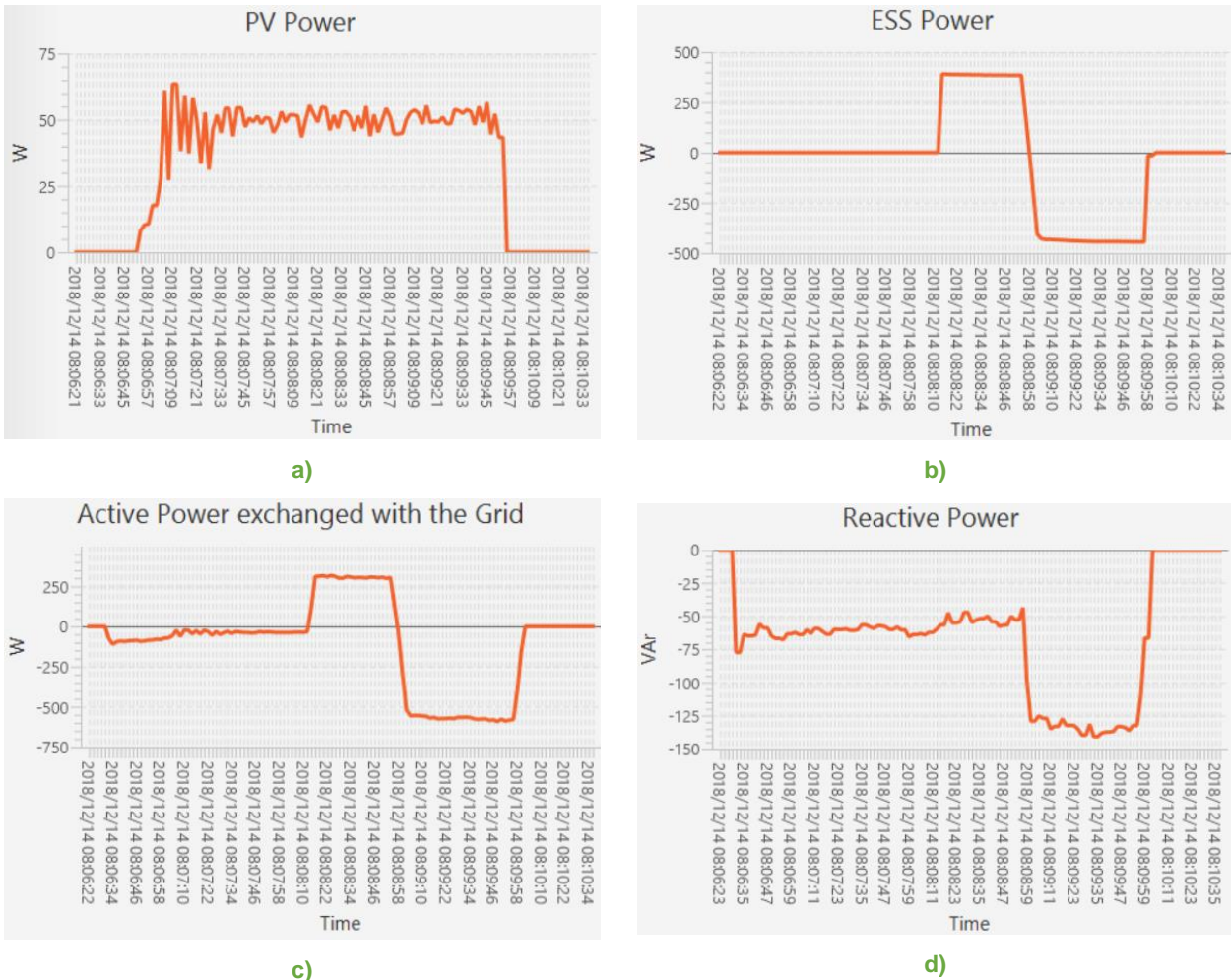


Figure 46. Scenario A2: Transient responses of the ER subsystems: a) PV power, b) Power exchanged with the ESS, c) Active power exchanged with the grid, and d) Reactive power.

8.3 Scenario A3

This scenario demonstrates the ER operation when the PV is OFF (e.g. night operation). In this scenario, the ESS is discharged and charged with a reference power of 600 W and -600 W (Figure 47 and Figure 48 respectively). The reactive power (Q) has a setpoint of 100 VAr.

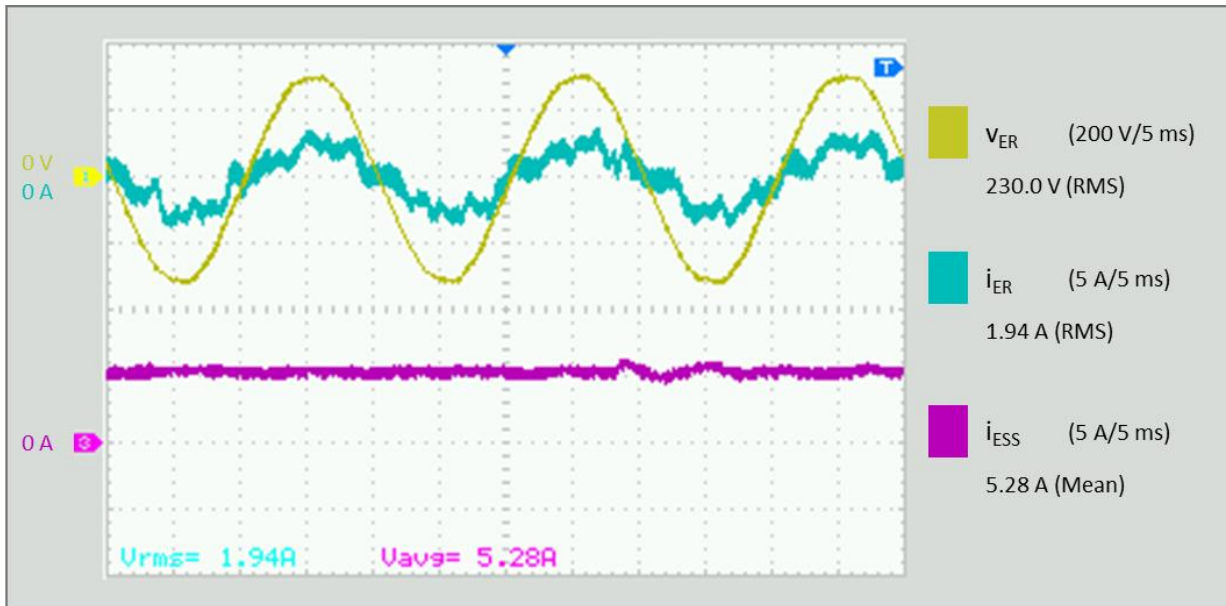


Figure 47. Scenario A3: ER voltage (v_{ER}), ER current (i_{ER}), and ESS current (i_{ESS}).

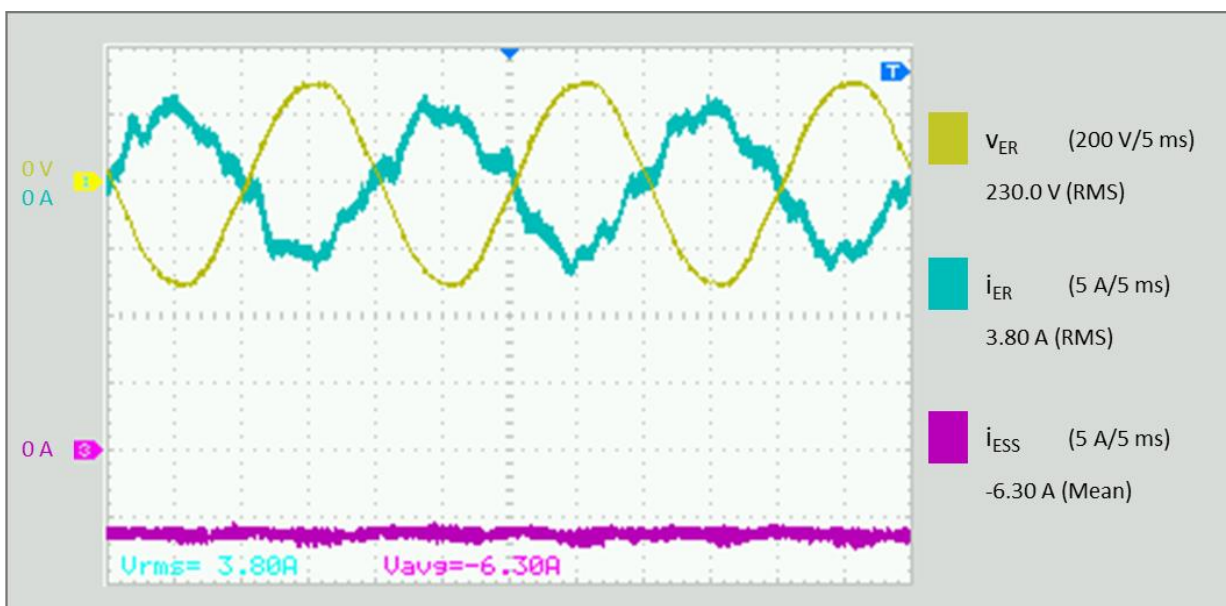


Figure 48. Scenario A3: ER voltage (v_{ER}), ER current (i_{ER}), and ESS current (i_{ESS}).

Figure 49 represents the transient responses of this scenario. Figure 49 a) shows the PV power, which is null during all the test (no PV available). Figure 49 b) shows the ESS being charged and discharged from/to the grid. An accurate response is observed in terms of active power balance (Figure 49 c)). Setpoints for the Q are also established and tracked properly (Figure 49 d)).

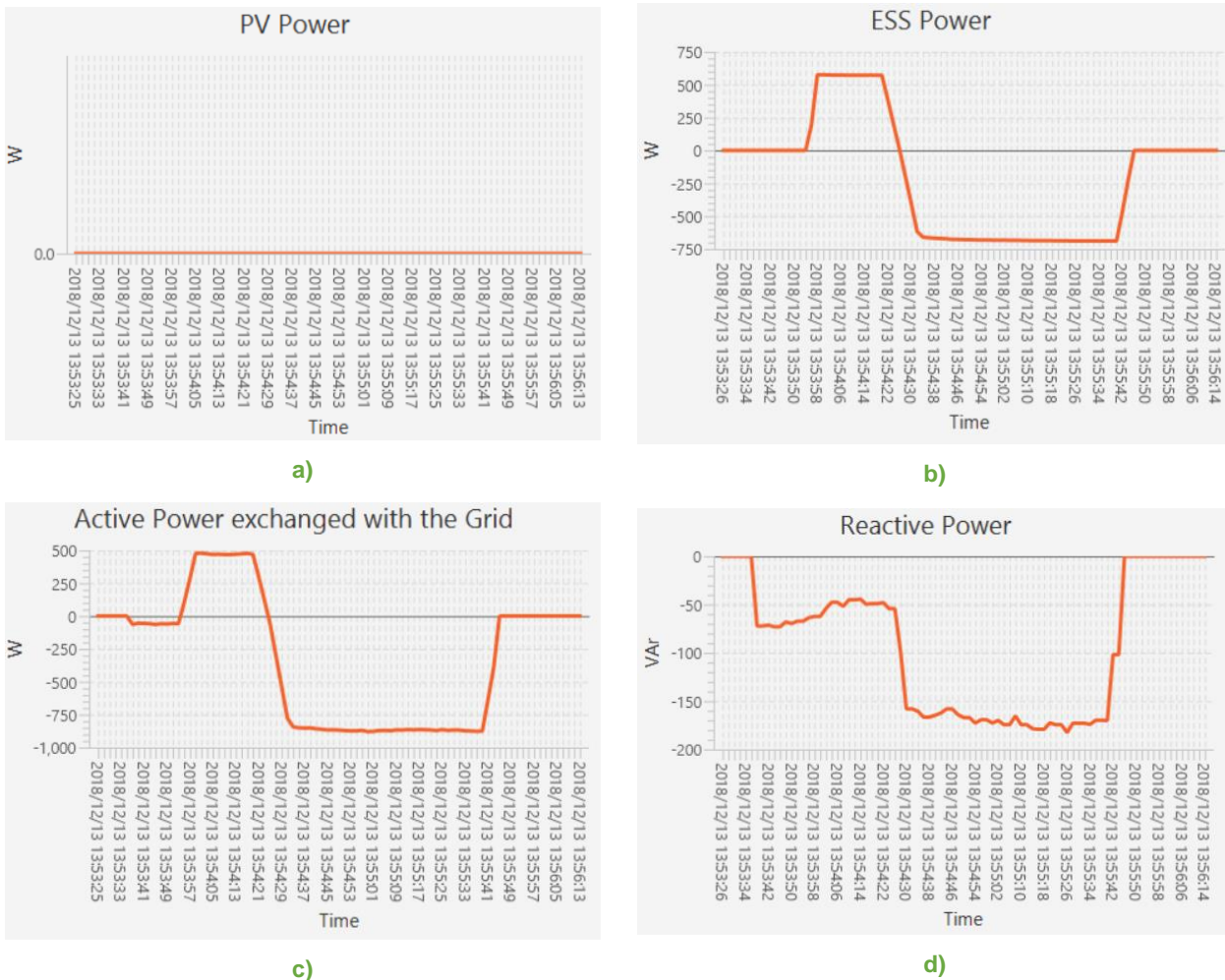


Figure 49. Scenario A3: Transient responses of the ER subsystems: a) PV power, b) Power exchanged with the ESS, c) Active power exchanged with the grid, and d) Reactive power.

8.4 Scenario B1

This scenario illustrates the ER operating in island mode in the test site. In this scenario, the DC-link is regulated by the ESS interface. The PV is operating in MPP condition and two different loads of 350 W and 700 W are connected to the AC side. The ESS injects the remaining power to regulate the DC-link voltage at the reference value (ESS discharges). These tests are illustrated in Figure 50 and Figure 51 respectively.

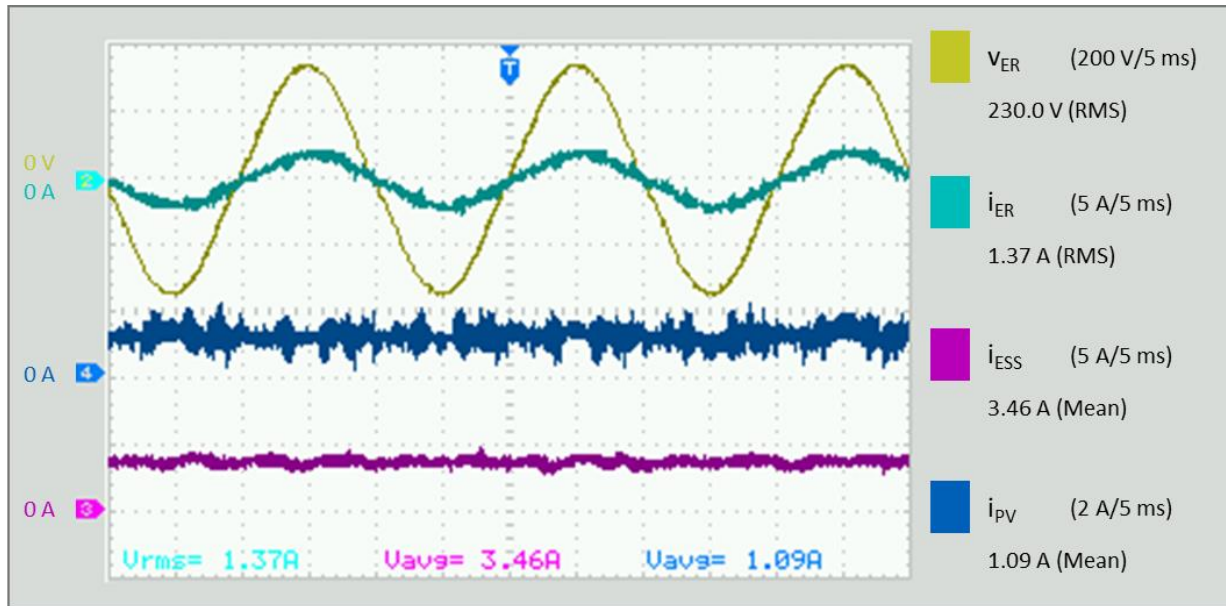


Figure 50. Scenario B1: ER voltage (v_{ER}), ER current (i_{ER}), ESS current (i_{ESS}), and PV current (i_{PV}) with 350 W load.

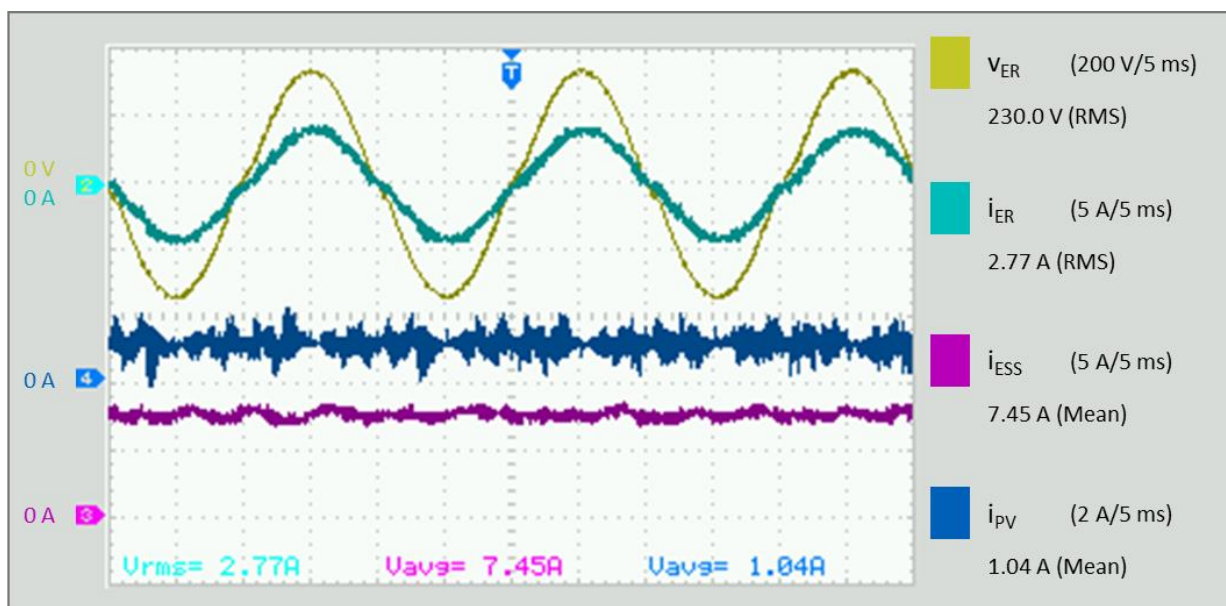


Figure 51. Scenario B1: ER voltage (v_{ER}), ER current (i_{ER}), ESS current (i_{ESS}), and PV current (i_{PV}) with 700 W load.

Figure 52 shows the power response of each ER subsystem under different setpoints. The PV generation is very low due to the weather conditions (Figure 52 a)). In Figure 52 b) the ESS tracks each reference value properly and that power is exchanged with the grid (Figure 52 c)). Setpoints for the Q are also established and tracked properly (Figure 52 d)).

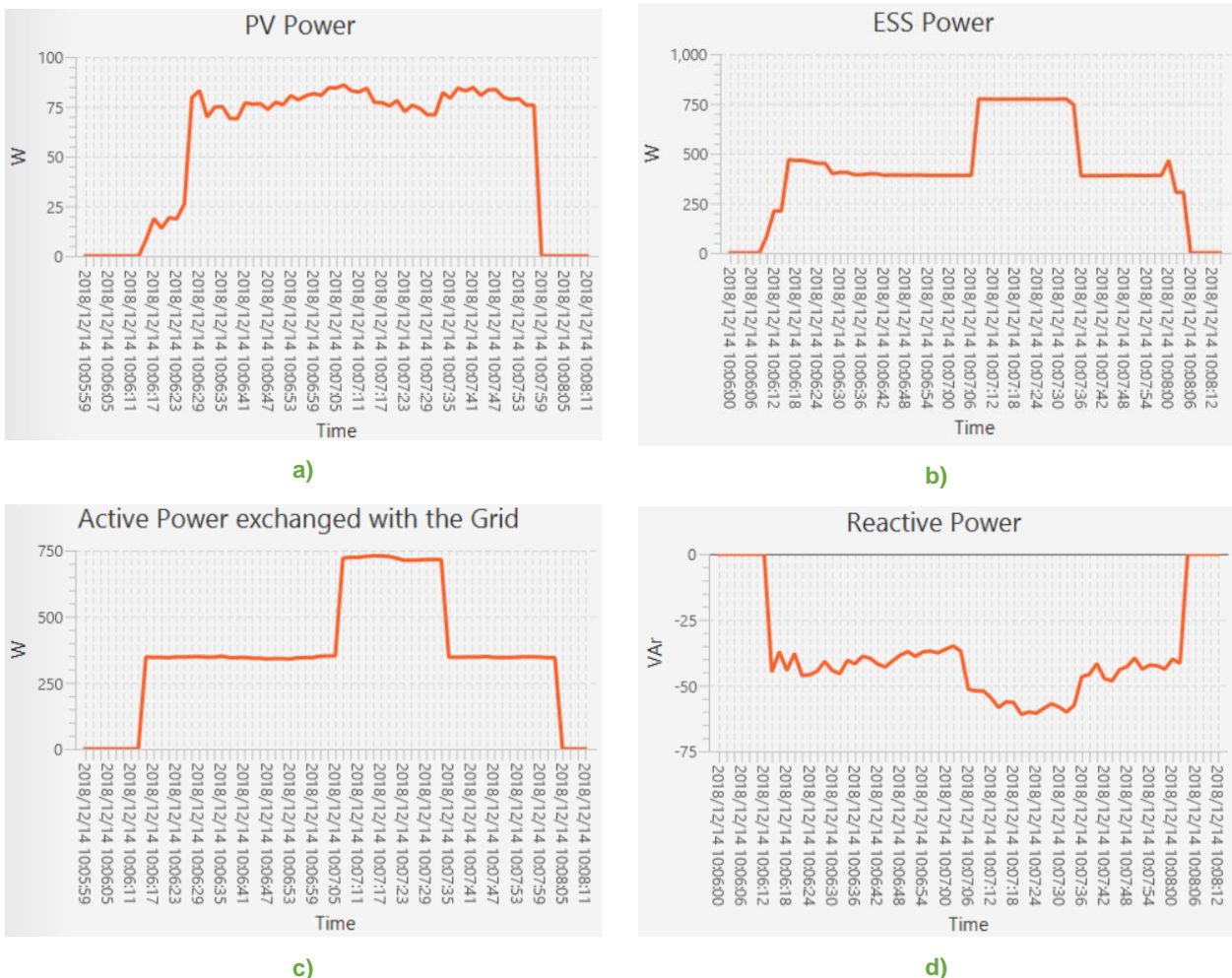


Figure 52. Scenario B1: Transient responses of the ER subsystems: a) PV power, b) Power exchanged with the ESS, c) Active power exchanged with the grid, and d) Reactive power.

8.5 Scenario B2

This scenario illustrates the ER operating in island mode with the PV operating in RPP condition with a 65 W setpoint, and the same two loads than in previous scenario were connected to the AC side. The ESS injects the remaining power to regulate the DC-link voltage at the reference value (ESS discharges). These tests are illustrated in Figure 53 and Figure 54 respectively.

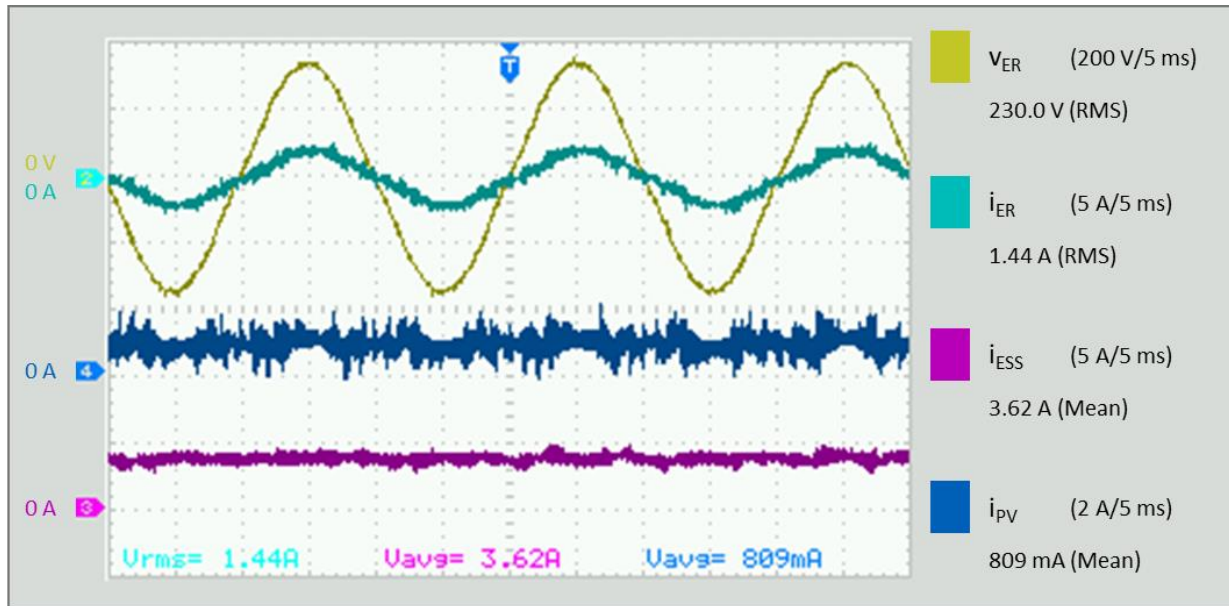


Figure 53. Scenario B2: ER voltage (v_{ER}), ER current (i_{ER}), ESS current (i_{ESS}), and PV current (i_{PV}) with 350 W load.

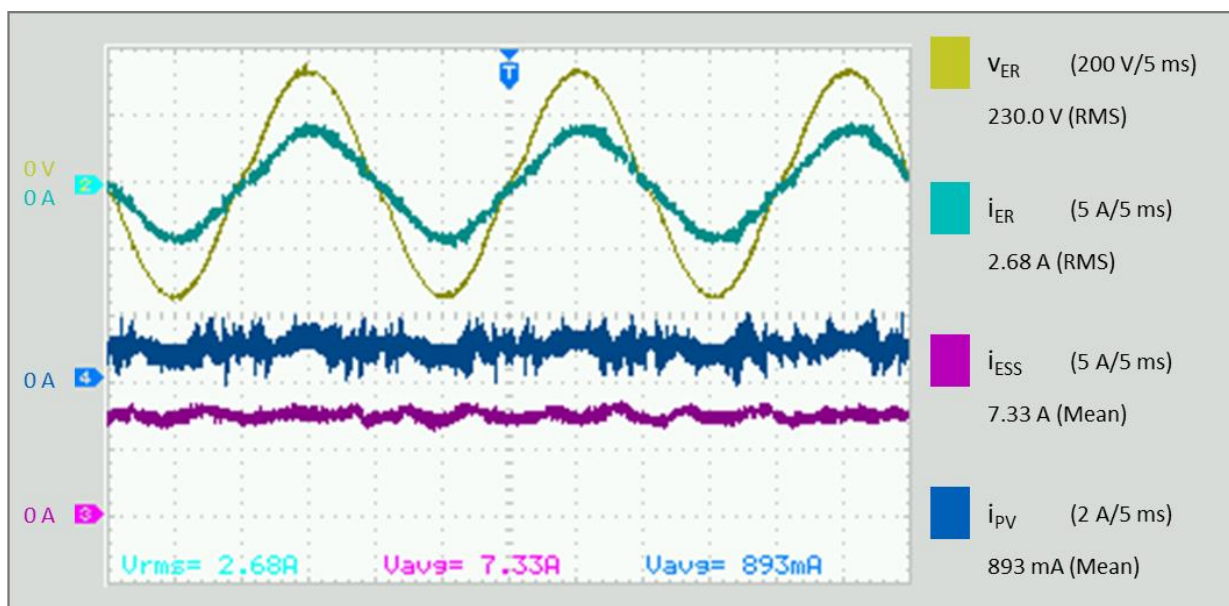


Figure 54. Scenario B2: ER voltage (v_{ER}), ER current (i_{ER}), ESS current (i_{ESS}), and PV current (i_{PV}) with 700 W load.

Lastly, Figure 55 shows the transient response during the scenario setpoints.

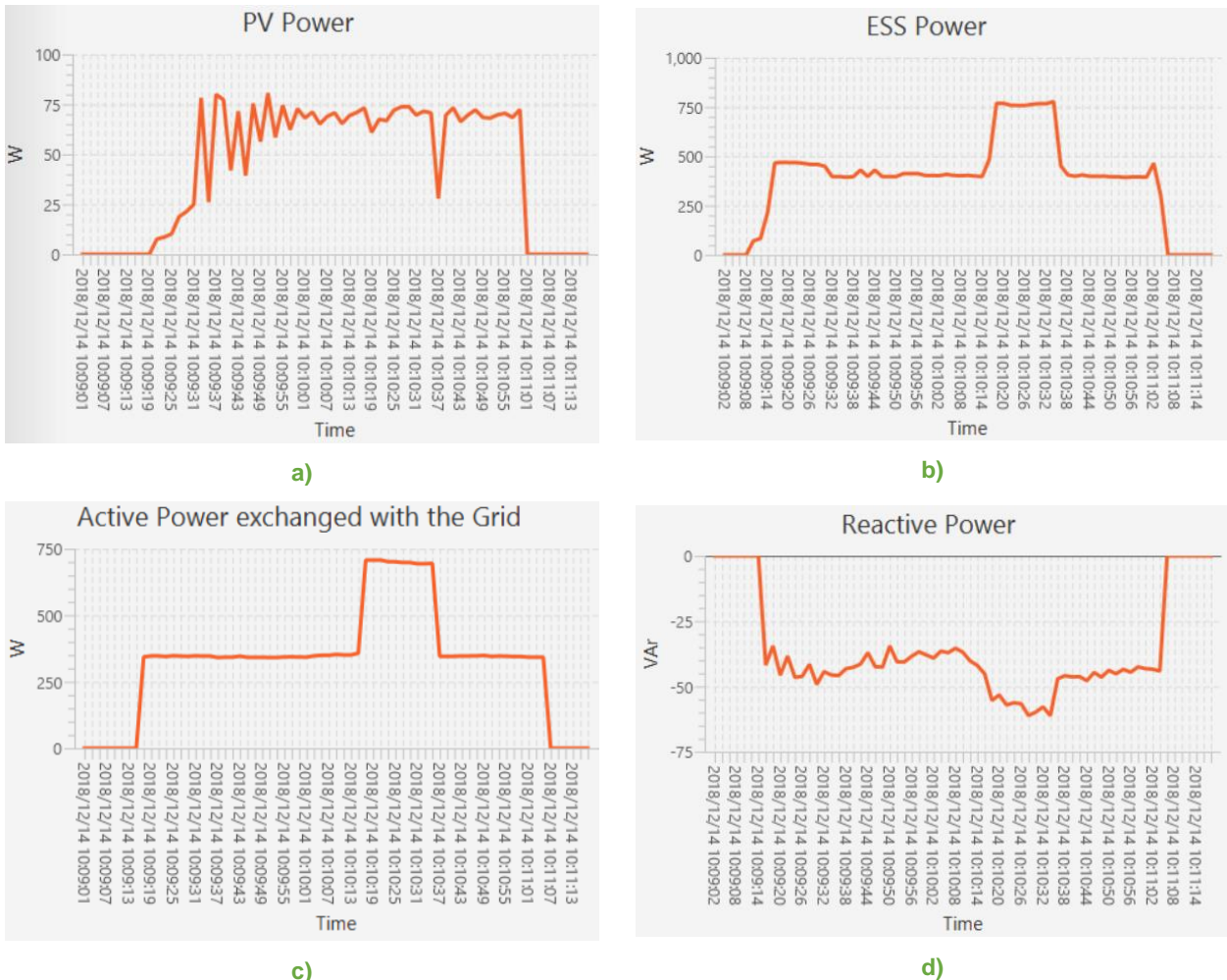


Figure 55. Scenario B2: Transient responses of the ER subsystems: a) PV power, b) Power exchanged with the ESS, c) Active power exchanged with the grid, and d) Reactive power.

8.6 Scenario C

This scenario demonstrates the ability of the ER to perform the black-start operation. The ER is feeding local loads by controlling its output voltage and output current. At a certain moment, the DSO grid is suddenly connected. Before the connection, the ER receives the information about the DSO grid angle and the ER synchronizes with the grid. With this procedure, the transient response during the DSO grid connection is smooth and the safe ER DSO grid connection is assured (Figure 56). Detailed waveforms of the ER current and voltage are shown in Figure 57 during the DSO grid connection.

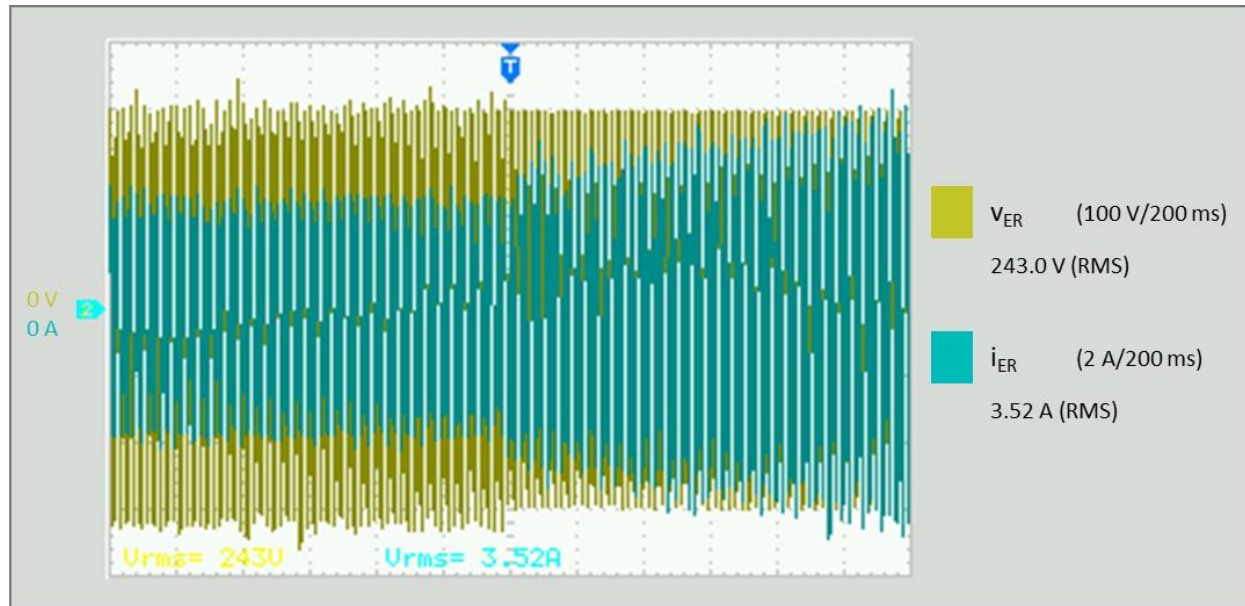


Figure 56. ER voltage (v_{ER}) and ER current (i_{ER}) during black-start.

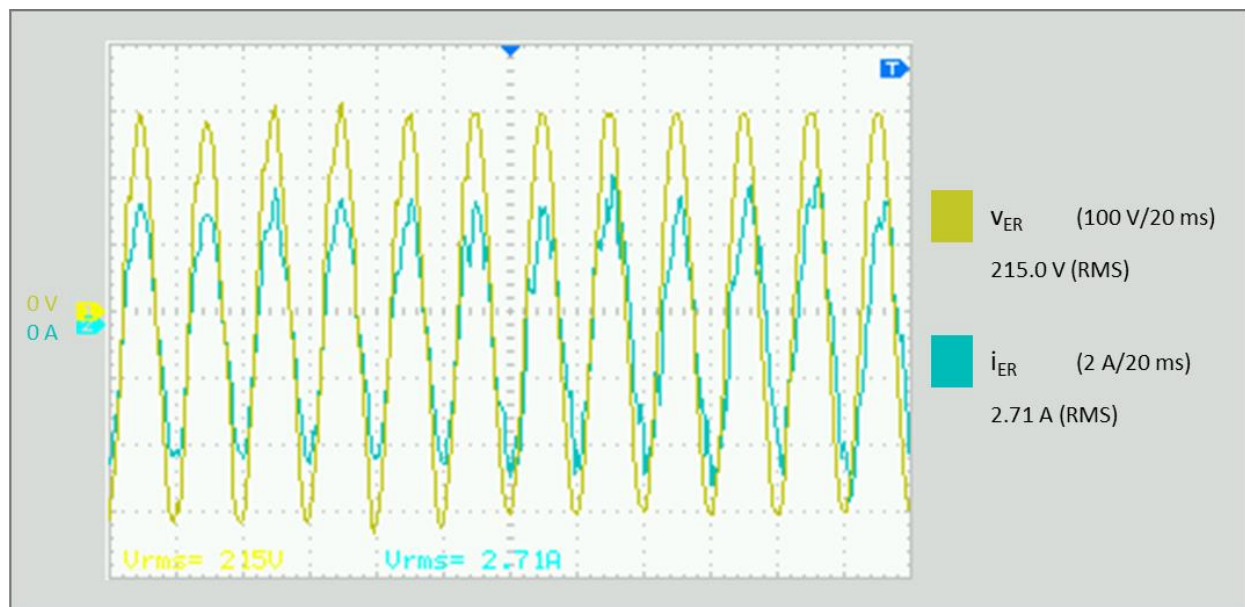


Figure 57. Scenario C: Detailed ER voltage (v_{ER}) and ER current (i_{ER}) during black-start.

9 Unidirectional neighbourhood DC-DC network

The Bucharest HLUCs specified in D2.2 [S4G-D2.2] will be tested and evaluated during phase 3 of the project. A DC network was deployed between two UPB laboratories to test HLUC-1-PUC-3: "Resilient hybrid cooperative Ecosystem" (described in D2.2 [S4G-D2.2]).

The DC network, which has a 400 V DC nominal voltage, is considered as a distribution line towards the neighbourhood. The 220 V ER DC bus is the source of the power transferred to the neighbourhood through the DC network, and a boost converter (DC/DC converter) was needed to increase the voltage from 220 V DC to 400 V DC. The boost converter was developed by UPB and its simplified block diagram is shown in Figure 58, where the dashed red lines show the control/measurement signals and the black ones show the power lines.

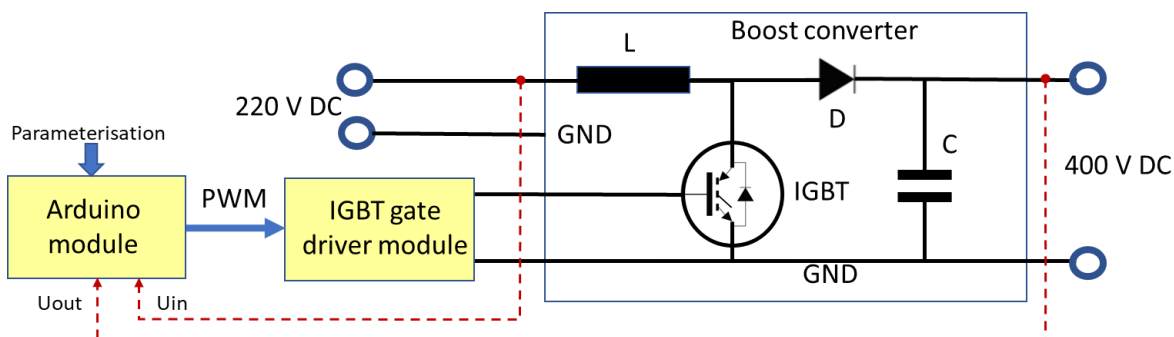


Figure 58. Boost converter (220 V DC to 400 V DC) block diagram.

The DC/DC converter is unidirectional (from the ER DC bus towards the neighbourhood 400 V DC network) and is implemented using a boost converter. The boost converter is composed of an IGBT (FGH25T120SMD-F155, ON Semiconductor) for switching the boost converter circuit (600 V or more, at least 30 kHz maximum switching frequency), an inductor ($L_{Boost} = 610 \mu\text{H}$), and a capacitor ($C_{Boost} = 470 \mu\text{F}$) to smooth the 400 V DC voltage level. Brief calculations for the most important components are followed presented.

The boost converter has been designed to work in Continuous Conduction Mode (CCM) at nominal power, which asks for the boost inductor (L_{Boost}) to be designed with the condition described in equation (20), where f is the switching frequency of the IGBT, R is the load on the higher voltage part and D_{Boost} is the PWM factor.

$$L_{Boost} > L_{Boost,m} = \frac{(1 - D_{Boost})^2 \cdot D_{Boost} \cdot R}{2 \cdot f} \quad (20)$$

For a maximum power of 1000 W on the 400 V part, the value R can be calculated using equation (21).

$$R = \frac{U^2}{P} = \frac{400^2}{1000} = 160 \Omega \quad (21)$$

The value for the PWM factor (D_{Boost}) is calculated with the equation (22).

$$D_{Boost} = 1 - \frac{U_{in}}{U_{out}} = 1 - \frac{220}{400} = 0.45 \quad (22)$$

For the switching frequency $f = 30 \text{ kHz}$, the minimum value of the boost inductor ($L_{Boost,m}$) is $363 \mu\text{H}$. The boost inductor (L_{Boost}) has been chosen at a higher value, implemented in the prototype with three inductors in series and totalling $610 \mu\text{H}$, as previously presented.

Targeting also teaching didactic purposes, the value and number of inductors can be increased or decreased, for coping with other parameters, such as frequency, load or IGBT type change.

The boost capacitor (C_{Boost}) on the 400 V DC voltage level needs to comply with equation (23), where $V_{Boost,r}$ is the boost voltage ripple and $V_{Boost,O}$ is the boost output voltage.

$$C_{Boost} > C_{Boost,m} = \frac{D_{Boost} \cdot V_{Boost,O}}{V_{Boost,r} \cdot R \cdot f} \quad (23)$$

For $V_{Boost,O} = 400$ V and $V_{Boost,r} = 4$ V (1%), the minimum boost converter value ($C_{Boost,m}$) is 9.3 μ F. A much higher value of 470 μ F has been chosen, to be able to stabilize the 400 V DC bus and to surpass sudden power changes (for the selected value of C_{Boost} it was obtained a time constant $T = RC = 72$ ms). Additional C_{Boost} values may be added during the phase 3 tests, if higher 400 V DC line stability will be needed, and eventual changes will be reported in D6.12 – “Phase 3 evaluation report”.

The experimental boost converter is normally operating for a maximum long-term power of 500 W and for 1000 W during short-term bursts (1-minute). During the development, different values of switching frequencies and of minimum L were tested, together with various IGBT types and of switching frequencies. A stable functionality has been finally achieved at a basic 30 kHz frequency, which can be still increased based on the IGBT capabilities (the implemented PWM control can easily exceed 50 kHz switching frequency). The FGH25T120SMD-F155 IGBT type which has been used works well within the operational conditions, as being designed for 50 A at a switching frequency of 40 kHz (duty cycle 50%, which brings a 25 A equivalent maximum current) and having a maximum voltage of 1200 V, thus leaving space for further developments towards higher frequencies and higher voltage on DC network.

An IGBT gate driver module is giving the appropriate signals (0 to 15 V, high sink/source current) for the IGBT control. The 400 V DC output voltage is regulated using a Proportional Integral (PI) controller (voltage control loop) for maintaining the output voltage in the range of $U=400$ V \pm 10 % and has an USB interface for changing the parameterisation and for software updates. The Arduino Mega microcontroller (8-bit Atmel technology) is controlling the IGBT using the PWM technique.

Section 10 shows the main tests, which were performed with the unidirectional boost converter, to evaluate the functionalities needed to power the unidirectional neighbourhood DC-DC network.

10 After deployment tests

Once the ER was fully installed in UPB's premises, two tests were performed, namely:

1. Local Energy Storage System Agent (LESSAg) integration with ER.
2. Boost converter evaluation.

10.1 LESSAg integration with ER

This test was performed to evaluate the real-time operation of the ER while receiving setpoints from the LESSAg (described in D4.3 [S4G-D4.3]). The test was performed with the ER in MPPT mode and receiving setpoints for charging (negative) and discharging (positive) the ESS (PBatRef), with the values in the range of -500 W to 500 W.

The ESS schedule was obtained by changing at various moments the setpoint sent by LESSAg, which was running on the SMX attached to the UPB smart meter connected in the Point of Common Coupling (PCC) with the main power system in the laboratory 1. LESSAg sends setpoints to the ER through Message Queuing Telemetry Transport (MQTT) messages (as described in D4.10 [S4G-D4.10]).

The tests were made on various intervals and targeting the telemetry of PV production and the ESS SoC during charging and discharging processes.

The main purpose of these tests was also to check the possibilities of making complex tests during phase 3, by using Hardware-in-the-Loop (HIL) technology, which is using ER, grid simulations and sets of consumption versus local production patterns. The tests for the LESSAg ER integration are recorded by using a 1-second sampling rate. Figure 59 shows the PV production evolution for one day. In this section, the time in the charts is in Greenwich Mean Time (GMT) zone.

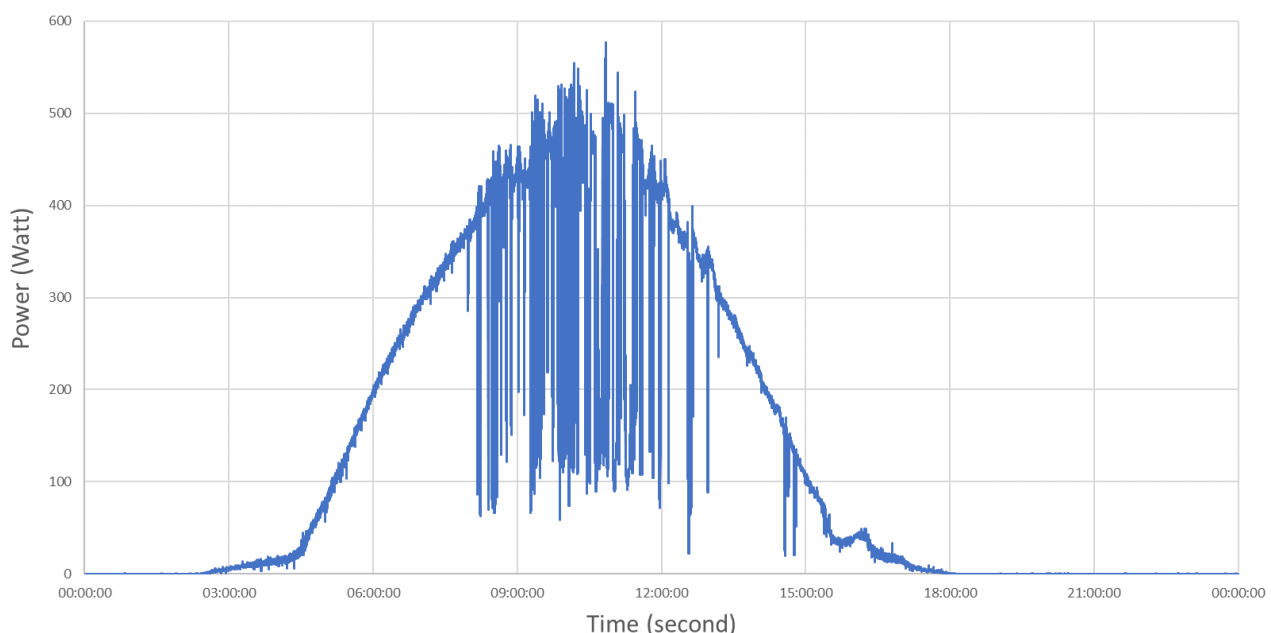


Figure 59. PV production (May 21st, 2019).

Figure 60 shows the SoC progress during a charging process and different ESS setpoints, starting from a discharged ESS. When the ESS is fully charged (SoC = 80 %, as defined the ER), the charging setpoints are no longer accepted by the ER to ensure the ESS integrity.

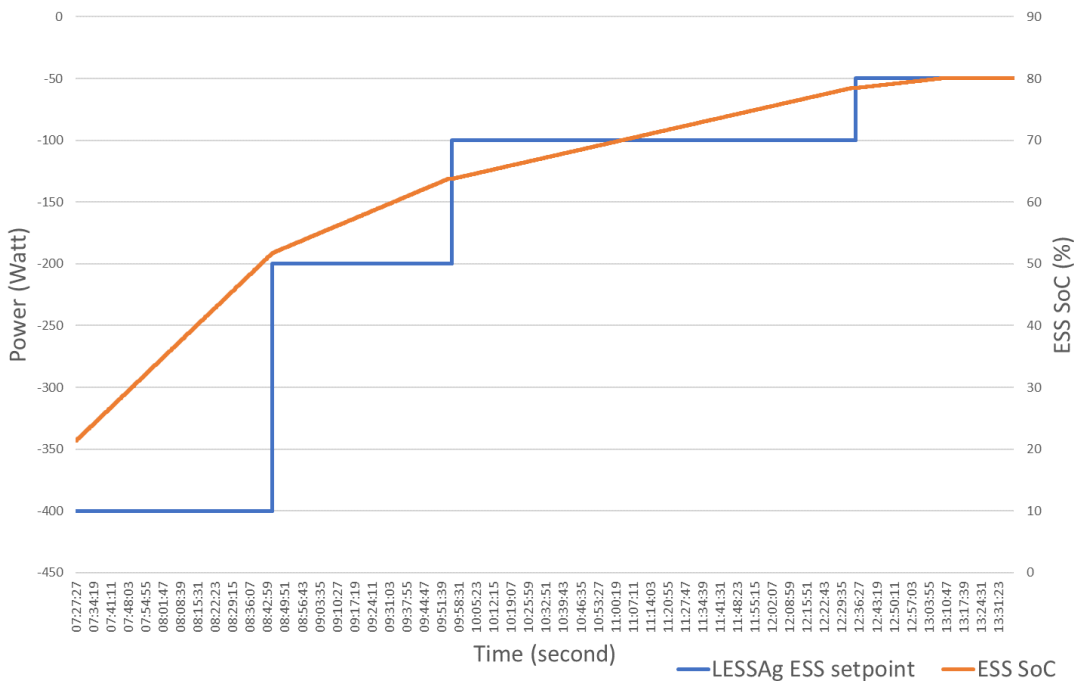


Figure 60. ESS charging SoC progress and LESSAg ESS setpoints (May 21st, 2019).

In the same day, a discharging sequence was requested with the SoC progress and different ESS setpoints presented in Figure 61. Similarly to the charging process, when the ESS is fully discharged (SoC = 20 %, as defined the ER), the discharging setpoints are no longer accepted by the ER to ensure the ESS integrity.

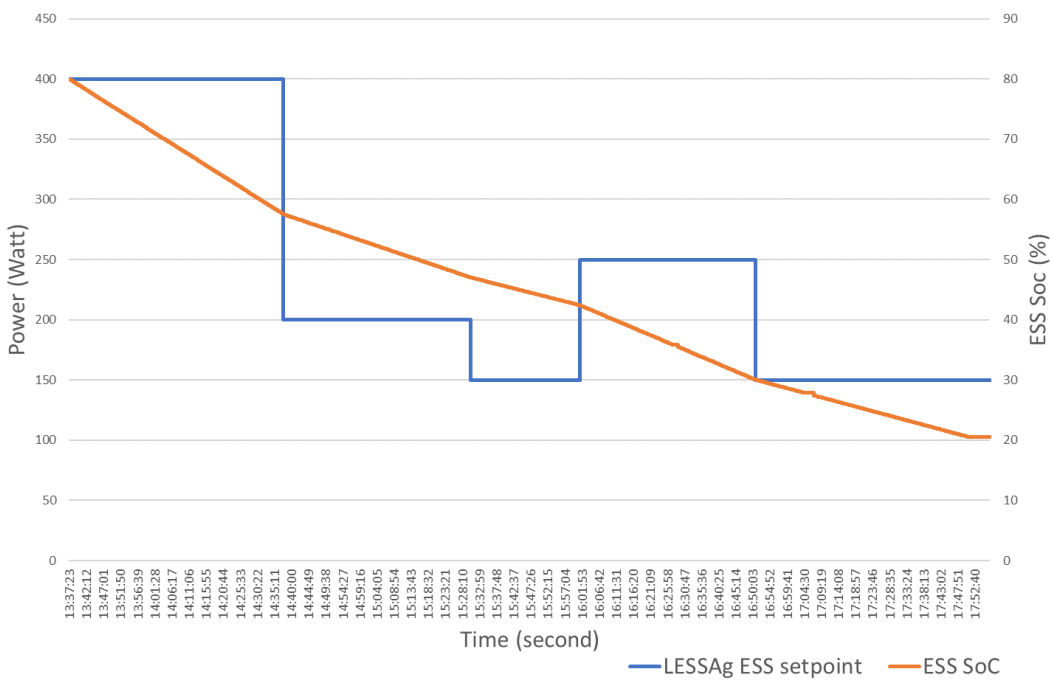


Figure 61. ESS discharging SoC progress and LESSAg ESS setpoints (May 21st, 2019).

The data records made within the interaction between LESSAg and ER will be used for the LESSAg refinements and for the improvement of HIL functionality, which will be tested in the phase 3 of the project.

10.2 Boost converter evaluation

This test was performed to evaluate the boost converter connected to the 220 V ER DC bus, which has the function to supply the 400 V DC unidirectional neighbourhood network. The S4G boost converter for the Bucharest test site needs to increase voltage from 220 V DC to 400 V DC (boost converter output), in order to be able to transport power at this higher voltage, thus having lower current between different neighbourhood locations.

The test was performed by supplying the boost converter with a 220 V DC power supply with capabilities for at least -20% to +10% voltage variation. Two tests were made to evaluate the boost converter capabilities.

- **Short-term burst capacity test:** sustain its output around 1000 W power on the 400 V DC side during at least 1-minute.
- **Long-term capacity test:** this test was also executed with 1000 W power on the 400 V DC side during a 5-minutes timeframe, to simulate a long-term power transfer (1-hour) of 500 W.

These tests are necessary to achieve a continuously power transfer on a 400 V DC network (to be accomplished until the end of the project), where the 400 V DC network will consume 500 W power during 1-hour interval. The fact that the targeted long-term power $P_{LONG_TERM} = 500$ W can be tested with higher $2 \times P_{LONG_TERM}$ power during the 5-minutes test has been also checked by running an additional test during 1-hour with $P = 500$ W.

The 400 V DC network load was implemented using power variable resistors (usually used for laboratory purposes), in order to allow a smooth variation of their resistance, while the heat of the resistors can be naturally transferred to the environment without damaging them. Therefore, the tests were made with appropriate resistors values, to be able to consume around 1000 W from the 400 V DC network during a 5-minutes timeframe, while the DC network voltage remains at $400\text{ V} \pm 10\%$ range.

Table 9 shows the first test made on a 1-minute timeframe, feeding a 1000 W DC load. Table 10 shows the second test, made on a 5-minutes timeframe, feeding the same 1000 W DC load, in order to check long-term stabilisation while the heating burden of the laboratory resistors remained in a safe operating temperature. Table 11 shows the long-term check test. The tests were extended by a 20 % period, to fully catch the desired time window of the tests (1- and 5-minutes, and 1-hour).

For fully covering the tests, the boost converter output DC voltage and the consumed power were chosen with slightly higher values over the targeted test values.

The voltage deviation is calculated compared to the nominal voltage $U_N = 400$ V DC. The power on the 400 V DC network is calculated by multiplying the boost converter DC current with its DC voltage, which were measured with the following devices:

- DC voltage: FLUKE 87 (true RMS multimeter).
- DC current: AX-588 (digital multimeter).

Table 9. Short-term test: 1-minute timeframe, with a 1000 W load on the 400 V DC network.

Time (mm:ss)	DC Current (A)	DC Voltage (V)	Power (W)	DC Voltage deviation (%)	Test assessment
00:00	2.56	405.30	1037.57	1.33	Passed
00:20	2.57	405.20	1041.36	1.30	Passed
00:40	2.57	405.70	1042.65	1.43	Passed
01:00	2.57	405.20	1041.36	1.30	Passed
01:20	2.57	405.10	1041.11	1.28	Passed

Table 10. Long-term test: 5-minutes timeframe, with a 1000 W load on the 400 V DC network.

Time (mm:ss)	DC Current (A)	DC Voltage (V)	Power (W)	DC Voltage deviation (%)	Test assessment
00:00	2.56	407.80	1043.97	1.95	Passed
01:00	2.58	408.90	1054.96	2.22	Passed
02:00	2.58	407.50	1051.35	1.88	Passed
03:00	2.59	407.90	1056.46	1.97	Passed
04:00	2.60	406.80	1057.68	1.70	Passed
05:00	2.60	407.40	1059.24	1.85	Passed
06:00	2.60	407.20	1058.72	1.80	Passed

Table 11. Long-term check test: 1-hour timeframe, with a 500 W load on the 400 V DC network.

Time (hh:mm)	DC Current (A)	DC Voltage (V)	Power (W)	DC Voltage deviation (%)	Test assessment
00:00	1.28	403.10	515.97	0.78	Passed
00:10	1.29	404.20	521.42	1.05	Passed
00:20	1.29	405.90	523.61	1.47	Passed
00:30	1.28	403.90	516.99	0.97	Passed
00:40	1.29	406.10	523.87	1.53	Passed
00:50	1.29	406.20	524.00	1.55	Passed
01:00	1.30	406.80	528.84	1.70	Passed
01:10	1.29	405.80	523.48	1.45	Passed

As the tests results shows, the DC-DC boost converter successfully passed the tests for 1-minute short-term burst capacity, and for 5-minutes long-term capacity, with an additional check test (Table 11) with lower power and long-term 1-hour timeframe capability.

11 Installation/Deployment instructions

An ER SMX South-bound connector needs to be present in the SMX to enable the interaction with the single-phase ER. This component and its installation/deployment instructions are detailed described in D4.9 [S4G-D4.9] and D4.10 [S4G-D4.10].

The ER deployment instructions are very extensive and require a very specific expertise. For this reason, the single-phase ER deployment should only be performed by the UNINOVA and UPB partners. Figure 62 shows the front view of the ER cabinet with the different components, while Figure 63 shows the top view. Figure 64 shows the single-phase ER deployed at UPB's premises. Lastly, Figure 65 shows the UPB's connection board in detail, enabling the ER connection with the ESS, PV panels, DSO grid, and unidirectional DC-DC neighbourhood network.

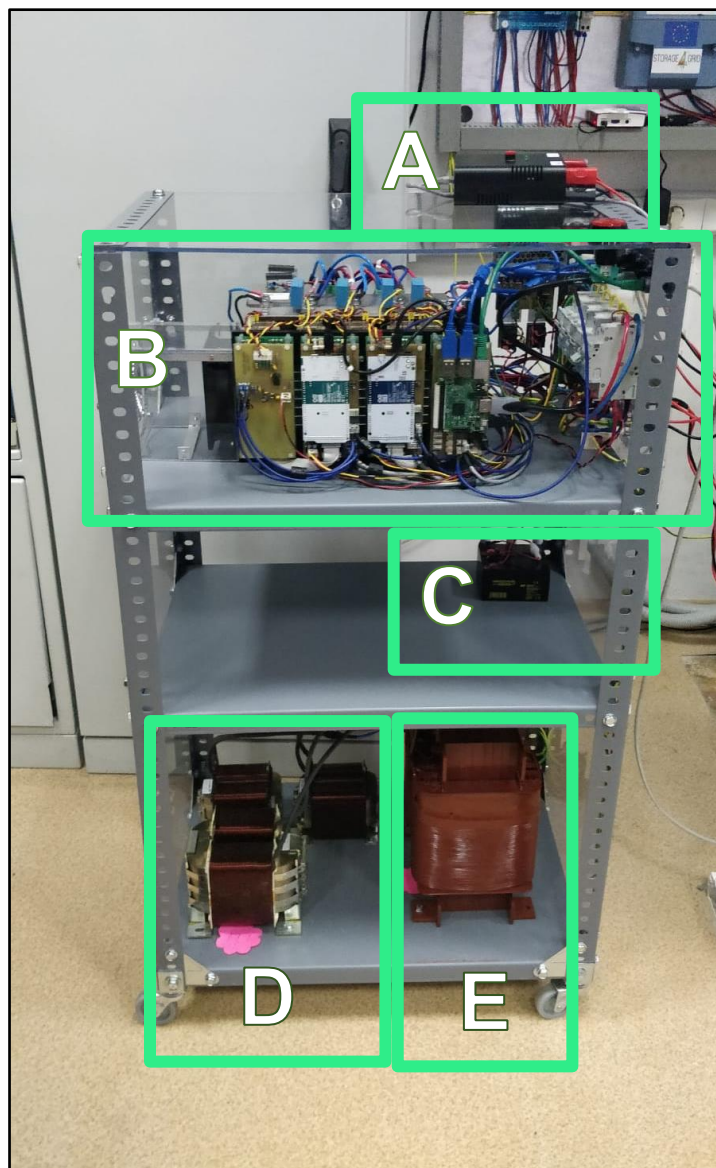


Figure 62. Single-phase ER cabinet front view (A – black-start box (S_{DSO}); B – PV, ESS and grid power converters, and measurement and control boards; C – UPS batteries; D – inductance filters; E – transformer).

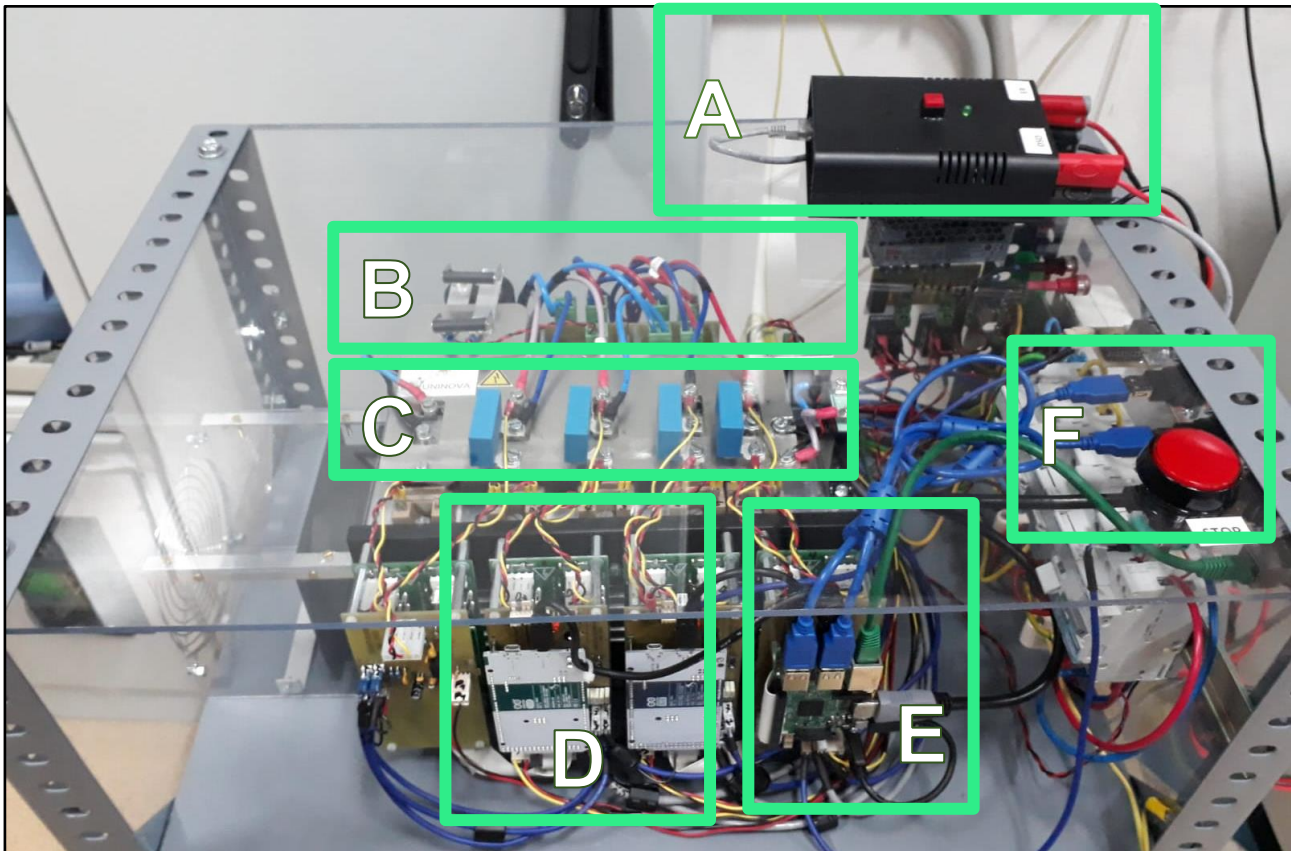


Figure 63. Single-phase ER cabinet top view (A – black-start box (S_{DSO}); B – measurement and control boards; C – Power converters, D – Grid, PV and ESS controllers; E – ER controller; F – emergency button).



Figure 64. Single-phase ER deployed at UPB's premises.



Figure 65. UPB's connection board.

12 Conclusions

A comprehensive simulation study was performed in the PSCAD/EMTDCⁱ software to validate the sizing values, the main functionalities, control algorithms, and modulation methods for the single-phase ER prototype. Different scenarios were defined in order to validate the correct operation of the single-phase ER, namely: A – DSO grid available, B – DSO grid unavailable (island mode), and C – black-start operation.

The scenarios were analysed and simulated, showing a correct operation of the ER in all the different scenarios. The single-phase ER prototype was tested in laboratory and validated at the UPB MicroDERLab facilities, obtaining similar results.

The boost converter of the unidirectional DC network intended to supply neighbourhoods at 400 V DC was implemented. It converts 220 V DC do 400 V DC and it was successfully tested and evaluated.

Acronyms

Acronym	Explanation
AC	Alternating Current
C	Capacitor
CC	Current Control
CCM	Continuous Conduction Mode
D	Diode
DC	Direct Current
DSO	Distribution System Operator
ER	Energy Router
ESR	Equivalent Series Resistor
ESS	Energy Storage System
GUI	Graphical User Interface
HIL	Hardware-in-the-Loop
HLUC	High-Level Use-Case
IGBT	Insulated-Gate Bipolar Transistors
L	Inductance
LESSAg	Local Energy Storage System Agent
MPP	Maximum Power Point
MPPT	Maximum Power Point Tracking
MQTT	Message Queuing Telemetry Transport
P	Active power
PI	Proportional Integral
PCC	Point of Common Coupling
GMT	Greenwich Mean Time
P&O	Perturb and Observe
PI	Proportional Integral
PLL	Phase-Locked Loop
PUC	Primary Use-Case
PV	Photovoltaic
PWM	Pulse Width Modulation
Q	Reactive power

Acronym	Explanation
RMS	Root Mean Square
RPP	Reference Power Point
RPPT	Reference Power Point Tracking
S	Switch
S4G	Storage4Grid
SB	South-bound
S _{DSO}	DSO (on-off) Switch
SMX	Smart Meter eXtension
SoC	State of Charge
SPWM	Sinusoidal Pulse Width Modulation
THD _I	Current Total Harmonic Distortion
UPB	University Politehnica of Bucharest
UPS	Uninterruptible Power Supply
USB	Universal Serial Bus
USM	Unbundled Smart Meter
VC	Voltage Control

Variables nomenclature

Variables	Description
η	Efficiency
$\Delta I_{L_{ESS}}$	ESS inductor current ripple
$\Delta I_{L_{PV}}$	PV inductor current ripple
ΔV_{DC_link}	Output DC-link voltage ripple
f_c	Cut-off frequency of the AC output filter
f_s	Minimum switching frequency
ω_1	Fundamental harmonic
C_{Boost}	Boost capacitor
$C_{Boost,m}$	Minimum Boost capacitor
C_{DC_link}	DC-link capacitor
$C_{DC_link,m}$	Minimum DC-link capacitor
C_{ER}	ER output capacitance filter
$C_{ER,m}$	Minimum ER output capacitance filter
C_{PV}	PV input capacitor
$C_{PV,m}$	Minimum PV input capacitor
D_{Boost}	PWM factor
D_{ER}	ER duty cycle
D_{ESS}	ESS duty cycle
$D_{ESS,M}$	Maximum ESS duty cycle
D_{PV}	PV duty cycle
$D_{PV,M}$	Maximum PV duty cycle
$G_L(h_{sw})$	Inductive filter transfer function
h_{sw}	Switching harmonic number
$I_{d,ref}$	Direct component reference current
i_{ER}	ER output current
i_{ER}	ER output current at the switching frequency
i_{ESS}	ESS current
$i_{ESS,M}$	Maximum ESS output current
$i_{ESS,ref}$	ESS reference current
I_{MPP}	Maximum power point current

Variables	Description
i_{PV}	PV current
$I_{PV,M}$	Maximum PV output current
I_{sc}	Short-circuit current
I_{sw}	Grid RMS harmonic current at the switching frequency
$I_{SW_{ESS}}$	Maximum ESS switch current
$I_{SW_{PV}}$	Maximum PV switch current
L_{Boost}	Boost converter inductor
$L_{Boost,m}$	Minimum Boost converter inductor
L_{ESS}	ESS inductance filter
$L_{ESS,m}$	Minimum ESS inductance filter
L_{ER}	ER output inductance filter
$L_{ER,m}$	Minimum ER output inductance filter
L_{grid}	Grid output inductance filter
L_{PV}	PV inductance
$L_{PV,m}$	Minimum PV inductance
L_t	Total output inductance filter
P_{MPP}	MPP power
P_{ER}	ER rated power
P_{ESS}	Nominal ESS power
$P_{ESS,ref}$	ESS reference power
$V_{Boost,O}$	Boost output voltage
$V_{Boost,r}$	Boost voltage ripple
V_{DC_link}	Nominal DC-link voltage
V_{ESS}	Nominal ESS voltage
$V_{ESS,m}$	Minimum ESS input voltage
$V_{ESS,M}$	Maximum ESS input voltage
V_{ER}	ER output voltage
$V_{ER(hsw)}$	ER output voltage at the switching frequency
V_{grid}	Grid voltage
V_{grid}	RMS grid voltage
V_{MPP}	Maximum power point voltage

Variables	Description
V_{oc}	Open circuit voltage
V_{PV}	PV input voltage
$V_{PV,m}$	Minimum PV input voltage
$V_{PV,M}$	Maximum PV input voltage
$V_{PV,ref}$	PV reference voltage

List of figures

Figure 1. Single-phase ER deployment architecture at Bucharest test site.....	7
Figure 2. Power topology of the single-phase ER.....	8
Figure 3. Typical harmonic spectrum of the grid current	13
Figure 4. Equivalent grid-connected ER with LC filter.....	14
Figure 5. Block diagram of the ER control strategy.....	16
Figure 6. Single-phase ER scenario A architecture.....	17
Figure 7. Single-phase ER scenario B architecture.....	18
Figure 8. Single-phase ER scenario C architecture.....	18
Figure 9. Scenario A1: PV voltage (v_{PV}), MPP reference voltage ($V_{PV,ref}$), and PV current (i_{PV}).....	19
Figure 10. Scenario A1: PV current ripple (i_{PV}).....	20
Figure 11. Scenario A1: Main magnitudes of the ESS interface: ESS SoC, ESS reference current ($I_{ESS,ref}$), ESS current (i_{ESS}), and ESS voltage (v_{ESS}).....	20
Figure 12. Scenario A1: ER voltage (v_{ER}) and ER current (i_{ER}) during ESS discharge and reactive power injection.	21
Figure 13. Scenario A1: ER voltage (v_{ER}) and ER current (i_{ER}) during ESS charge and reactive power injection.	21
Figure 14. Scenario A1: Evolution of the main DC-link voltage (v_{DC_link}) during ER start-up.	22
Figure 15. Scenario A2: PV voltage (v_{PV}), RPP reference voltage ($V_{PV,ref}$), and PV current (i_{PV}).....	22
Figure 16. Scenario A2: Main magnitudes of the ESS interface: ESS SoC, ESS reference current ($I_{ESS,ref}$), ESS current (i_{ESS}), and ESS voltage (v_{ESS}).....	23
Figure 17. Scenario A2: ER voltage (v_{ER}) and ER current (i_{ER}) during ESS discharge and reactive power injection.	23
Figure 18. Scenario A2: ER voltage (v_{ER}) and ER current (i_{ER}) during ESS charge and reactive power injection.	24
Figure 19. Scenario A3: Main magnitudes of the ESS interface: ESS SoC, ESS reference current ($I_{ESS,ref}$), ESS current (i_{ESS}), and ESS voltage (v_{ESS}).....	24
Figure 20. Scenario A3: ER voltage (v_{ER}) and ER current (i_{ER}) during ESS discharge and reactive power injection.	25
Figure 21. Scenario A3: ER voltage (v_{ER}) and ER current (i_{ER}) during ESS charge and reactive power injection.	25
Figure 22. Scenario B1: ER voltage (v_{ER}), ER current (i_{ER}), ESS current (i_{ESS}), and PV current (i_{PV}) with a 500 W AC load.....	26
Figure 23. Scenario B1: ER voltage (v_{ER}), ER current (i_{ER}), ESS current (i_{ESS}), and PV current (i_{PV}) with a 1500 W AC load.....	26
Figure 24. Scenario B2: ER voltage (v_{ER}), ER current (i_{ER}), ESS current (i_{ESS}), and PV current (i_{PV}) with a 500 W AC load.....	27
Figure 25. Scenario B2: ER voltage (v_{ER}), ER current (i_{ER}), ESS current (i_{ESS}), and PV current (i_{PV}) with a 1500 W AC load.....	27
Figure 26. Scenario C: Evolution of the ER voltage (v_{ER}) and ER current (i_{ER}) during black-start operation.	28
Figure 27. Scenario C: Detailed evolution of the ER voltage (v_{ER}) and ER current (i_{ER}) during black-start operation.....	28
Figure 28. Scenario C: ER current (i_{ER}) during active and reactive power steps.....	29
Figure 29. Scenario A1: ER voltage (v_{ER}), ER current, and PV current (i_{PV}).....	31
Figure 30. Scenario A1: ER voltage (v_{ER}), ER current (i_{ER}), ESS current (i_{ESS}), and PV current (i_{PV}).....	31
Figure 31. Scenario A2: ER voltage (v_{ER}), ER current (i_{ER}), ESS current (i_{ESS}), and PV current (i_{PV}).....	32
Figure 32. Scenario A2: ER voltage (v_{ER}), ER current (i_{ER}), ESS current (i_{ESS}), and PV current (i_{PV}).....	32
Figure 33. Scenario A3: ER voltage (v_{ER}), ER current (i_{ER}), ESS current (i_{ESS}), and PV current (i_{PV}).....	33
Figure 34. Scenario A3: ER voltage (v_{ER}), ER current (i_{ER}), ESS current (i_{ESS}), and PV current (i_{PV}).....	33
Figure 35. Scenario B1: ER voltage (v_{ER}), ER current (i_{ER}), ESS current (i_{ESS}), and PV current (i_{PV}) with 500 W load.....	34
Figure 36. Scenario B1: ER voltage (v_{ER}), ER current (i_{ER}), ESS current (i_{ESS}), and PV current (i_{PV}) with 1500 W load.....	34
Figure 37. Scenario B2: ER voltage (v_{ER}), ER current (i_{ER}), ESS current (i_{ESS}), and PV current (i_{PV}) with 500 W load.....	35
Figure 38. Scenario B2: ER voltage (v_{ER}), ER current (i_{ER}), ESS current (i_{ESS}), and PV current (i_{PV}) with 1500 W load.....	35
Figure 39. Scenario C: Transient responses of the ER subsystems: a) PV power, b) Power exchanged with the ESS, c) Active power exchanged with the grid, and d) Reactive power.	36
Figure 40. Weather conditions during the last on-site test days (December 11 th to 14 th , 2018).	37
Figure 41. Scenario A1: ER voltage (v_{ER}), ER current (i_{ER}), ESS current (i_{ESS}), and PV current (i_{PV}).....	38
Figure 42. Scenario A1: ER voltage (v_{ER}), ER current (i_{ER}), ESS current (i_{ESS}), and PV current (i_{PV}).....	38

Figure 43. Scenario A1: Transient responses of the ER subsystems: a) PV power, b) Power exchanged with the ESS, c) Active power exchanged with the grid, and d) Reactive power.....	39
Figure 44. Scenario A2: ER voltage (v_{ER}), ER current (i_{ER}), ESS current (i_{ESS}), and PV current (i_{PV}).....	40
Figure 45. Scenario A2: ER voltage (v_{ER}), ER current (i_{ER}), ESS current (i_{ESS}), and PV current (i_{PV}).....	40
Figure 46. Scenario A2: Transient responses of the ER subsystems: a) PV power, b) Power exchanged with the ESS, c) Active power exchanged with the grid, and d) Reactive power.....	41
Figure 47. Scenario A3: ER voltage (v_{ER}), ER current (i_{ER}), and ESS current (i_{ESS}).....	42
Figure 48. Scenario A3: ER voltage (v_{ER}), ER current (i_{ER}), and ESS current (i_{ESS}).....	42
Figure 49. Scenario A3: Transient responses of the ER subsystems: a) PV power, b) Power exchanged with the ESS, c) Active power exchanged with the grid, and d) Reactive power.....	43
Figure 50. Scenario B1: ER voltage (v_{ER}), ER current (i_{ER}), ESS current (i_{ESS}), and PV current (i_{PV}) with 350 W load.....	44
Figure 51. Scenario B1: ER voltage (v_{ER}), ER current (i_{ER}), ESS current (i_{ESS}), and PV current (i_{PV}) with 700 W load.....	44
Figure 52. Scenario B1: Transient responses of the ER subsystems: a) PV power, b) Power exchanged with the ESS, c) Active power exchanged with the grid, and d) Reactive power.....	45
Figure 53. Scenario B2: ER voltage (v_{ER}), ER current (i_{ER}), ESS current (i_{ESS}), and PV current (i_{PV}) with 350 W load.....	46
Figure 54. Scenario B2: ER voltage (v_{ER}), ER current (i_{ER}), ESS current (i_{ESS}), and PV current (i_{PV}) with 700 W load.....	46
Figure 55. Scenario B2: Transient responses of the ER subsystems: a) PV power, b) Power exchanged with the ESS, c) Active power exchanged with the grid, and d) Reactive power.....	47
Figure 56. ER voltage (v_{ER}) and ER current (i_{ER}) during black-start.....	48
Figure 57. Scenario C: Detailed ER voltage (v_{ER}) and ER current (i_{ER}) during black-start.....	48
Figure 58. Boost converter (220 V DC to 400 V DC) block diagram.....	49
Figure 59. PV production (May 21 st , 2019).....	51
Figure 60. ESS charging SoC progress and LESSAg ESS setpoints (May 21 st , 2019)	52
Figure 61. ESS discharging SoC progress and LESSAg ESS setpoints (May 21 st , 2019)	52
Figure 62. Single-phase ER cabinet front view (A – black-start box (S_{DSO}); B – PV, ESS and grid power converters, and measurement and control boards; C – UPS batteries; D – inductance filters; E – transformer)	55
Figure 63. Single-phase ER cabinet top view (A – black-start box (S_{DSO}); B – measurement and control boards; C – Power converters, D – Grid, PV and ESS controllers; E – ER controller; F – emergency button).....	56
Figure 64. Single-phase ER deployed at UPB's premises.....	56
Figure 65. UPB's connection board.....	57

List of tables

Table 1. Specifications of the PV interface and calculated values (in bold) for L	10
Table 2. Specifications of the PV interface and calculated values (in bold) for C.....	10
Table 3. Specifications of the PV interface and calculated values (in bold) for C.....	11
Table 4. Specifications of the ESS interface and calculated values (in bold) for L.....	12
Table 5. Specifications of the ESS interface and calculated values (in bold) for C.....	13
Table 6. Specifications of the grid interface and calculated values (in bold) for L and C.	14
Table 7. Final values of the single-phase ER selected components.	15
Table 8. Laboratory specifications of the experimental setup.	30
Table 9. Short-term test: 1-minute timeframe, with a 1000 W load on the 400 V DC network	53
Table 10. Long-term test: 5-minutes timeframe, with a 1000 W load on the 400 V DC network.	54
Table 11. Long-term check test: 1-hour timeframe, with a 500 W load on the 400 V DC network.....	54

References

-
- ⁱ PSCAD, *Power systems computer-aided design*, <https://hvdc.ca/>, accessed 08 October 2018.
 - ⁱⁱ M. Liserre, F. Blaabjerg and S. Hansen, "Design and control of an LCL-filter-based three-phase active rectifier," in IEEE Transactions on Industry Applications, vol. 41, no. 5, pp. 1281-1291, Sept.-Oct. 2005.
 - ⁱⁱⁱ P. Channegowda and V. John, "Filter Optimization for Grid Interactive Voltage Source Inverters," in IEEE Transactions on Industrial Electronics, vol. 57, no. 12, pp. 4106-4114, Dec. 2010.
 - ^{iv} T. G. Habetler, R. Naik and T. A. Nondahl, "Design and implementation of an inverter output LC filter used for dv/dt reduction," in IEEE Transactions on Power Electronics, vol. 17, no. 3, pp. 327-331, May 2002.
 - ^v TimeAndDate, *Past weather in Bucharest - Romania*,
<https://www.timeanddate.com/weather/romania/bucharest/historic>, accessed 21 January 2019.